GRI-93/0270

GRI

MICROFICHE

Topical Report

Core Based Stress Measurements: A Guide to Their Application

Prepared by:
Sandia National Laboratories

Gas Research Institute

Drilling and Completion Gro
June 1993

GRI-93/0270 SAND 93-2239

CORE BASED STRESS MEASUREMENTS: A GUIDE TO THEIR APPLICATION

TOPICAL REPORT
(July 1991-June 1993)

Prepared by
N. R. Warpinski, L.W. Teufel
J. C. Lorenz and D.J. Holcomb

Sandia National Laboratories
Divisions 6114 & 6117
P.O. Box 5800
Albuquerque, New Mexico 87185

For
GAS RESEARCH INSTITUTE
Contract No. 5089-211-2059

GRI Project Manager
Steve Wolhart
Tight Gas Sands Field Evaluation

June 1993

50272-101

REPORT DOCUMENTATION PAGE	1. REPORT NO. GRI-93/0270	2.	3. Recipient's Accession No.
4. Title and Subtitle: Core Based Stress Measurements: A Guide to their Application			5. Report Date: 6/1/93 Preparation 6.
7. Author(s): N.R. Warpinski, L.W. Teufel, J.C. Lorenz & D.J. Holcomb			8. Performing Organization Rept. No. SAND93-2239
9. Performing Organization Name and Address: Sandia National Laboratories Division 6253 P.O. Box 5800 Albuquerque, New Mexico 87185			10. Project/Task/Work Unit No. 11. Contract(C) or Grant(G) No. (C) 5089-211-2059 (G)
12. Sponsoring Organization Name and Address: Gas Research Institute 8600 Bryn Mawr Avenue Chicago, Illinois 60631			13. Type of Report & Period Covered: Topical Report 14.

15. Supplementary Notes

16. Abstract (Limit: 200 words)

This report is a summary and a guide to core-based stress measurements. It covers anelastic strain recovery, circumferential velocity anistropy, differential strain curve analysis, differential wave velocity analysis, petrographic examination of microcracks, overcoring of archived core, measurements of the Kaiser effect, strength anisotropy tests, and analysis of coring-induced fractures. The report begins with a discussion of the stored energy within rocks, its release during coring, and the subsequent formation of relaxation microcracks. The interogation or monitoring of these microcracks form the basis for most of the core-based techniques (except for the coring induced fractures). Problems that can arise due to coring or fabric are also presented. Coring induced fractures are discussed in some detail, with the emphasis placed on petal (and petal-centerline) fractures and scribe-knife fractures. For each technique, a short description of the physics and the analysis procedures is given. In addition, several example applications have also been selected (where available) to illustrate pertinent effects. This report is intended to be a guide to the proper application and diagnosis of core-based stress measurement procedures.

17. Document Analysis a. Descriptors

Tight gas sands, in situ stress, core, core analysis, stress measurement, hydraulic fracturing,

b. Identifiers/Open-Ended Terms

anelastic strain recovery, circumferential velocity anisotropy, differential strain curve analysis, differential wave velocity analysis, Kaiser effect, strength anisotropy, coring induced fractures, rock fabric, petal fractures, relaxation microcracks, tectonic microcracks,

c. COSATI Field/Group

18. Availability Statement	19. Security Class (This Report)	21. No. of Pages
Release unlimited	unclassified	
	20. Security Class (This Page)	22. Price

(See ANSI-Z39.18) See Instructions on Reverse

OPTIONAL FORM 272 (4-77)
(Formerly NTIS-35)
Department of Commerce

GRI DISCLAIMER

LEGAL NOTICE This report was prepared by Sandia National Laboratories as an account of work sponsored by the Gas Research Institute (GRI). Neither GRI, members of GRI, nor any person acting on behalf of either:

a. Makes any warranty or representation, express or implied, with respect to the accuracy, completeness, or usefulness of the information contained in this report, or that the use of any apparatus, method, or process disclosed in this report may not infringe privately owned rights; or

b. Assumes any liability with respect to the use of, or for damages resulting from the use of, any information, apparatus, method, or process disclosed in this report.

Title	Core-Based Stress Measurements: A Guide to Their Application
Contractor	Sandia National Laboratories
	GRI Contract Number: 5089-211-2059
Principal Investigator	N. R. Warpinski
Report Period	July 1991-June 1993 Topical Report
Objective	The objective is to develop a practical manual on the application of core-based measurements for determining *in situ* stresses. This manual would include the methods, analyses techniques, example applications, and strategies for obtaining optimal data.
Technical Perspective	*In situ* stresses are important for many processes in tight gas reservoirs, ranging from siting the well, to drilling, completion and long-term production. The orientation of the stress field, which controls the azimuth of the hydraulic fracture, is important for field development, as optimum drainage in a tight reservoir will depend on the elliptical drainage from a hydraulic fracture. If wells are not sited properly, then drainage patterns will overlap and production may be uneconomic. Stress magnitudes are important for wellbore stability and hydraulic fracturing. For fracturing, in particular, the stress difference between lithologies is the major control on fracture height growth. Since fracture length decreases as height increases (for a given volume), understanding the amount of height growth is crucial for developing optimum stimulation schemes. The focus of this study is a suite of core-based methods for determining both the orientation and the magnitudes of the stresses.
Results	This report provides information on the technical background, procedures, equipment, analyses, and case studies of currently available core-based techniques. Included in this report are circumferential velocity analysis (CVA), Anelastic Strain Recovery (ASR),

Differential Strain Curve Analysis (DSCA), Differential Wave Velocity Analysis (DWVA), petrographic examination of microcracks, overcoring of archived core, measurements of the Kaiser effect, strength anisotropy tests, and examination of coring induced fractures. When appropriately applied, these procedures can yield valuable data on the stress field at depth.

Technical Approach

The technical approach is to review each of the concepts separately and discuss the basic concepts, the core preparation procedures, the data acquisition techniques and equipment, and the data analysis procedures. Where available, example data are presented for each of the techniques, and limitations and problems are explained through example data. Also explained are the relative merits of each technique for discriminating fabric problems and for providing information on the stress magnitudes.

Project Implications

The determination of the orientation and magnitude of *in situ* stresses is a key element in the effective development of tight gas sand reservoirs. GRI research has shown that a number of methods must be applied to obtain reliable *in situ* stress data. This report is a guide to core-based techniques for determining *in situ* stresses.

Steve Wolhart
Project Manager, Tight Sands Field Evaluation

TABLE OF CONTENTS

LIST OF FIGURES

LIST OF TABLES

1.0 RESEARCH OBJECTIVES

The purpose of this report is to give petroleum engineers a manual that can be used to make decisions on the applicability of various core-based techniques for determining the *in situ* stress at depth in a gas reservoir. Available measurement techniques are reviewed, and example applications are provided for each. Where possible, relative merits and complexity of each technique are described, as well as the importance of the type of data that can be obtained.

2.0 INTRODUCTION

The *in situ* stresses at depth, including both orientation and magnitude, have many effects on gas and oil completion and production processes. Stress orientation is important for optimal well locations in a field that is to be hydraulically fractured or waterflooded. Stress magnitudes are important for hydraulic fracture design, wellbore stability and sand production, as well as many other aspects of drilling and production.

Stress measurement techniques that can be made at depth are logically divided into three categories The first is direct measurement, as with a hydraulic fracture. The primary objective of a hydraulic-fracture test is the determination of the minimum *in situ* stress at depth. If the fracture is created open hole, performed during drilling, or monitored with diagnostics, then fracture orientation may also be obtained. In some open-hole tests, the data may also be adequate to estimate the maximum horizontal stress, but there are many problems associated with this measurement.

The second category of techniques is borehole measurements. Examples include the formation microscanner (FMS), televiewer and TV camera measurements of breakouts and drilling-induced fractures for stress orientation, as well as estimates of the minimum *in situ* stress from sonic logs. These techniques have the advantage of being a standard industry technique, but the disadvantage of having large uncertainties due to the qualitative discrimination between breakouts and washouts and between drilling-induced and natural fractures.

The third category of stress measurement techniques are core-based methods. These include Anelastic Strain Recovery (ASR), Differential Strain Curve Analysis (DSCA) and Differential Wave Velocity Analysis (DWVA), Circumferential Velocity Anisotropy (CVA), examination of coring induced fractures, petrographic examination of microcracks, measurements of acoustic emissions based on the Kaiser effect, measurements of petrophysical anisotropy (e.g., strength, permeability etc.), and overcoring of archived core. Most of these techniques are used primarily for stress orientation, but ASR, DSCA, and Kaiser effect techniques offer the potential for providing stress magnitude data as well. It is this third category of techniques that is the subject of this report.

It should be noted that some other stress measurement techniques have not been considered because of their lack of application for gas and oil applications. For example, overcoring is a very useful technique in mines, but is impractical in boreholes at depth. Focal point mechanisms may provide some information on regional stress fields, but their inaccuracy and their distance from producing strata make them useless for this application.

3.0 BACKGROUND

With the exception of the analysis of coring induced fractures, all of the core-based measurements derive their information from the measurement or perturbation of relaxation microcracks that develop in a piece of core upon stress relief. These techniques are much more understandable if the basic relaxation concepts are clear. These concepts will be discussed in some detail.

3.1 Stored Energy within Rocks

The behavior of core upon stress relief during drilling actually has its roots in the first deposition and lithification of the sediments (Friedman[1]). During burial and lithification of the sedimentary materials, individual grains (in this case, consider sand grains) eventually become stressed, resulting in compression and distortion of the grains. Fluids permeating through the sediments then precipitate cementing materials which lock in the altered shape of the sand grain. The compressed and distorted sand grain is analogous to several springs that have been pre-loaded and set. There is a considerable amount of stored energy within the grain, and it may vary in different directions depending upon the amount of stress that was applied in each orientation. This situation is shown in Figure 1.

Through time, however, conditions change and the sand grain may be buried deeper, undergo heating, experience pore-pressure changes, or even be altered. These processes apparently happen slowly enough that cement materials are dissolved and reprecipitated in some equilibrium manner so that the stored energy within the sand grains reflects the current stresses on the sample. Of course, if the stresses become large enough that failure occurs, then tectonic microcracks develop and the relaxation process may not apply. Such problems will be discussed later.

Obviously, the directions of energy storage, or strain, within a single sand grain are entirely dependent upon the contact points with neighboring particles. However, if a large enough ensemble of grains is chosen, then the domain-averaged principal directions of stored strain will be co-aligned with the principal stress directions. Thus for relaxation techniques to be valid, there are two primary conditions that must be met. First, the geologic processes are slow and equilibrium conditions are maintained so that the stored energy within the rock is proportional to the current stress on the sample. Second, the grain size of the sample is small compared to the sample size. The first assumption may not always be true, but based upon the cumulative measurements to date, it appears to hold for most sedimentary rocks in petroleum basins and some other types of rocks and conditions. This situation of differentially stored strain is the initial condition for the core-based relaxation techniques.

3.2 Unloading of a Core Specimen

When a rock stratum is cored, the core undergoes an immediate relief of part of the stress on it. The external stress on the sample changes from some deviatoric stress state to one of

hydrostatic stress due to the mud pressure. Figure 2 shows the immediate change in stress that takes place. This immediate response begins the strain relaxation process just after coring, and the process continues as the core is retrieved and the hydrostatic stress due to the mud weight decreases. The final stress state of the sample at the surface is zero external stress.

When the external stresses are relieved, the sand grains attempt to expand elastically, but they are held back by cement materials which form bonds across grains. Many of these cement bonds will eventually be broken, leaving grain-boundary microcracks. Since the largest amount of stored strain is in the direction of the largest principal stress, more grain boundaries will be broken at contacts that are perpendicular to the maximum stress. Thus the anisotropy in stress state creates an anisotropy in stored strain which results in an anisotropy in the orientation of grain boundary microcracks. The net effect is a time-dependent expansion of the core which is preferentially oriented in the direction of the stress field.

Figure 3 shows a schematic of the strain recovery of a piece of core for one orientation, as first proposed by Emery.[2] This behavior is essentially that which will be considered for ASR applications (discussed later) and was verified in several ASR experiments (Teufel,[3,4] Teufel and Warpinski;[5] Smith et al.,[6] Warpinski and Teufel,[7]). When the core is cut at time t_o, there is an initial elastic recovery of the core, followed by the anelastic recovery which may occur for as much as two days. If the core is brought to the surface and instrumented with strain or displacement gages at time t_s, then some of the anelastic part of the recovery may be measured. The elastic part can only be measured using overcoring techniques, which are good techniques in mines, but which are impractical for oil and gas applications in deep boreholes.

The essential mechanism, that the relaxation is caused by the formation of microcracks, was proved by Teufel[8] using acoustic emissions. Figure 4 shows relaxation data correlated with acoustic emissions from a sandstone sample. In this case, core relaxation was measured in four orientations, starting approximately six hours after the core was cut. Acoustic emissions, which are a signature of microcracking, are prevalent during the period of relaxation, but they stop when the core relaxation stops. As shown in Figure 5, there is a one-to-one correspondence between the number of acoustic emissions and the volumetric strain of the sample for three different rocks tested.

The time dependence is not well understood, but a plausible mechanism is stress corrosion cracking. Water is found to some extent in all rocks at depth, and it is also introduced during drilling. When the stresses are relieved and the expansion of the grains puts a tensile stress on the cement material, stress corrosion begins to weaken the cement material at any flaw site. With time some of the grains will be sufficiently weakened to crack. Cracking at some locations will likely cause additional stress at other grain boundaries, thus resulting in a cascading effect until the stresses are relieved. As cracks begin to appear and the strength characteristics of the rock change, frictional sliding along grain boundaries may occur,

particularly if there are clays, carbonaceous material, liquid hydrocarbons, or water to lubricate the process.

Cooling of the rock, which introduces tensile thermal stresses if grains and cement have different coefficients of thermal expansion, may also aide the process and account for some of the time dependency, although the general effect of cooling is shrinkage. Decay of the pore pressure, which provides effective tension within the rock, probably has a significant role in some samples, but the decrease in pore pressure also results in a volumetric shrinkage (Warpinski and Teufel[7]). Drying and chemical reactions may also contribute to the process in some rocks.

3.3 Effect of Relaxation Microcracks

The end result of the relief of the *in situ* stresses by coring is the formation of a population of microcracks that is preferentially aligned with the stress field (Teufel[8]). A schematic of this population is shown in Figure 6, where it can be seen that there are more (and probably larger) cracks that are opening normal to the original maximum *in situ* stress direction. However, it is important to stress that there still are a large number of microcracks with different orientations.

An oriented population of microcracks has some interesting and useful effects on many of the rock's petrophysical properties, and these effects are used to deduce stress conditions. In order to illustrate some of these effects, it is first useful to define a coordinate system oriented on the microcracks, as shown in Figure 7. If the principal crack orientation (i.e., the cracks opening up in the direction of the maximum *in situ* stress) is considered, then the normal to the crack surface is directed at an angle φ with respect to some reference angle (usually north). All following discussions will be with respect to this principal crack normal, and the angle φ will be its orientation.

A preferentially oriented population of microcracks has a lower modulus, acoustic velocity, permeability, and tensile strength at an orientation φ than at any other orientation. This behavior can be easily explained by examining effects of the microcracks in Figures 6 or 7. Open cracks are highly compliant, so modulus will be low. This was clearly shown by Walsh,[9] who developed formulae for estimating the change in bulk modulus due to cracks. For example, Walsh estimated that a rock with N aligned penny-shaped microcracks, having a length c and residing in a volume V, would have a bulk modulus

$$K_{eff} = \frac{K}{\left[1+\frac{16(1-\nu^2)Nc^3}{9(1-2\nu)V}\right]}, \qquad (1)$$

where K is the bulk modulus of the uncracked material. Thus as the crack length increases, or the number of cracks increases, the effective bulk modulus decreases.

Microcracks are very effective at slowing acoustic waves, as would be expected from the effects on the elastic property shown above. Garbin and Knopoff[10] calculated the variation of velocity through a set of dilute parallel microcracks as

$$V_{P_{eff}} = \frac{V_p}{\left[1+\frac{8Nc^3}{3V}\left\{\frac{8}{7}(\cos^2\theta-\cos^4\theta)+\frac{1}{4}(1+2\cos^2\theta)^2\right\}\right]^{\frac{1}{2}}}, \quad (2)$$

where c, N and V are defined as above and θ is the angle of incidence to the parallel cracks. V_{po} is the compressional velocity of the uncracked material. Similar analyses will be used for analyzing the effects of a population of microcracks, and applications of this property will be discussed in the section on CVA.

Permeability is much greater along the crack length, so the permeability of the sample will be higher in the direction normal to the maximum stress. Ostensen[11] provides an estimate of the permeability anisotropy due to a population of microcracks under an anisotropic stress. Such analyses can also be used to develop a model of permeability anisotropy under lab conditions.

Microcracks normal to a tensile stress weaken rock strength. In this case, the tensile strength is most likely affected by the length of the cracks. Ingraffea and Schmidt[12] have developed a relationship between crack size and tensile strength for Indiana limestone. Such relationships could presumably be developed for many materials. Point load and Brazilian tests (Logan and Teufel[13]) have been used to exploit this effect.

Thus, there is a large suite of petrophysical properties that can be used to interrogate the population of microcracks. When the behavior and relative orientation of the microcracks are known, much information can be gleaned about the original stress state on the rock when it was at depth.

3.4 Coring and Orienting

One of the major difficulties with core-based techniques is the necessity to have oriented core that is in relatively good condition.[14-16] Orienting of core is not always successful, as orientation surveys may fail, scribe knives may not cut the core, or core may spiral, crack or break during cutting. Without a successful orientation survey, none of these core-based methods provide quantitative results.

When excessive damage is done to the core, as when chattering or spiraling is observed, there may be little or no measurable development of preferentially oriented microcracks. The reason for this is not known, but it likely that rough treatment of the core produces shock loadings that cause many intergranular cracks irrespective of the stress state. A preferential population of microcracks, superposed on a much broader damage, may not produce significant petrophysical changes. Thus, the most important aspect of core-based techniques is obtaining good quality oriented core.

In order to avoid the problems of standard oriented core, it is sometimes possible to orient core using other techniques. Paleomagnetism is occasionally used to orient core, but it has a relatively large uncertainty and may not work on all rocks. If bedding is present, and if the bedding has significant dip with respect to the borehole, then an oriented borehole imaging log may allow the core to be oriented by comparison with the logs. Unfortunately, the applicability of this technique for a given well is difficult to assess *a priori.*

3.5 Fabric

Perhaps the most difficult problem associated with these techniques is a group of problems that has collectively come to be characterized as rock fabric. A population of preferentially oriented microcracks will have observable effects on petrophysical properties in a homogeneous isotropic material, but their effects may not be evident if the rock is highly anisotropic. Furthermore, some types of fabric, or anisotropy, may actually overwhelm the effects of the relaxation microcracks and yield inaccurate data on the *in situ* stresses. Understanding the various types of rock fabric and devising methods to diagnose their occurrence is an ongoing research topic. Examples of fabric problems will be presented with the discussion of individual techniques.

The simplest types of fabric to diagnose are those which are visible in the core. A few examples include bedding planes, which for a vertical well provide a fabric along the axis of the core (transverse anisotropy), draping bedding planes or shale streaks which provide a full 3D anisotropy, natural fractures, and large grain sizes (e.g., conglomerates).

When bedding planes are found perpendicular to the axis of the core, then velocity, ASR, or DSCA data taken circumferentially around the core may still be of value for estimating stress orientation in that plane, but nothing can be determined about the stresses in the axial direction. On the other hand, permeability measurements taken circumferentially will be useless because they will only measure the permeability of the bedding planes. Draping features make a core sample unsuitable for most core-based methods as all techniques will have their results distorted in all directions.. Features as subtle as crossbeds in a sandstone may skew the results.

Macroscopic natural fractures will affect all petrophysical properties in its vicinity, and thus naturally fractured specimens should be avoided for all of these techniques. If the natural

fracture only cuts a small slice of the core, then it may be possible to obtain some velocity, permeability, or petrographic data that is of value.

The grain size of the rock relative to the core size is an important limitation for most of these techniques. The preferentially oriented population of microcracks which is co-aligned with the maximum *in situ* stress can only develop if there are large numbers of microcracks so that an averaged ensemble of these cracks reflects the original stress condition. If there are few grains, then the grain contacts may be oriented such that the orientation of grain contacts is more important than the *in situ* stress condition. Rocks such as conglomerates should be avoided. Other features, such as vugs and aligned or distorted grains may have the same effect. Cores with any macroscopic anisotropies should be avoided if reliable data are desired.

More difficult to assess are the sub-visible fabric features such as tectonic microcracks and the microcracks that might have been induced during the coring process. Tectonic microcracks are pre-existing features within a core sample that were formed during burial in the subsurface. Like natural fractures, such features tend to be highly aligned, and they may be inter- or intra-granular. Figure 8 shows a photograph of a thin section where the tectonic microcracks are clearly visible. Many of these cracks are intragranular. On a broader scale, as seen in Figure 9, the tectonic microcracks form regions of highly oriented, sub-parallel fractures.

Because of their high degree of alignment, these fractures tend to dominate strain relaxation, modulus, permeability, velocity and most other petrophysical properties. Such microcracks form parallel to the maximum *in situ* stress (just the opposite of relaxation microcracks), and if the stress state that caused the microcracks is still prevalent at the time of coring, the core-based measurements will be dominated by the microcracks and the predicted stress orientation will be 90° in error. If the stress that formed the tectonic microcracks has changed orientation, then the core-based measurements will be in error by 90° minus the rotation angle. The end result is: In the presence of tectonic microcracks, most of these techniques will yield unreliable results. Thus it becomes important to develop a strategy for assessing if fabric is present. Such strategies will be discussed along with the individual techniques.

The other type of sub-visible fabric, that induced by coring damage, appears to yield the manifestations of a homogeneous stress state. Cores exhibit no ASR response and rocks show no velocity anisotropy. It is speculated that chattering, spiraling, and scribe knife chipping are the external evidence that the cores have undergone significant shock during the coring, recovery, and handling process. This shock probably induces microcrack damage in random orientations, and there may be sufficient damage that any relaxation microcracks have little differential effect above that of the shock-induced damage. Cores exhibiting this type of damage should be used carefully.

4.0 TECHNIQUES

The techniques considered here include circumferential velocity anisotropy (CVA), petrographic examination of microcracks, anelastic strain recovery (ASR), overcoring of archived core, differential strain curve analysis (DSCA) and differential wave velocity analysis (DWVA), examination of coring induced fractures, and measurements of the Kaiser effect. In each case, the concept will be discussed first, followed by data acquisition techniques, data analysis (including problems and limitations), example applications, and a general discussion of the technique, its value and its advantages.

4.1 Circumferential Velocity Anisotropy (CVA)

4.1.1. Concept

Circumferential velocity anisotropy is a technique that is used to determine the stress azimuth and to deduce information about rock fabric problems. Measurements of the circumferential velocity anisotropy of a core sample appears to have been first made by Nur and Simmons,[17] but they did not attempt to use the data for stress measurement purposes. Teufel[3,4] first used velocity information as a stress indicator by correlating velocity data with ASR results. Other CVA results have been presented by Teufel,[8] Warpinski and Teufel,[18] Miller et al.,[19] and Walls et al.[20] These results have shown that CVA provides a useful indicator of the *in situ* stress orientation . Teufel[3] also showed the value of measuring velocity anisotropy under confining stress.

As discussed earlier, the acoustic velocity is anisotropic because of the population of preferentially oriented microcracks. Referring again to Figure 7, the velocity parallel to **n** will be lower because of the effect of crossing a large number of open microcracks. Since the averaged direction of maximum crack opening, **n**, is co-aligned with the maximum *in situ* stress, the minimum velocity orientation is co-aligned with the maximum stress orientation. Thus, if one can measure the velocity at several orientations around the core, the orientation that has the lowest velocity will be the maximum stress orientation.

4.1.2. Core Preparation

The first step to an accurate reliable measurement of the circumferential velocity anisotropy is choosing pieces of core that are relatively homogeneous and free from noticeable fabric. Bedding may be present if it is perpendicular to the axis of the core, but it is generally best to pick locations without any observable bedding. Natural fractures, even if healed, should also be avoided.

Core specimens can be used as received, and good results are often obtained with as-received samples. However, many cores have a thin skin-damage zone that can interfere with the acoustic signals. If anisotropies are small, or if there is a large amount of scatter in

the data, the skin damage can be removed by grinding down the surface of the sample about $1/16$ in and retesting.

Velocity anisotropy generally works best on dry samples, because fluid-filled cracks do not affect the velocity nearly as much as air filled cracks. If cores were sealed and are then tested immediately, they may show very little anisotropy. However, a couple of days of drying under room conditions may yield completely different results.

4.1.3. Data Acquisition Technique

While the data acquisition scheme is relatively simple, some sophisticated equipment is needed to obtain accurate reliable data. It is recommended that a graduated (in degrees) rotating stand be used to hold the sample during testing. The core should be mounted on the stand in some fashion and transducers applied with mechanical, pneumatic, hydraulic, or solenoid actuated devices. Figure 10 shows a schematic of such an apparatus (the type used at Sandia). Once the sample is positioned on the stand, the transducers are applied to the core surface and the velocity at one position is taken. The actuators are released, the core is rotated a specified amount, the transducers are re-applied, and data are again taken. This process is repeated until a full 180° circuit of the core is completed.

To obtain good coupling between the core and the transducer, some type of viscous material should be applied at each position. Glycerin and molasses are two materials that work well.

The transducers can be either p-wave or s-wave transducers, and generally should have a frequency range of 500 kHz. One of the transducers is a source which is excited with a pulsed power supply, while the other transducer is the receiver. Data from the two transducers can be analyzed in many ways, but a simple one is to use a versatile oscilloscope like a Nicolet. The input to the source receiver is used as a trigger while the output of the receiver is displayed on the scope. The signal is captured and held and the timing of the input signal and the first arrival of the output signal are determined.

The difference in time of the two signals gives the Δt across the sample and transducer platens. The time to cross the platens must be determined and subtracted to get the Δt across the core, but this need be done only once prior to or after the entire suite of tests are completed. To obtain velocity, the diameter of the core is divided by the Δt at each position.

4.1.4. Data Analysis

The simplest method of analyzing the velocity data is to take the orientation of the minimum velocity point as the orientation of the stress field, and this approach is commonly taken. However, there are other approaches that offer the potential of extracting considerably more information from the data. The approach suggested here is to compare the data to the

theoretical distribution of a population of preferentially oriented microcracks, and make decisions about the validity of the data based on the fit. The fit also provides a more accurate estimate of the orientation at which the minimum velocity occurs. A similar procedure has been used by Plumb et al.[21] to model microcrack fabric.

The theoretical velocity distribution for a preferentially oriented population of microcracks has been worked out by Sayers,[22] yielding a velocity distribution given simply by

$$V(\theta) = V_{avg} + A\cos(2\theta+\varphi) + B\cos(4\theta+\varphi). \quad (3)$$

In this equation, the velocity at any orientation, $V(\theta)$, is a function of the average velocity through the sample plus a 2θ and a 4θ component.

The phase angle, φ, is simply the offset angle that makes $V(\theta)$ a maximum at $2\theta+\varphi=0°$ (assuming B is much smaller than A). φ is required because the orientation of the minimum (or maximum) velocity is not known *a priori*. A regression using this equation will provide the parameters A and B, but more importantly it gives the best fit value of φ. Thus, the orientation of the minimum velocity, $2\theta+\varphi=180°$, is the direction in which the most cracks are crossed. A simple FORTRAN computer program to extract A, B and φ is given in appendix A.

In actual practice there are a number of factors which can cause problems with the CVA technique. In some rocks, there is very little microcrack development, microcracks are overwhelmed by other factors, or the microcracks have little effect on the velocity, so that the anisotropy is small. A good example is a high porosity rock, where additional microcracks have a minimal effect on velocity through the highly voided rock. When velocity variations are on the order of 2-3% or less, the inferred stress orientation should be considered unreliable.

A second major problem for the CVA technique is the prior existence of a rock fabric, due to cracks, layering, oriented grains or crystals, or many other factors. Such a fabric can often produce a velocity anisotropy that overwhelms the microcracks velocity anisotropy. However, fabrics usually have a completely different velocity character than microcracks, and this becomes very apparent in fitting the theoretical curve to the data. For relaxation microcracks, the theoretical fit is generally good, and the sinusoidal character of the anisotropy is evident. For the cases with fabric, a poor fit of the theoretical curve is often obtained, and the velocity data have a blocky structure. This difference provides a qualitative diagnostic for fabric problems. Examples of this blocky structure will be shown below.

4.1.5. Example Applications

Several examples from different formations and locations are shown to demonstrate the capabilities of this technique. Some of the examples also demonstrate the effect of fabric, natural fractures, and coring damage.

4.1.5.1 SFE-4 Frontier

An example of high-quality CVA data comes from the GRI-funded S.A. Holditch & Assoc. SFE-4 well in the Moxa Arch region of the Green River Basin in Wyoming. In this example, the formation tested was the Frontier at a depth of about 7400 ft.

Sample ASR 13, shown in Figure 11 and data given in Table 1, was a fluvial sandstone taken from 7419 ft. The data for this sample are taken at 15° increments and shown by the square symbols. The data point at about 105° was taken twice to provide an estimate of the reproducibility of the measurement. The solid line is the fit obtained by the regression on Equation 3, and it shows that the data are well fit by the theoretical distribution and clearly have the desired sinusoidal character. The velocity anisotropy is about 13%, suggesting that the horizontal stresses have a large stress anisotropy. The stress orientation of N21°E, agrees with other diagnostic techniques (Laubach et al.[23]).

Table 1. SFE-4 CVA data for ASR-13

ORIENTATION	VELOCITY (ft/sec)
1	10647
16	10371
31	10507
46	10719
61	11129
76	11367
91	11700
106	11874
106	11918
121	11787
136	11743
151	11287
166	10865

4.1.5.2 MWX Mesaverde

Another successful example is taken from a coastal sandstone from the Mesaverde in the Piceance Basin of Colorado at the Multiwell site. This core was taken from a depth of

about 6520 ft from CER MWX-2. The CVA data and the resultant fit are shown in Figure 12. The data for this sample are given in Table 2.

In this example, the velocity anisotropy is about 15%, and the theoretical equation provides an excellent fit to the data. The orientation is N96E°, which is in agreement with other techniques at this depth (Warpinski and Teufel[24]).

Table 2. MWX-2 CVA data at 6520 ft

ORIENTATION	VELOCITY (ft/sec)
0	12795
15	12801
30	12467
45	12205
60	11811
75	11385
90	11089
105	10991
120	11417
135	11811
150	12270
165	12598
180	12795

4.1.5.3 Fuelco Cozzette

Another example taken from the Mesaverde in the Piceance basin is from the Fuelco EM22-10-94-S well. This sample was cored from a depth of 6937 ft in the Cozzette sandstone, a marine sandstone near the base of the Mesaverde. As seen in Figure 13 and Table 3, there is a 12% anisotropy and a good fit of the data by the theoretical velocity distribution. The orientation here is N94°E, essentially the same as the previous example, which is about 20 miles to the north of this well.

A second core, taken three feet deeper, is shown in Figure 14 and the data are given in Table 4. The same essential behavior is observed, although the anisotropy is only about 7%. In this example, however a shallow (0.5 in) scribe-knife-induced fracture cuts into the core at about the 25° location. Because of this fracture (and possibly some other damage associated with it), the data between 15° and 50° are not well fit by the theoretical distribution. Had the scribe knife fracture been deeper, it is likely that the data quality would have been more seriously degraded.

Table 3. Fuelco CVA data at 6937 ft

ORIENTATION RELATIVE TO PSL	VELOCITY (ft/sec)
10	10961
25	10814
40	10741
55	10850
70	11152
85	11594
100	11936
100	11895
115	12119
130	12165
145	11939
160	11594
175	11269

Table 4. Fuelco CVA data at 6940 ft

ORIENTATION RELATIVE TO PSL	VELOCITY (ft/sec)
2.5	10165
17.5	10070
32.5	9855
47.5	9916
62.5	10070
77.5	10345
92.5	10565
107.5	10705
107.5	10687
122.5	10652
137.5	10634
152.5	10345
167.5	10181

4.1.5.4 Phillips Canyon Sands

Some interesting results were obtained from core obtained from the Phillips Petroleum Ward C11 well in a GRI sponsored Canyon Sands test in Sutton County, Texas. Only one of four cores yielded reliable data, but other cores showed some of the problems that may occur.

A sandstone sample at 5581 ft, shown in Figure 15 and given in Table 5, was the one test in which the data appeared to be high quality, with an anisotropy of about 6%. The orientation of this test was N24°E, about 10° different from a suite of other tests conducted at this site (Miller et al.[19]). This result has similar characteristics to the previous examples.

A sample taken at 5528 ft, shown in Figure 16 and given in Table 6, is a muddy siltstone, and it clearly exhibits fabric response. A minimum velocity is measured over a span from about N30°W to N50°E. This type of plateau in the minimum velocity is typical of many tests where the CVA data is not well fit by the theoretical distribution and where the stress orientation from CVA does not agree with the stress determined by other techniques (difference of 25 degrees). The velocity anisotropy is about 4%.

A third Canyon Sands sample, from a sandstone at 5577 ft is shown in Figure 17 and given in Table 7. This case shows both unground (as received) and ground results. In this sample there is a large difference in the response of the as-received sample compared to the ground sample. Even the ground sample is a poor set of data, and there appears to be indications of

fabric, but this test illustrates the improvement in data that can be obtained by surface preparation of the core.

Table 5. Canyon Sands CVA data for 5581 ft

ORIENTATION	VELOCITY (ft/sec)
0	13386
15	13302
30	13247
45	13330
60	13555
75	13729
90	13938
105	13908
120	13999
135	13938
150	13818
165	13527

Table 6. Canyon Sands CVA data for 5528 ft

ORIENTATION	VELOCITY (ft/sec)
5	13882
20	14064
35	13972
50	14003
65	14412
80	14412
95	14543
110	14543
125	14348
140	14252
155	14064
175	14126

Table 7. Canyon Sands CVA for 5577 ft

UNGROUND ORIENTATION	UNGROUND VELOCITY (ft/sec)	GROUND ORIENTATION	GROUND VELOCITY (ft/sec)
3	16411	10	16114
18	16131	25	16074
33	16131	40	16114
48	16053	55	16074
63	16092	70	16444
79	16053	85	16572
93	16092	100	16745
108	16290	115	16701
123	16250	130	16833
138	16210	145	16966
153	16330	160	16701
168	16492	175	16444

4.1.5.4 HEYCO Bone Spring

Another example of fabric is seen in a carbonate sample from the HEYCO AJ 11 Federal #1 well in the Bone Spring formation, New Mexico (Lorenz et al.[24]). These results are shown in Figure 18. As in the previous Canyon Sand test, there is a broad minimum plateau extending over 45-60° and a poor fit by the theoretical distribution.

A better test in the Bone Spring, taken from the Second sandstone at 8708 ft, is shown in Figure 19. The anisotropy is about 4% and the fit to the data is acceptable. Although there is not much good stress data available from this site, a few indicators suggest that the stress orientation is NE (Lorenz et al.[24]).

A second well in the Bone Spring, the Can Ken 4 Federal #2, had many coring problems and the core came up with significant damage. All of the CVA tests had results similar to those shown in Figure 20, which was taken from a depth of 8222 ft. There was no velocity anisotropy within the accuracy of the measurements, and no useful results were obtained from this well. Because of data such as these, it is believed that the coring damage induces random microcracks throughout the sample that mask an relaxation microcracks. From the previous well, it was clear that a significant anisotropy exists in this formation, but some element of the coring process has destroyed it.

4.1.5.5 Maxus Cleveland formation

Several samples from a GRI co-op well, the Maxus Exploration H.T. Glasgow # 2, in the Cleveland formation of Ochiltree County, Texas, were tested with very poor results. Depths of the test samples were about 7200 ft. All four of these samples were sandstones, but with some amount of dipping and undulating bedding in all samples. In the deltaic depositional environment of the Cleveland formation, these were the cleanest sandstones that could be found.

A sample at 7227 ft, shown in Figure 21, has a velocity anisotropy of about 1% (with the exception of one point). These results are not reliable for stress azimuth and should be discarded. What is not clear, however, is why there is no velocity anisotropy. The core was retrieved in relatively good condition, and there is no reason to suspect an isotropic stress state at this location.

A second sample, at 7236 ft and shown in Figure 22, has a large velocity anisotropy (8%), but the velocity distribution in no way resembles the expected theoretical distribution. We suspect that the undulating bedding planes are responsible for this unusual behavior, and the minimum velocity point is only indicative of bedding. This result should not be trusted for stress orientation.

All samples from the Cleveland formation had these same kinds of problems and no reliable data were obtained. These tests indicate that there will be some formations and some wells where CVA will not provide any useful information.

4.1.5.6 UPRC Frontier

Further evidence of fabric and coring damage were found in a GRI co-op well in the Frontier. The UPRC Fabian Ditch #4-34 well, in the Moxa Arch region of the Green River Basin, encountered the Frontier at about 11,000-12,000 ft. Most of the core was heavily damaged in the coring process, and typical CVA results (at 11625 ft) are shown in Figure 23. In this case, no discernible velocity anisotropy was measured. However, previous tests in the Frontier had consistently measured large anisotropies. We again believe that the coring-induced damage, as evidenced by spiraling scribe marks and chatter, has masked any relaxation behavior.

One sample that did have a large anisotropy, a test at 11573 ft, is shown in Figure 24. In this case, however, we again see the blocky structure, that is, the broad minimum plateau from -20° to 50°, that we believe is typical of fabric problems.

4.1.6. Discussion

CVA is an excellent technique for determining *in situ* stress orientation and for diagnosing the results from other techniques. Using CVA, one can determine if preferentially oriented microcracks exist, and if they are oriented in the direction indicated by other techniques. CVA is in large measure self-diagnosing, because many fabric problems yield velocity distributions that are much different from a population of preferentially oriented microcracks. Furthermore, by using the theoretical distribution in a regression process, one is then able to determine a stress orientation that is the best fit of all of the data. The accuracy of the technique is limited primarily by the accuracy of the orientation survey, because angular increments can be made as small as possible to provide large amounts of information for the regression. Accuracy of the velocity measurement is typically ±100-200 ft/sec out of an average velocity of around 12000 ft/sec, so anisotropies greater than 2-3% are generally meaningful.

The disadvantages to CVA are the same as those for all core-based techniques. The core must be oriented, which is expensive and sometimes difficult, and the core must be recovered in good shape. If non-normal bedding, fractures, or fabric are present, then no results can be obtained using CVA.

The advantage to CVA is that it can be performed at any time after oriented core is available, and archived core provides excellent results. It should be considered as a diagnostic anytime that ASR or DSCA/DWVA are used, and it can be used as a primary technique, although many samples should be tested to assure good results (some samples

may have fabric and it is worthwhile to have at least three good tests for statistical purposes).

If oriented core is being recovered for other reasons, then CVA offers a low cost opportunity to measure the stress orientation. A typical CVA survey takes about one hour of a technician's time and 15 minutes for analysis. If surface grinding is performed, shop costs may be $50-100.

4.2 Anelastic Strain Recovery

The Anelastic Strain Recovery (ASR) technique is a field method that estimates stress orientation and magnitude from time-dependent strain relaxation measurements of oriented core at the well site. The ASR technique has evolved from the observation that when a core is cut at depth, it undergoes differential relaxation in relief of the *in situ* stresses, and that the total strain includes both an instantaneous, elastic component and an anelastic component which may relax over tens of hours. Principal *in situ* stress directions can be determined directly from partial ASR measurements of oriented core by making the assumption that anelastic strains are proportional to the total recoverable strains and that the relaxation process can be described by linear viscoelastic behavior. Determination of the *in situ* stress magnitudes from ASR data is considerably more difficult and requires a constitutive model of the relaxation process.

4.2.1. Concept

The determination of the *in situ* stress state in deep formations from anelastic strain recovery measurements of oriented core is in part, an extension of the stress relief method used to determine *in situ* stresses near underground openings. The stress relief method is generally accomplished by an overcoring process which allows the physical detachment of a body of rock from the rock mass, thus permitting the body to undergo differential relaxation in relief of *in situ* stored strain energy. The recovered strain is measured with strain or displacement gages and generally involves both an instantaneous, elastic component and an anelastic component, as shown in Figure 25. Usually gages are installed at the bottom of a borehole prior to overcoring and stress relief, and the measured strain recovery can be related to the total stress components which acted prior to relief.

A measure of the total strain relief (both elastic and anelastic) and the calculated stress state is restricted to shallow depths. However, if gages are installed subsequent to stress relief, a partial component of the anelastic strain recovery can still be determined. Voight[25] first suggested that if the assumption is made that the partial recoverable strain is proportional to the total recoverable strain, then an approximate estimate of the *in situ* stress state at depth can be made by instrumenting oriented cores immediately upon removal from the borehole. Voight noted that there is empirical justification to consider that the recovered anelastic strains will be proportional to the total recoverable strain, and hence, will be related to the *in situ* stress state. If the rock is isotropic or transversely isotropic and homogeneous at depth and the recovery behavior is linearly viscoelastic, then the strain relief along principal strain directions will be uniform with time, and the directions of principal strain relief determined over a given time interval will correspond to the initial *in situ* strain conditions. Thus, principal strain directions determined from anelastic strain recovery measurements will be homothetic with the principal *in situ* stress directions. If there is no mechanical anisotropy due to rock fabric to distort the results the maximum strain direction is coincident with the maximum stress direction.

Teufel[27] found good agreement between stress directions inferred from elastic and anelastic strain recovery measurements and hydraulic fractures exposed by a mineback operation in volcanic tuff at the Nevada Test Site. Smith et al,[6] Lacy,[28] and Warpinski and Teufel,[24] found good agreement between principal horizontal stress directions determined from ASR and other methods.

The determination of the stress magnitudes is more complicated and requires a constitutive model for the ASR process. Blanton[29] and Warpinski and Teufel[7] have developed different types of viscoelastic models to explain the behavior. Blanton's model assumes constant properties throughout the relaxation process and results in a simple relationship between the stresses and the relaxation strains. Warpinski and Teufel's model fit the relaxation data to a full viscoelastic model to arrive at relationships between the strain parameters (from the fit) and the stresses. These models will be described in the data analysis subsection.

4.2.2. Core Procedure

Immediately upon retrieval from the wellbore, the oriented core must be carefully examined to select pieces without natural fractures or significant non-homogeneities. Core samples are sealed with a polyurethane coating, which is brushed on and cured within 15 minutes, and with polyurethane wrapping. The displacements associated with anelastic strain recovery are determined with spring-loaded, clip-on gages, which incorporate precision gage heads (Holcomb and McNamee[30]). Prior to applying the gages, a drill should be used to put a small dimple on the surface of the core so that gages do not slip. If cores are from vertical wellbores in flat-lying to shallow dipping strata, only three independent displacement measurements are required to determine the directions and magnitudes of the two principal horizontal strains. The best procedure is to use four gages that are mounted at 45 degrees to each other in the horizontal plane of each core, as seen in Figure 26. Using combinations of any three gages that principal horizontal strains can be calculated from the strain-rosette equations (see data analysis subsection). The vertical strain is determined by mounting a gage parallel to the center axis of the core. Deviated holes require at least six gages, but it becomes more difficult to perform this technique as the number of gages increases.

4.2.3 Data Acquisition

Displacement data are obtained using precision gage heads that have been calibrated prior to the test. These gages are mounted in a ring with an adjustable screw for loading the gage (essentially zeroing the gage). Thermocouples are used to record the temperature of the room and the core. Displacement data for each gage and the temperatures are recorded with a data logger or directly onto a personal computer. All displacements are normalized to strain from the initial gage length settings. The resolution of the strain measurements is one microstrain. During the field tests temperature variations of the cores must not exceed 1° C. Otherwise thermal corrections to the field data must be made later using thermal

conductivity data from laboratory measurements in each gage direction of the core. Data from a core run is usually taken for 10-48 hours, depending upon changes in the strain with time and the arrival of the next set of oriented core to be instrumented.

4.2.4. Data Analysis

The orientation of the stress field can be found by determining the orientation of the principal recovered strains. The strain-rosette equations can be found in any elementary rock mechanics or stress analysis book (e.g., Obert and Duvall[31]). Given gage angles of 0°, 45° and 90°, the principal strains in the horizontal plane can be calculated directly from the ASR strains as

$$\varepsilon_1 = \frac{\varepsilon_0 + \varepsilon_{90}}{2} + \frac{\sqrt{2}}{2}\sqrt{(\varepsilon_0 - \varepsilon_{45})^2 + (\varepsilon_{45} - \varepsilon_{90})^2} \tag{4}$$

and (12)

$$\varepsilon_2 = \frac{\varepsilon_0 + \varepsilon_{90}}{2} - \frac{\sqrt{2}}{2}\sqrt{(\varepsilon_0 - \varepsilon_{45})^2 + (\varepsilon_{45} - \varepsilon_{90})^2} \tag{5}$$

where ε_1 and ε_2 are the maximum and minimum principal strains, respectively, assuming that all of the strains are positive (expansion). The directions of the principal strains can be found as

$$\theta = \frac{1}{2}\tan^{-1}\left\{\frac{2\varepsilon_{45} - \varepsilon_0 - \varepsilon_{90}}{\varepsilon_0 - \varepsilon_{90}}\right\} \tag{6}$$

but θ must be inspected carefully to ascertain whether it is the angle from the 0° gage to the maximum or the minimum principal horizontal *in situ* stress.

4.2.4.1 Blanton's Procedure for magnitudes

The stress magnitudes can be estimated using a solution developed by Blanton.[29] His analysis yields a direct calculation of the stresses from the principal strains as

$$\sigma_1 = (\sigma_v - \alpha p)\frac{(1-\nu)\Delta\varepsilon_1 + \nu(\Delta\varepsilon_2 + \Delta\varepsilon_v)}{(1-\nu)\Delta\varepsilon_v + \nu(\Delta\varepsilon_2 + \Delta\varepsilon_1)} + \alpha p \tag{7}$$

and

$$\sigma_2 = (\sigma_v - \alpha p)\frac{(1-\nu)\Delta\varepsilon_2 + \nu(\Delta\varepsilon_1 + \Delta\varepsilon_v)}{(1-\nu)\Delta\varepsilon_v + \nu(\Delta\varepsilon_2 + \Delta\varepsilon_1)} + \alpha p \tag{8}$$

where the $\Delta\varepsilon$ are the change in principal strains between any two times, ν is Poisson's ratio, p is the pore pressure, α is a poroelastic constant, and the subscripts 1 and 2 refer to the maximum and minimum horizontal strain directions, respectively, while v refers to the overburden. Important assumptions for the direct model include (1) linearly viscoelastic behavior, (2) constant Poisson's ratio throughout the relaxation process, (3) step unloading of the *in situ* stresses at the moment of coring, (4) a constant α throughout the process, (5) a vertical overburden stress and wellbore, and (6) isotropic behavior. Note that the strain-rosette equations must be used prior to applying these equations.

4.2.4.2 Warpinski and Teufel method for integrated analysis

The basic idea of the viscoelastic analysis of Warpinski and Teufel[7] is to extract as much information as possible from the entire set of ASR relaxation data. This is achieved by using a model of the time-dependent response, fitting the model to the experimental data, and calculating stress and material property information. The full derivation of the equations are given in Warpinski and Teufel[7] and the computer code to solve these equations are given by Warpinski.[32] The final viscoelastic form of the equations is

$$\varepsilon_r(t) = \left[2\sigma_1\cos^2\theta + 2\sigma_2\sin^2\theta - \sigma_1\sin^2\theta - \sigma_2\cos^2\theta - \sigma_v\right]J_1\left\{1-e^{-t/t_1}\right\} + \left[\sigma_1+\sigma_2+\sigma_v-3p\right]J_2\left\{1-e^{-t/t_2}\right\} \quad (9)$$

$$\varepsilon_v(t) = \left[2\sigma_v-\sigma_1-\sigma_2\right]J_1\left\{1-e^{-t/t_1}\right\} + \left[\sigma_1+\sigma_2+\sigma_v-3p\right]J_2\left\{1-e^{-t/t_2}\right\} \quad (10)$$

In Equations. (9) and (10), ε is the strain in a radial (ε_r) or vertical (ε_v) direction, σ_1 and σ_2 are the maximum and minimum horizontal stresses, respectively, σ_v is the overburden stress, and p is the pore pressure. The parameter J_1 is the distortional creep compliance argument (i.e., equilibrium value) and J_2 is a dilatational creep compliance argument. t_1 and t_2 are relaxational time constants associated with distortional and dilatational creep, respectively, while t is the actual time since the core was cut. The angle θ is the angle in the horizontal plane between a particular gage and a principal stress. This will be discussed in more detail later.

In Equations (9) and (10), the distortional part is the useful part of the relaxation data for stress calculations. This is because pore pressure effects do not enter into the distortional component so that these terms are independent of the pore pressure behavior and effective stress law used.

4.2.4.2.1 Parameter Estimation

For this application, ASR measurements for core from a vertical borehole use three horizontal gages at 0°, 45°, and 90° and a vertical gage. The strains for each of these gages

can be written in terms of Equations. (1) and (2), but with x_i to be determined from the field data. This yields

$$\begin{aligned}
\varepsilon_0(t) &= x_1 - x_2 e^{-t/x_9} - x_{10} e^{-t/x_{11}} \\
\varepsilon_{45}(t) &= x_3 - x_4 e^{-t/x_9} - x_{10} e^{-t/x_{11}} \\
\varepsilon_{90}(t) &= x_5 - x_6 e^{-t/x_9} - x_{10} e^{-t/x_{11}} \\
\varepsilon_v(t) &= x_7 - x_8 e^{-t/x_9} - x_{10} e^{-t/x_{11}}
\end{aligned} \tag{11}$$

by suitable combination of Equations. (9) and (10) for appropriate values of θ. The representations of the x_i will be given in the next section. Note that $x_9 = t_1$ and $x_{11} = t_2$. In addition, geometry considerations require that

$$x_2 + x_6 + x_8 = 0$$

so only 10 parameters are independent. The actual experimental data are then least-squares fit with Equations. (3) and (4) using a modified Levenberg-Marquardt procedure.

4.2.4.2.2 Extracting Stress and Compliance Information

Upon comparing Eq. (11) to Equations. (9 and (10), relations for the x_i can be written, but only four of them (x_2, x_4, x_6, x_8) are useful for determining stress information. These relations are

$$\begin{aligned}
x_2 &= \left[\sigma_1(3\cos^2\theta - 1) + \sigma_2(3\sin^2\theta - 1) - \sigma_v\right] J_1 \\
x_4 &= \left[\sigma_1(1/2 - 3/2\sin 2\theta) + \sigma_2(1/2 + 3/2\sin 2\theta) - \sigma_v\right] J_1 \\
x_6 &= \left[\sigma_1(3\sin^2\theta - 1) + \sigma_2(3\cos^2\theta - 1) - \sigma_v\right] J_1 \\
x_8 &= \left[-\sigma_1 - \sigma_2 + 2\sigma_v\right] J_1
\end{aligned} \tag{12}$$

where θ was replaced by $(\theta + \pi/4)$ for the x_4 term and by $(\theta + \pi/2)$ for the x_6 term. Since $x_2 + x_6 + x_8 = 0$, only three equations are independent. Also, the only information that can be extracted from one of the independent horizontal strain equations is the angle θ. This can be evaluated by

$$\theta = \frac{1}{2}\tan^{-1}\left[\frac{x_2 + x_6 - 2x_4}{x_2 - x_6}\right] \tag{13}$$

but the angle θ must be inspected to check whether it is the angle of maximum stress or the minimum stress with respect to the 0° gage. This is easily checked (usually) by comparing the magnitudes of x_2 and x_6. If x_2 is greater than x_6, then the largest strain (and thus the largest stress) is closer to the 0° gage. Additionally, a negative value of θ indicates that the orientation is between the 0° and 45° gages.

Only two independent equations remain to calculate four unknowns--σ_1, σ_2, σ_v and J_1. σ_v is obtained as the integrated weight of the overburden rocks. The value for σ_2 can be determined with a minifrac or J_1 can be obtained from previous data in the same (or similar) material or possibly in the lab. However, laboratory results may not be feasible because of the irreversibility of the process. Without any previous information on J_1, the optimum arrangement is to conduct a minifrac in tandem with the ASR measurement. Using both the minimum stress from a minifrac and the overburden stress as calibration points yields an accurate estimate of the maximum horizontal stress, particularly if the maximum horizontal stress is the intermediate stress (magnitude less than the overburden).

If a minifrac is conducted, then the other two parameters can be found from

$$\sigma_1 = \frac{x_2(-\sigma_2 + 2\sigma_v) - x_8\left[(3\sin^2\theta - 1)\sigma_2 - \sigma_v\right]}{\text{Det}} \tag{14}$$

and

$$J_1 = \frac{\text{Det}}{(3\sin^2\theta - 1)\sigma_2 - \sigma_v + (3\cos^2\theta - 1)(-\sigma_2 + 2\sigma_v)} \tag{15}$$

with $\text{Det} = x_2 + (3\cos^2\theta - 1)x_8$. If J_1 is known from lab results or previous field data, then

$$\sigma_1 = \frac{\left[\sigma_v + x_2/J_1\right] - (3\sin^2\theta - 1)\left[2\sigma_v - x_8/J_1\right]}{\text{Det}} \tag{16}$$

and

$$\sigma_2 = \frac{(3\cos\sin^2\theta - 1)\left[2\sigma_v - x_8/J_1\right] - \left[\sigma_v + x_2/J_1\right]}{\text{Det}} \tag{17}$$

with $\text{Det} = 3(\cos^2\theta - \sin^2\theta)$.

Finally, the dilatational creep compliance argument, J_2, can be computed from

$$x_{10} = [\sigma_1 + \sigma_2 + \sigma_v - 3p]J_2 \tag{18}$$

In general, this will not be a good estimate of J_2 because other dilatational effects, such as those due to unbalanced drilling, thermal viscoelastic effects, and slow diffusion of pore fluids from the core, should be included in the x_{10} term. Since there is no good way to calculate such effects, J_2 will always be considered an approximate value.

4.2.4.2.3 Calculating Apparent Poisson's Ratio

One interesting result of this model is the ability to estimate the variation of "Poisson's ratio" throughout the relaxation process. This can be written as

$$\nu(t) = \frac{\frac{\nu}{E} + J_1\left[1 - e^{-t/t_1}\right] - J_2\left[1 - e^{-t/t_2}\right]}{\frac{1}{E} + 2J_1\left[1 - e^{-t/t_1}\right] + J_2\left[1 - e^{-t/t_2}\right]} \tag{19}$$

A constant value for Poisson's ratio in this analysis would partition the creep compliances according to

$$J_2 = J_1\left\{\frac{1-2\nu}{1+\nu}\right\} \tag{20}$$

for $t_1 = t_2$.

4.2.5. Field Parameters Affecting ASR Measurements

At least nine different parameters affect the ASR measurements, and in some cases, significantly limit the application of the ASR method in determining *in situ* stresses. Proper understanding of how these parameters influence ASR behavior and the interpretation of ASR results is critical to the successful application of the method, as well as defining the field situations where the method should not be employed.

4.2.5.1 Temperature

Temperature variations contribute thermal strains which must be separated from ASR. Thermal strains can arise from the cooling of cores taken from deep wells or from temperature fluctuations during the field measurements. A correction must be made for the thermal strain contribution to the field data by determining the thermal expansion coefficient of the cores in the directions that strain recovery measurements were made. Thermal measurements on the core can be made in the laboratory after completion of the field test using an environmental chamber. In making the thermal correction one must ascertain if the core has a thermal anisotropy. Experience has shown that some cores can exhibit up to a 20 percent difference in the thermal expansion coefficient for different directions. The highest thermal expansion coefficient occurring in the direction of maximum strain (expansion). Thermal anisotropy is believed to be related to microcrack development in the core during recovery or to an existing, tectonic microcrack fabric in the rock.

4.2.5.2 Dehydration

Dehydration due to improper sealing of the core can occur, particularly in shale, and can result in shrinkage and large contractions of the core. If this occurs the ASR data is invalid.

4.2.5.3 Pore-fluid pressure diffusion.

Pore-fluid pressure diffusion can occur for several hours to days depending on how low the permeability of the rock is and the saturation of the pore fluids and gases in the rock. This process will cause contraction of the core as the internal pressure in the core is depleted. This contraction can be isotropic or anisotropic depending upon whether or not the core has a permeability anisotropy. Contraction due to fluid pressure diffusion is superposed on expansions related to ASR and can significantly affect interpretation of the data, particularly if the diffusion is anisotropic. Contractions in all strain measurement directions for sealed cores (low porosity and permeability shale and siltstone) have been observed when the strains due to pore fluid pressure diffusion were greater than the ASR expansions. For these cores the minimum contraction direction agreed with the maximum expansion direction of higher porosity and permeability cores in the same well, and the maximum stress direction as determined independently by wellbore breakout data.

4.2.5.4 Homogenous recovery deformation

Homogeneous deformation of the core is a basic assumption to infer stress directions from the strain response and to calculate stress magnitudes from the linear viscoelastic constitutive models. If the core is heterogeneous on the scale of the core (for example a conglomerate) the results will reflect local deformation-recovery fields within the core. Accordingly, the technique is not applicable when the rock has been highly deformed or when the core contains complex sedimentary structures.

4.2.5.5 Anisotropy

Anisotropy due to deformation (tectonic) or sedimentary fabrics significantly bias ASR results. If a fabric is present, the total ASR response will be due to a combined effect of the fabric and stress state. Moreover, if the fabric is sufficiently well developed and a strong anisotropy exists, the observed recovery deformation is dominated by the fabric's contribution to ASR and the stress state cannot be determined. Therefore, accurate interpretation of the ASR results for stress directions and magnitudes cannot be made without doing proper complimentary geologic and petrophysical studies of the core and reservoir.

4.2.5.6 Drilling mud-rock interaction

Chemical reactions and invasion of drilling mud into the core can create a "skin effect" on the outside of the core. This interaction can cause unusually large strains when strain measurements are made using the entire diameter cross-section of the core. This commonly occurs in shales which have a high clay content and are cored with water based muds. Strain measurements made using displacement gages mounted from 1 to 2 cm deep in pilot-holes drilled into the core usually eliminate this problem.

4.2.5.7 Residual strains

Several studies have shown that rocks are not perfectly elastic mechanical systems and that strain energy can be stored in the system by an interlocking fabric of anisotropic grains, cement between the grains, or shear stresses along grain boundaries and fractures. Since a rock mass at depth is in equilibrium, we will have a situation where the sum of the internal stresses (grains + cement) in a rock volume is equal to the tractions (i.e. stress state) on the rock element. Accordingly, all processes, natural or induced by man, by which the state of loading is altered will to some degree involve residual stress and stored energy. Thus, when a rock is cored, the material must establish equilibrium, where its internal, residual stress state is balanced with its new stress free boundary. Because of the interlocking nature of the rock fabric, some of the stored strain energy will recover instantaneously, some of it will be recovered over a period of time, and a certain amount will not be recovered as long as the volume of material forms a coherent, inter-reacting fabric. A practical consequence of residual stress and stored energy on *in situ* stress measurements by strain relief methods has been pointed out by several studies. If the measurement sample is equal to or larger than the equilibrium volume that is required by the internal balanced force systems for zero external load, then that part of the measured system that can be assigned to residual stress will be zero. On the other hand, if the measurement sample is smaller than the equilibrium volume, then the residual strain component will be finite and will probably approach some maximum limiting value as the sample size becomes negligible compared with the equilibrium volume.. Accordingly, for ASR measurements, if the scale of the core is smaller than the equilibrium volume, then residual strains could affect ASR behavior.

4.2.5.8 Core recovery time

In doing ASR measurements it is imperative that the core recovery time be sufficiently long relative to core retrieval time so that an adequate representation of the recovery deformation can be measured in order to determine if a linear viscoelastic response is a valid approach to modeling the ASR behavior. Total relaxation times for a variety of rock types ranges from less than 4 hours to over 100 hours. Therefore, core must be retrieved and instrumented as quickly as possible, which means ASR measurements must be done at or near the well site.

4.2.5.9 Accuracy of core orientation survey

The accuracy of stress directions determined using the ASR method can be only as good as the core orientation survey. The quality of the survey can vary for different coring trips within a given well and from one well to another in a field. It is estimated that the accuracy of the survey can vary from 5 degrees to unusable, because of internal rotation of the survey instrument, severe rotation of the scribeline on the core, or poor quality core. In order to improve the reliability of the ASR measurements, it is necessary to make several measurements on cores taken from at least three coring runs within a stratigraphic section. The total error of the ASR measurements and core survey would be included in the mean ± standard deviation of all of these measurements.

4.2.6. Example Applications

4.2.6.1. Mounds Experiment

ASR measurments were made on oriented core in conjunction with the Amoco/DS/Sandia/GRI fracture diagnostics test in the Skinner Sandstone near Mounds, Oklahoma. ASR was one one of seven techniques that were used to determine hydraulic fracture azimuth. Four cores were taken from a depth of approximately 1050 ft. The strain recovery of one of the four instrumented cores is presented in a strain relief-time plot of the temperature corrected vertical and principal horizontal strain magnitudes and the azimuth of the maximum horizontal strain in Figure 27. Strain relief monitoring began 3.1 hours after the core was cut. Expansion occurred in all directions and the recovery rate decreased rapidly with time. All of the relaxation took place with in 20 hours after the core was cut and initial strain recovery began. Beyond this period of relaxation the rock assumed a state of equlibrium and maintained a permanent set.

The anelastic strain recovery measurments of the four oriented cores from the Mounds Test well are summarized in Table 8. All of the cores showed expansion in the principal directions of strain recovery, except the core from depth 1056 ft, which showed contractions in the minimum strain recovery direction. The maxium horizontal strain direction, which corresponds to the maximum horizontal stress direction and the azimuth of a vertical hydraulic fracture, ranged from N86°E+14° to N100°E+9°. The mean orientation of σ_{Hmax} for all four cores is N86°E+14°. The mean orientation of σ_{Hmax} for each coring trip is N75°E+6° and N97°E+3° for coring trips 1 and 2, respectively.

Table 8 Summary of Mounds ASR data

Coring Trip 1

Depth (ft)	ε_V (με)	ε_{Hmax} (με)	ε_{Hmin} (με)	$\varepsilon_{Hmax}/\varepsilon_V$	$\varepsilon_{Hmin}/\varepsilon_V$	$\varepsilon_{Hmax}/\varepsilon_{Hmin}$	Azimuth of ε_{Hmax}
1056	148	126	-88	0.95±.14	-0.49±.15	-0.53±.14	N69°E±8°
1064	214	162	112	0.72±.18	0.39±.19	0.47±.16	N81°E±10°

All data							N75°E±6°

Coring Trip 2

1079	142	136	46	1.02±.23	0.28±.21	0.26±.19	N94°E±9°
1081	174	144	92	0.91±.15	0.45±.17	0.51±.13	N100°E±9°
All data							N97°E±3°

Coring Trips 1 and 2

All data							N86°E±14°

The direction of the principal horizontal strains (stresses) determined from ASR measurements is dependent on the accuracy of the core orientation survey. It should be noted that the error associated with the principal strain directions determined for the two measurements made in each coring trip is much reduced relative to the error of all four measurements. The mean σ_{Hmax} direction of each coring trip has an error of less than 7 degrees, compared to 14 degrees for all four measurements of the two coring trips. This suggests that the error in determining principal horizontal stress directions is due in part to the accuracy of the core orientation survey, and that the survey may be a limiting factor in the quality of the ASR or any core based method.

Table 9 summarizes the results of all seven techniques used to detemine the maxium horizontal stress direction and hydraulic fracture azimuth at the Mounds site. There was good agreement between the borehole logs, tiltmeter, and ASR measurements, showing a maximum horizontal stress direction of essentially east-west.

Table 9 Summary of Mounds azimuth results

Procedure	Azimuth
Borehole Logs - Downhole Television	N95°E
Tiltmeters	N95°E
Core Analysis - Anelastic Strain Recovery	N86°E
Core Analysis - DSCA and DWVA	N30°W
Borehole Seismic Monitoring	N70°E

4.2.6.2 Multiwell Experiment

The most extensive ASR data set is from the Multiwell Experiment site in the Piceance Basin of Colorado. ASR measurements were made on sandstone and mudstone cores that were taken from depths of about 4600 to 8150 feet. The relaxation behavior of these two lithogies is very different and are shown in Figures 28 and 29. The actual ASR data for the vertical and three horizontal strains taken at one hour intervals and the calculated strain-

history fit of the data using the Warpinski and Teufel model are given. Using this model the total time-dependent strain that the core has experienced can be estimated. Accordingly, the format in Figures 28 and 29 do not imply that the cores experienced neagative strains in early times. For convience the original form of the data is preserved (i.e., all strains started at zero at the time the core is instrumented), and the early negative strains represent the anelastic strains that the core experienced before being instrumented. For both cores the data quality is excellent and the theoretical viscoelastic strain-history model fits the measured response well.

For all of the MWX sandstone cores that were instrumented the horizontal strains were anisotropic and principal horizontal strain magnitudes and orientations could be determined for each core. In sharp contrast, the mudstone cores exhibited horizontally isotropic strain behavior and there was no principal horizontal strain direction, and by implication no preferred principal horizontal stress direction in the mudstone horizons at this site.

The maximum horizontal strain direction as a function of depth for sanstone cores from MWX-1, 2, and 3 wells is shown in Figure 30. Only sandstone results are shown, because the mudstones have no preferred orientation. The scatter in the ASR data is typical of a large data set of ASR measurements and is the result of several parameters, but primarily is due to the accuracy of the core orientation survey and core heterogeneities. The average orientation for each of the three wells is given in Table 10.

Table 10 Summary of MWX ASR results by well

Well	Number of Measurements	Stress Azimuth
MWX-1	28	N81°W±13°
MWX-2	18	N70°W±14°
MWX-3	27	N73°W±16°
All data	73	N75°W±15°

In general the maximum horizontal stress direction is essentially east-west, but a 30 degree clockwise rotation of the stress field apparently occurs with depth. This rotation has been interpreted to be a result of severe topography surrounding the MWX site.

Figure 30 also shows data for sandstone cores from each of the wells that had well developed tectonic microcrack fabric. In these cores the strain response associated with the pre-existing fabric and the resulting mechanical anisotropy dominated the total strain respones of the core. Thus, the maximum strain recovery directions in these cores do not reflect the present *in situ* stress state. It is interesting to note that the maximum horizontal strain directions for cores with a tectonic microcrack fabric is about 90 degrees to the cores

with no fabric, as shown in Figure 31. Tectonic microcracks and regional extension fractures typically are oriented parallel to the maxium horizontal stress.

For magnitudes, it is necessary to implement one of the viscoelastic models. Figure 32 shows both raw data and the data with the theoretical fit of the model developed by Warpinski and Teufel. Fitting the theoretical model has the advantage of determining an azimuth that is a best fit of all of the data, but it can also be used for magnitude estimates if the overburden stress is known (determined from a density log) and the minimum stress is known from a microfrac. In this example, both the minimum and maximum stress were estimated from an open-hole microfrac (Teufel and Warpinski,[33]) so good comparative data are available. The parameters estimated from the fit of the data are given in Table 11.

Table 11 ASR model fit results

Parameter	Value
x_1	176.7 με
x_2	35.6 με
x_3	148.3 με
x_4	-26.8 με
x_5	94.2 με
x_6	-130.3 με
x_7	211.2 με
x_8	94.7 με
x_9	9.56 hr
x_{10}	278.1 με
x_{11}	11.75 hr
θ	-6.95°
J_1	0.069×10^{-6} psi^{-1}
σ_{Hmax}	7620 psi

The value for σ_{Hmax} is in good agreement with the measured value of 7600 psi. For this calculation, σ_V was 7900 psi and σ_{Hmin} was 6800 psi. Using Blanton's model, with ν=0.2 and α=1.0, σ_{Hmin} is estimated to be 7150 psi and σ_{Hmax} is estimated to be 7700 psi. In both cases the agreement is relatively good. With sufficiently accurate input data, ASR can provide a good estimate of the *in situ* stresses.

4.2.6.3 SFE-4

Examples from the SFE-4 experiment show some of the difficulties and problems that can develop using ASR. Figure 33 shows the results for ASR-3, a core extracted from 7313 ft. In this case, only three horizontal gages were used (no vertical), and all gages showed

contraction. Contraction often occurs in tight rocks where pore pressure bleeds off very slowly, and as it does so, the core actually shrinks. This shrinkage is often greater than the relaxation expansion, but in a homogeneous rock it should occur the same amount in all directions. Therefore, the differential contraction is still a meaningful record of the differential relaxation behavior, and these results can be used for orientation. In this particular example, the orientation of stress field is N50°E, which is in good agreement with the NE orientation obtained from other techniques.

Figure 34 shows the results for ASR-7, taken from 7368 ft. In this example, three of the four gages show a contraction, but in fact the 90° gage contracts throughout most of the recording time. The initial sharp rise in the 90° response is probably due to a thermal or drying effect which is over in 2-3 hours. Afterwards, this orientation responds similarly to the other orientations. In cases such as this, the first three hours of data should be subtracted from the data set, and the data should be reanalyzed. The stress orientation from this sample is N46°E, but there is low confidence on this azimuth because the strain recoveries are very small. A temperature change of 2°F (a typical change in an ASR test) will induce about 12 με of recovery in a core sample, so strain-recovery data should be at least four times this amount to obtain data in which there is any confidence (application of Equation 6). In this test, the largest horizontal response is about 35 με and the other two are much less. It is recommended that data having less than 50 με recovery be used very carefully, if at all.

An example of an ASR test in which the response has nothing to do with relaxation is shown in Figure 35. This test (ASR-19) was taken from a depth of 7488 ft in a mudstone. Relaxation behavior should be exponential in nature, as shown in previous examples. This case has a bi-linear response, that is, two nearly straight-line slopes before and after 12 hours. Although the response is large, there is no doubt that this test is due to the rock fabric and not to relaxation behavior. In a later examination of the core, it was found that there were numerous planes of weakness in the core that were probably responsible for this behavior. Data such as these should be discarded.

An interesting summary of all of the data taken at SFE-4 are shown in the rose diagram of Figure 36. Originally, all of the SFE-4 data were reported by the ASR contractor, giving an orientation response shown by the outlined results. Although the azimuth is primarily NE, there are large numbers of data in all directions and it would be difficult to predict the stress azimuth with certainty. After a close inspection of the results for fabric (seen in core after the test), low strain recoveries (anything less than 50 με were discarded), non-functioning gages (one tests was reported in which one of the gages was not working) and early time thermal anomalies, the only results that could pass a reliability criterion are those shown shaded. While there is still a large amount of uncertainty in the results, the NE pattern is much clearer. ASR data should always be carefully scrutinized by the operator.

4.3 Differential Strain Curve Analysis and Differential Wave Velocity Analysis

Differential Stain Curve Analysis (DSCA) is a laboratory technique that estimates stress orientation and magnitudes by comparing the relative strain induced in different directions with the application of confining pressure (Strickland and Ren,[34] Ren and Roegiers.[35]) As discussed earlier, and shown by Nur and Simmons,[17] the relaxation microcracks have a significant effect on the various rock moduli, and a preferentially oriented set of microcracks will yield different moduli in different orientations, at least for low stress values (until the cracks close). This differential strain behavior is used to extract the stress information. Application of DSCA is straightforward for estimates of the stress orientation, and will be considered first. Differential Wave Velocity Analysis (DWVA) (Ren and Hudson[36]) follows a similar development to DSCA and will be considered together with DSCA. Magnitudes will be discussed later.

4.3.1. Concept

The strain response in one direction due to the application of a hydrostatic confining stress on a core sample with a population of preferentially oriented microcracks is shown in Figure 37. At low confining stresses, the rock is highly compliant because of the existence of open or partially open microcracks. As confining stress is increased, the cracks begin to totally close (the transition zone), and eventually only the response of the matrix rock remains (low compliance or high modulus). The slope of the initial strain behavior has two components, that of the microcracks (denoted ε') and that of the matrix (denoted β). By subtracting out the matrix portion, β, as determined from the high confining-stress conditions, from the total, θ, the microcrack contribution, ε' can be obtained directly. Of course, if the matrix is homogeneous and isotropic, there is no need to subtract it out for orientation purposes.

These types of measurements are made in multiple orientations, and the differential behavior is used to deduce relative differences in the strain response. An example of the differential response of three strain gages is shown in Figure 38. These types of data would be obtained from a 2-D analysis (e.g., assuming the wellbore is vertical and is aligned with the overburden), from which only three gages are needed to determine orientation in the plane of interest. A full 3-D analysis would use a minimum of 6 gages. Assuming the microcracks are relaxation and not fabric, then two assumptions are needed in order to use this information for stress purposes. First, the cracks must be proportional volumetrically to the corresponding *in situ* stress. This assumption was verified by Teufel[8] using acoustic emissions. Second, by reversing the expansion of the sample by subjecting it to hydrostatic pressure, the contraction of the rock in any specific direction will be analogous to the original strain in that direction. This last assumption is not strictly true, as the strain relaxation process is irreversible (as evident from the fact that it always takes more stress to close the microcracks than was originally on the rock at depth), but it appears to be sufficiently applicable that the technique provides good results for many conditions.

DWVA follows a similar development, except that the acoustic velocity of the material is measured, rather than the strain. Differences in the acoustic travel time between low-stress (cracks plus matrix) and high-stress (matrix alone) conditions for several orientations are compared. One additional assumption that must be made for DWVA is that the velocity field is a tensor field. However, Sayer's[22] analysis (Equation. 3) shows that a microcrack population will not have tensor properties if the $\cos(4\theta)$ multiplier, B, is significant. As shown in some of the CVA examples, B is usually small, but cases can arise where it is significant.

4.3.2. Core Preparation and Data Acquisition

As with the other strain-relaxation techniques, the first step to obtaining high-quality data is to choose core specimens with minimal bedding, fractures, or other signs of fabric. Closure of shaly bedding planes, natural fractures, or vugs will typically overwhelm any microcrack behavior.

Many different specimen geometries can be used for DSCA, but Strickland and Ren[34] and Ren and Roegiers[35] cut a cubed specimen from the rock core, and instrument three sides with strain gage rosettes, as shown in Figure 39. Machining must be done carefully (to avoid creating more cracks) and precisely so that the corners are square. These authors also add a fourth strain gage (shown in Figure 39) for redundancy and error analysis. The sample is then coated with a jacket material to exclude pressure from the internal pore space of the rock.

The sample is incrementally pressurized and strain gage data are taken using a standard bridge. Other than a pressure vessel with feed-throughs, no additional sophisticated equipment are needed. However, Ren and Roegiers[35] suggest using a fused silica sample as a reference for avoiding experimental errors due to temperature or pressure.

For DWVA, the core specimen is cut into a dodecahexahedron (18 sides), as shown in Figure 40, and each pair of parallel sides are fitted with transducers (total of 9 measurements). If the material is isotropic, testing is conducted on a benchtop with no confining stress. If isotropy cannot be assumed, the sample must be jacketed, placed in a pressure vessel, and incrementally loaded while data is obtained. An oscilloscope is used to measure the travel time across the sample.

4.3.3. Data Analysis

Orientation data analysis for both DSCA and DWVA is similar, being simply the manipulation of a tensor field. The easiest case to apply is the 2-D analysis, where three strains, ε'_1, ε'_2, and ε'_3, are oriented 45° apart from each other. The orientation of the principal strain axes are then given by

$$\theta_{min|max} = \frac{1}{2}\tan^{-1}\left\{\frac{2\varepsilon_2' - \varepsilon_1' - \varepsilon_3'}{\varepsilon_1' - \varepsilon_3'}\right\}, \tag{21}$$

or if velocity data are used, the ε'_i are replaced by the inverse of the Δt_i. $\theta_{min|max}$ is an angle that could be either the maximum or minimum principal strain orientation relative to the orientation of ε'_1, and which one it is can be deduced by inspection, or by a relative comparison of the strains. For example, if ε'_1 is the largest strain of the three, then the angle, θ, is the orientation of the maximum strain orientation (or vice versa if it is the smallest strain). If θ is an intermediate strain, then it becomes necessary to compare the other two strains. The principal strains are given by

$$\varepsilon_p', \varepsilon_q' = \frac{\varepsilon_1' + \varepsilon_3'}{2} \pm \frac{\sqrt{2}}{2}\sqrt{(\varepsilon_1' - \varepsilon_2')^2 + (\varepsilon_2' - \varepsilon_3')^2} \tag{22}$$

For the 3-D case, the 2nd order tensor transformation rules apply. The analysis is most easily accomplished by defining

$$\begin{aligned}
\varepsilon_x &= \varepsilon_1' \\
\varepsilon_y &= \varepsilon_3' \\
\varepsilon_z &= \varepsilon_6' \\
\gamma_{xy} &= 2\varepsilon_2' - \varepsilon_1' - \varepsilon_3' \\
\gamma_{yz} &= 2\varepsilon_5' - \varepsilon_4' - \varepsilon_6' \\
\gamma_{xz} &= 2\varepsilon_8' - \varepsilon_7' - \varepsilon_9'
\end{aligned} \tag{23}$$

Note that there are several redundant gages which can be averaged together or used to develop statistics on the process. The principal strains are found by solving

$$\begin{aligned}
&\varepsilon_i^{\,3} - (\varepsilon_x + \varepsilon_y + \varepsilon_z)\varepsilon_i^{\,2} + (\varepsilon_x\varepsilon_y + \varepsilon_y\varepsilon_z + \varepsilon_x\varepsilon_z - \gamma_{xy}^2/4 - \gamma_{yz}^2/4 - \gamma_{xz}^2/4)\varepsilon_i' \\
&-(\varepsilon_x\varepsilon_y\varepsilon_z - \varepsilon_x\gamma_{yz}^2/4 - \varepsilon_y\gamma_{xz}^2/4 - \varepsilon_z\gamma_{xy}^2/4 + \gamma_{yz}^2\gamma_{xz}^2\gamma_{xy}^2/4) = 0
\end{aligned} \tag{24}$$

where the ε_i are the three principal strains. Once the ε_i are known, the direction cosines are found from

$$l = \frac{A_i}{\sqrt{A_i^2 + B_i^2 + C_i^2}}$$
$$m = \frac{B_i}{\sqrt{A_i^2 + B_i^2 + C_i^2}} \qquad (25)$$
$$n = \frac{C_i}{\sqrt{A_i^2 + B_i^2 + C_i^2}}$$

where

$$A_i = (\varepsilon_y - \varepsilon_i)(\varepsilon_z - \varepsilon_i) - \gamma_{zy}\gamma_{yz}/4$$
$$B_i = \gamma_{zy}\gamma_{xz}/4 - \gamma_{xy}/2(\varepsilon_z - \varepsilon_i) \qquad (26)$$
$$C_i = \gamma_{xy}\gamma_{yz}/4 - \gamma_{xz}/2(\varepsilon_y - \varepsilon_i)$$

As before, the ε are replaced with $1/\Delta t$ for DWVA analyses. Thus, successful application of DSCA or DWVA can provide an estimate of the orientation of the stress field

4.3.4. Analysis for Stress Magnitudes

DSCA and DWVA have been used for the determination of magnitudes, but the theory behind this procedure is still unclear. The fundamental assumption for obtaining magnitudes is that the ratio of the principal strains, or the principal velocities, is directly proportional to the effective *in situ* stress ratio, much as it would be for an overcore technique. Since microcracks clearly exhibit hysteresis, and pressure in excess of the original *in situ* stress is required to close the microcracks, it is likely that this assumption will not always hold. Nevertheless, DSCA and DWVA have been shown to yield good estimates of the stresses in many applications.

Given principal *in situ* stresses σ_2 and σ_3 in the horizontal plane and σ_1 in the vertical (overburden) plane, then a 2-D analysis (Ren and Roegiers[35]) yields

$$\frac{\varepsilon_3 + \nu\varepsilon_1}{\varepsilon_1 + \nu\varepsilon_3} = \frac{(\sigma_3 - \alpha p)}{(\sigma_1 - \alpha p)}, \qquad (27)$$

with a similar equation for the ε_2 ratio. If the overburden stress and pore pressure are known, and if the poro-elastic parameter α can be determined, then estimates of the stress magnitudes can be readily made.

For a 3-D transversely anisotropic situation, Ren and Roegiers give the ratios as

$$(\sigma_1 - \alpha p):(\sigma_2 - \alpha p):(\sigma_3 - \alpha p) = (C_{11}\varepsilon_1 + C_{12}\varepsilon_2 + C_{13}\varepsilon_3): (C_{12}\varepsilon_1 + C_{11}\varepsilon_2 + C_{13}\varepsilon_3):(C_{13}\varepsilon_1 + C_{13}\varepsilon_2 + C_{33}\varepsilon_3) \quad (28)$$

where

$$C_{11} = \frac{E_1(1 - \nu_{31}\nu_{13})}{(1+\nu_{12})(1 - \nu_{12} - 2\nu_{31}\nu_{13})}$$

$$C_{12} = \frac{E_1(\nu_{12} + \nu_{31}\nu_{13})}{(1+\nu_{12})(1 - \nu_{12} - 2\nu_{31}\nu_{13})} \quad (29)$$

$$C_{13} = \frac{E_3\nu_{13}}{(1 - \nu_{12} - 2\nu_{31}\nu_{13})}$$

$$C_{33} = \frac{E_3(1 - \nu_{12})}{(1 - \nu_{12} - 2\nu_{31}\nu_{13})}$$

4.3.5. Application Examples

4.3.5.1 MWX

A simple example of the 2-D analysis can be shown using data from an MWX core taken from a depth of 6520 ft in a fine-grained, homogeneous sandstone. This particular example was not cubed, but rather three horizontal plugs were taken at orientation 45° apart, and a strain gage along the axis of each plug recorded the strain for each orientation. Figure 41 shows the strain data taken at increments of 1000 psi and Table 12 gives the data.

Table 12 MWX-6520 DSCA data, 2-D analysis

STRESS	ε_1	ε_2	ε_3
0	0	0	0
1000	0.1359	0.1585	0.0928
2000	0.1758	0.2042	0.1219
3000	0.2148	0.2490	0.1506
4000	0.2459	0.2831	0.1741
5000	0.2698	0.3097	0.1942
6000	0.2886	0.3297	0.2099
7000	0.30423	0.3467	0.2234
8000	0.3188	0.3624	0.2359

A quick calculation of the stress orientation can be made by considering the strain slope from 1000-2000 psi to represent the cracks plus matrix and the strain slope from 7000-8000 psi to represent the matrix material. Table 13 gives these θ_i and β_i, as well as the resultant ε'_i. Using the three ε'_i in equation 4, the angle is -32° which corresponds to an orientation of N74°W, in agreement with the stress orientation from other techniques.

Table 13 MWX-6520 DSCA strain slopes

	1	2	3
θ (1000-2000 psi)	0.0457	0.0291	0.0400
β (7000-8000 psi)	0.0157	0.0125	0.0146
$\varepsilon' = \theta - \beta$	0.0300	0.0166	0.0254

Strickland and Ren[34] and Ren and Roegiers[35] take considerably more data and it is used to develop polar plots, as shown in Figure 42. For this MWX fluvial sandstone at 5727.5 ft, the maximum stress is approximately east-west, in general agreement with other stress techniques.

Figure 43 shows a comparison of DSCA measurements with several other stress orientation techniques across a depth interval from 4500-7600 ft at MWX. As can be seen, the DSCA orientations agree well with all other techniques. The largest source of error in the core-based techniques is due to the orientation survey. Figure 44 shows a comparison of several techniques used to measure or estimate stress magnitudes. Of particular interest in this figure are the minimum stress data, as they can be compared with direct measurements using microfracs. In the coastal zone from 6400-6500 ft, there are six DSCA tests in the sandstone, and five of those tests provide an accurate estimate of the minimum stress. In the paludal zone between 7100-7200 ft, there is one DSCA test in a siltstone which gave a minimum stress magnitude that was approximately 900 psi lower than the measured value in an adjacent sandstone. Other lithologies (e.g., mudstone, shale, siltstone, coal) generally have stresses that are greater than or equal to the stress in the sandstone.

4.3.6. Discussion

DSCA and DWVA are techniques that can be used to determine the orientation of the *in situ* stress field by performing relatively simple laboratory measurements. Under some conditions, it is also possible to make estimates of the magnitudes of the stress. Like all other relaxation techniques, DSCA and DWVA will not provide accurate results if rock fabric is present. The technique is very useful for studying archived core and is relatively inexpensive. Some problems may arise with mudstones and shales if aging, drying, or drilling-fluid interactions alter the material.

Simple 2-D DSCA tests can be easily conducted in the lab by cutting oriented plugs, putting axial strain gages on the samples, jacketing the plugs, and stressing in a pressure vessel. If full cubical (DSCA) or dodecahexahedron (DWVA) samples are used, the procedure and analysis become somewhat more complicated, but the advantage of enhanced statistics more than compensates for the complexity.

4.4 Kaiser Effect

4.4.1. Concept

The Kaiser-effect stress-measurement technique holds promise for both stress azimuth and magnitudes. The Kaiser effect is the phenomenon whereby acoustic emissions are stress-history dependent, such that acoustic emissions will not be observed in most rocks until the rock is loaded to the peak stress attained in a previous load cycle (Holcomb[37,38]). For example, if a rock is placed in a load frame and uniaxially loaded to 10,000 psi, there would likely be an increasing rate of acoustic emissions throughout the loading cycle. However, if the sample is unloaded and then restressed uniaxially, very few emissions would occur until the stress reached the previous maximum of 10,000 psi, at which point emissions would become numerous. Because most rocks exhibit this behavior, the Kaiser effect has been proposed as a technique for measuring both stress orientation and magnitude. The advantage of such a technique is that it is a direct stress measurement; there is no need to measure strains or velocity and then convert to stress through some material model.

The technique is conducted by attaching piezo-electric transducers to a sample, loading the sample uniaxially, and recording the acoustic emissions (Momayez and Hassani[39]). This procedure is performed on plug samples taken at different orientations, so that principal stresses and the principal stress orientation can be calculated (e.g., the rosette equations). Such an approach is very straightforward and yields a direct measurement of the stresses.

Although there is considerable promise, there are still questions about the accuracy reliability and theoretical basis of the Kaiser effect. Holcomb[37,38] has shown that for rock stresses in the laboratory, the Kaiser effect responds to the full 3-D stress state This is analogous to the observation that rock failure is dependent on the confining stresses. Therefore, it is not clear how uniaxial tests can provide accurate stress data. One possibility, proposed by Holcomb,[37] is that the Kaiser effect measured by most researchers is a different effect than the failure-Kaiser effect seen in the laboratory, and a good possibility for the stress-Kaiser effect is acoustic emissions formed by closing of microcracks. In such a scenario, acoustic emissions would occur due to asperity crushing during crack closure. Considerably more research needs to be conducted before this can be considered a reliable technique, but it does offer great promise for the future.

4.4.2. Core Preparation

Core preparation for this technique is simple and only requires that oriented plugs be taken from a core sample. For a 2-D analysis (say stresses in a horizontal plane), only three plugs are required, and these can be taken at any conventional rosette angles (45° or 60° spacing). For a semi-3-D analysis, where the overburden stress is known (or assumed) to be vertical, then three horizontal and one vertical core are required. For a full 3-D analysis, six plugs at six different orientations are needed.

4.4.3. Data Acquisition Technique

The standard technique for conducting these tests is to place the plug sample in a load frame (unconfined), with care taken to isolate the sample from apparatus-induced noise (Momayez and Hassani[39]). A piezo-electric transducer is attached to the sample and signal-conditioning instrumentation. The sample is loaded uniaxially at a constant displacement or load rate and emissions are monitored and counted. Various graphical or numerical techniques can be employed to determine the point where the emissions begin, and error bars on this point can be determined. By using several samples in each direction, good statistics can be developed for error analyses.

The principal stress and the stress orientations can be determined using the same equations developed earlier for the strain techniques.

For the 2-D analysis, where three stresses, σ_X, σ_Y, and σ_Z, are oriented 45° apart from each other, the orientation of the principal strain axes are then given by

$$\theta_{min|max} = \frac{1}{2}\tan^{-1}\left\{\frac{2\sigma_y - \sigma_x - \sigma_z}{\sigma_x - \sigma_z}\right\}. \qquad (30)$$

$\theta_{min|max}$ is an angle that could be either the maximum or minimum principal stresses orientation relative to the orientation of σ_X, and which one it is can be deduced by inspection, or by a relative comparison of the stresses. The principal stresses are given by

$$\sigma_p, \sigma_q = \frac{\sigma_x + \sigma_z}{2} \pm \frac{\sqrt{2}}{2}\sqrt{(\sigma_x - \sigma_y)^2 + (\sigma_y - \sigma_z)^2} \qquad (31)$$

For the 3-D case, the 2nd order tensor transformation rules apply, and the form used for determining the principal stresses and the orientations depend on the orientations at which the sample is loaded. Several techniques can be used for this purpose (Obert and Duvall[32]).

4.4.4. Application Example

4.4.4.1 Atomic Energy of Canada Underground Research Lab

The best example of use of the Kaiser effect is from Momayez and Hassani,[39] who analyzed stresses at the Atomic Energy of Canada underground research lab site. No actual curves were shown in this paper, but inferred horizontal stresses from three orientations are given in Table 14. From these results, the principal stresses, using Equation 31, are

calculated. The Kaiser-effect stresses and stresses obtained from several different techniques are compared in Table 15.

Table 14 Kaiser effect stress data

Borehole	Dip Angle (deg)	Samples Tested	Estimated Stress (psi)	Standard Deviation (psi)
1	90	10	1591	485
2	45	12	4914	933
3	135	12	5559	678

Table 15 Principal stresses from Kaiser effect

Stress Axis	Major (σ_1)	Minor (σ_3)
Kaiser Effect	8850 ± 870 psi	1600 ±580 psi
Other Techniques	7980 ± 730 psi	2030 ± 150 psi

No comparison of the stress orientation was given for this study.

While there is general agreement between the various stress measurement techniques, the uncertainties and the differences in the different results suggest that the Kaiser effect needs additional development before it can be routinely and confidently used for stress data in petroleum applications.

4.4.5. Discussion

While there have been no definitive studies, the potential of such a technique is great, as it offers a direct measurement of stress, rather than an indirect one (i.e., strain or velocity). The laboratory setup is somewhat more complicated than other lab techniques (although simpler than DSCA or DWVA), as a load frame and piezo-electric transducers are required, but the possibility of obtaining a direct measurement technique makes this investment worthwhile. At this time, however, it is not clear what problems or disadvantages may arise. Further research work is needed to develop a better understanding of the basic physics.

4.5 Strength Anisotropy Tests

4.5.1. Concept

Strength anisotropy tests have been found to be useful for determining the stress azimuth from oriented core. The concept was proposed by Logan and Teufel[13] who used both point-load and Brazil tests. Based upon tests conducted in the Wattenburg field, it was found that the strength anisotropy correlated with the hydraulic fracture azimuth. Gregg[40] also used point-load and Brazil tests to determine the rock microstructure, but in attempting to relate the microstructure to stress azimuth, he failed to account for the differences between relaxation microcracks and other fabric. As a result, his analysis gave inconsistent results. Laubach et al.[23] used point-load testing to determine stress orientations in the Frontier formation, but found a bimodal distribution of strength.

Point-load testing,[41] being the easier procedure, is the one recommended for such tests. It is performed by applying a hemispherical indenter to the top and bottom of a core disk and loading the indenter until the rock fails. The pattern of failure is used to deduce the microstructural fabric of the rock. If the microstructure is due entirely to relaxation microcracks, then the induced fractures will align with the microcracks and their orientation will be perpendicular to the maximum stress. If the microstructure is due to tectonic microcracks, then the induced fractures will align with these and thus will not be perpendicular to the maximum stress. As with all of the other core-based techniques, it is important to know if fabric is present.

Brazil tests consist of a compression of a core disk across its diameter until failure occurs. This test can be used for strength anisotropy, but was generally used by researchers to check the point-load results. It is not clear that this test would provide any different data than the point-load test.

4.5.2. Core Preparation

Core preparation for a point-load test requires that a circular disk with parallel ends be cut from the core. To obtain the orientation of the maximum horizontal stress, this disk must have its parallel surfaces in the horizontal plane. The thickness of the disk is not an important parameter, but generally it is less than 0.5 in. Care must be taken to keep track of the orientation of the sample when it is being prepared.

4.5.3. Data Acquisition

To obtain the point-load response, the core disk is placed in a load frame between two hemisperical indenters, as shown in Figure 45. The sample is loaded until failure, removed from the frame, and examined for fracture orientations. Moderate load rates should be used to minimize any dynamic effects (Clift et al.[41] use one pound per second).

4.5.4. Data Analysis

Data analysis consists of measuring the orientations of fractures within the core disks for several samples and obtaining a statistical average and standard deviation of the orientations. Since there is no method to determine if fabric is dominating the response, point-load tests should be performed in tandem with CVA or petrographic examination.

4.5.5. Example Application

The best example of the correlation of point-load data with other results can be found in Gregg's[40] analysis of Appalachian data. A comparison of orientations from CVA and point-load testing from samples taken in several states is shown in Table 16. These results show a good correlation between the two types of tests.

Table 16 Comparison of CVA with point-load tests

Location	CVA azimuth	Point Load azimuth
KY-1	30	30
KY-2	60	60
KY-3	30-60	60
KY-4	60	90,120
NY-1	60	60
NY-2	–	90
NY-3	150	120,150
OH-1	0,90	0,90
OH-2	60	60
OH-3	120	60
OH-4	90	90
OH-5	30	60
OH-6	90	30
OH-7	90	120
OH-8	–	90,120
OH-9	90	90-120
OH-10	120	–
OH-11	60	60
OH-12	0	0
PA-1	60	60
PA-2	30	30
PA-3	120	90
PA-4	30	30
PA-5	30	30
TN-1	60	30
VA-1	60	30
WV-1	0	30
WV-2	30,60	60,150
WV-3	60	60
WV-4	45	45
WV-5	60	60
WV-6	30	30
WV-7	30	30

4.5.6. Discussion

Point load tests are a good technique for determining strength anisotropy in a core sample, and they are fast and easy to conduct. Some machining of the core is required, but the apparatus is simple and so is the analysis. The major difficulty with this technique is that there is no way to tell if the strength anisotropy is due to relaxation microcracks or due to other fabric, as all resulting fractures will look similar. Thus, this technique should never be used alone.

This technique is simple and cheap, and large numbers of samples can be processed. This is an excellent technique for developing statistics based on a large number of samples. However, it should not be used on non-homogeneous samples, as bedding and other types of fabric can mask the desired effect.

4.6 Petrographic Examination of Microcracks

4.6.1. Concept

One of most valuable techniques for assessing the microstructure of a core is to perform petrographic analyses on thin sections, and such an examination will often provide information on the stress azimuth and rock fabric. Many structural features, including those lumped into the category of "fabric", can be seen under a microscope. Standard blue-dye thin sections can often be used to detect important features, but techniques using fluorescent-dye epoxies have made detection even easier. Gies[42] and Soeder[43] describe the process and usefulness of this technique, and Walls et al.[20] show how the technique can be used to obtain stress information and how well it compares with CVA and directional permeability measurements.

Petrographic examination can often be used to distinguish between relaxation microcracks and tectonic microcracks. Relaxation microcracks are primarily intergranular, and they typically have uniform widths, or at least monotonically varying widths. Tectonic microcracks can be either intergranular or intragranular, and their widths typically are quite variable, presumably because of solution processes that have occurred since the cracks were created. Thus, an experienced examiner can often distinguish between different types of cracks, and petrographic examination becomes a valuable technique for deducing fabric as well as stress orientation.

4.6.2. Core Preparation

Thin sections are prepared in the same manner as with a standard blue-dye system, except that the blue dye is replaced by a fluorescent dye, usually rhodamine B. The same epoxy is used in both cases, and the thin section must also be oriented if stress azimuth or fracture azimuth is to be obtained. The thin section is typically cut to a thickness of about 30 microns.

4.6.3. Data Acquisition

The primary difference in using fluorescent epoxy rather than blue dye is the need for an incident light source to stimulate autofluorescence. Filters are needed so that the dye can be made to fluoresce in a desired color. Typically a green filter is used, which causes the dye to fluoresce in a bright red or orange color. While the porosity fluoresces in a chosen color, all non-porous material remains black. A primary benefit of this technique is that the microstructure becomes more apparent (brighter colors, more contrast) as the magnification increases.

Microfractures and other microporosity can be easily seen through the microscope without the distracting effects of other features within the grains. Figure 46 shows an example of a 200x magnification of a relaxation microcrack connecting two pores. Figure 47 shows an

example of a 200x microcrack that is interpreted as being a tectonic microcrack because of its variable width. As mentioned before, some expertise is needed to make decisions on what features are relaxation and what features are tectonic.

4.6.4. Data Analysis

Orientations of all of these features are recorded for each thin section and rose diagrams of the resulting azimuths are created. If the microcracks are relaxation, then the stress azimuth is normal to the preferred crack direction. If the microcracks are not relaxation, then nothing can be said about the stress direction, but the information can be used as a diagnostic on whether other core-based techniques are providing reliable information.

4.6.5. Example Application

4.6.5.1 Multiwell Experiment

An example application of this technique comes from the Multiwell experiment discussed in earlier examples. Figure 46, the relaxation microcrack, comes from MWX at a depth of 6459 ft. Figure 48 shows the rose diagram of all microcracks at depth, and it can be seen that there is a preferred strike of N35°E, corresponding to a stress orientation of N55°W. This orientation is only about 10° different from the average strike of N65°W taken from the average of various other techniques.

On the other hand, the microcrack in Figure 47 comes from a depth of 5490 ft where there is no preferred orientation, as shown in Figure 49. In this example, the microcracks are aligned with the *in situ* stress orientation and they are clearly not relaxation in origin. However, this information is important because it suggests that other core-based techniques may not give reliable results in this interval.

4.6.5.2 SFE-4

Fluorescent microscopy was performed on 9 samples from SFE-4 in the Frontier formation. Of the nine tests, seven showed a preferred stress orientation of NNE, while the other two were due east and NNW, respectively. Figure 50 shows an example of the microcrack distributions found in a sample at 7384 ft where 11 relaxation microcracks were observed. In the same core, 16 tectonic cracks were noted, so it is obviously important to distinguish between the two types. Relaxation cracks should be considered a population with some cracks in all directions, but more in the preferred direction. In this case, the preferred crack orientation is slightly north of west, so the inferred stress azimuth is slightly east of north.

Figure 51 shows a similar pattern, but only three relaxation microcracks were observed. The orientation is again NNE, which happens to be aligned with the tectonic microcrack orientation.

4.6.6. Discussion

Petrographic examination of microcracks is a valuable technique for determining stress orientation and the possible effect of tectonic microcracks. If the analyst can distinguish between the two types of cracks, then this technique provides a valuable diagnostic on all other core-based measurements.

The technique is not expensive, as thin sections are cheap to make and petrographic microscopes are abundant. However, special equipment is needed for the incident light feature with filters. A considerable amount of time is also required to examine the thin sections and determine which features are relevant.

This technique should be routinely used as a diagnostic of fabric whenever there is any question about the reliability of other core-based measurements. It is the only technique that can immediately determine if sub-visible fabric is affecting the data.

4.7 Over-Coring of Archived Core

4.7.1. Concept

Overcoring is a technique that can be used to determine the stress azimuth and may eventually be used to determine stress magnitudes as well. The concept of over-coring of archived core is one that has a long history dealing with the development of a theory for residual stresses (or strains) found in rocks. Friedman[1] proposed the mechanism whereby residual stresses developed by cementation of deformed sand grains under an *in situ* load. Hoskins and Russel[44] used over-coring techniques to measure the residual strains in the Black Hills and found a favorable comparison with the stress orientation deduced from direct overcoring of outcrop rocks.

Apparently, the coring process causes the rock to relieve much of the stored energy through microcracking (as measured with ASR), but not all of the residual stress can be relieved. Successively smaller overcores will continue to relieve additional stored energy, and this energy can be measured in terms of residual strains. The procedure is fairly simple, as it only requires that a strain-gage rosette be epoxied onto the core and a plug be taken. The change in strain, post-coring minus pre-coring, in each direction gives a measure of the differential residual strains/stresses stored in the rock. Since such strains are likely to be generally aligned with the *in situ* stresses, the principal strain orientation can be determined using the rosette equations.

4.7.2. Core Preparation and Data Acquisition

Core is prepared by taking a full piece of archived (or new) core and cutting a flat surface perpendicular to the axis of the core. This surface is cleaned and a strain-gage rosette is epoxied to the surface. The gages are connected to bridge circuits, the circuits are balanced, and the sample is plugged over the rosette. Plugging can be accomplished without disconnecting the wires (for example, on a lathe), or by disconnecting the wires, plugging the sample on a drill press, and then reconnecting the wires. Since there is likely to be a small contact resistance, this last technique may introduce some additional noise into the data, but the noise can be quantified by connecting and disconnecting the leads several times and recording the variability of the output voltage (or strain). Generally, the contact resistance is small.

4.7.3. Data Analysis

Data analysis of the sample is straightforward. Prior to plugging, the voltage of each gage is recorded and averaged if necessary (i.e., if the data are noisy). After plugging, the voltages of each gage are again recorded and an average voltage change for each channel is calculated. These voltage changes can be converted to strains, giving three strains, ε_0, ε_{45}, and ε_{90}, in the plane of the surface of the core (assuming a strain-gage rosette with 45° spacing). The rosette equation,

$$\theta_{min|max} = \frac{1}{2}\tan^{-1}\left\{\frac{2\varepsilon'_{45} - \varepsilon'_0 - \varepsilon'_{90}}{\varepsilon'_0 - \varepsilon'_{90}}\right\}, \quad (32)$$

can be used to determine the orientation of the principal strains, and thus, the stress orientation. An alternate technique for processing all of these rosette techniques is to fit the equation

$$r = r_{avg} + A\cos(2\beta + \theta) \quad (33)$$

to the data, where θ is the direction of the maximum strain and r_{avg} and A can be used to determine the principal strains. This equation is nonlinear and requires iteration, but it is simple to code (this same regression is used for the velocity analysis and is included in Appendix A).

4.7.4. Example Applications

An example of the data obtained using this technique is taken from SFE-4, in the Frontier formation in western Wyoming. The strain data taken from this test are shown in Table 17. Strain recovery from these tests are relatively small, but still an order of magnitude larger than the measurable limit of most equipment.

Table 17 Over-coring data, SFE-4, 7419 ft

GAGE	ORIENTATION	STRAIN
0	61	29 με
45	16	52.3 με
90	151	17.6 με

Using Equation 33, the data are fit to the regression and then compared to the CVA data taken on this sample. These results are shown in Figure 52. The maximum strain recovery is aligned with the minimum velocity azimuth, which is in turn aligned with the maximum horizontal stress.

4.7.5. Discussion

Over-coring of archived core has the potential to be a valuable technique for estimating stress azimuth because it is simple to use and it can be used on any archived oriented core. Unlike CVA, which requires measurements at a large number of orientations because it is not a tensor, the strain field in one plane can be deduced from only three points.

The principal difficulties with this technique are (1) not all rocks will exhibit much strain recovery upon overcoring and (2) fabric will cause errors in this technique the same as in

any of the other core-based techniques. However, this is a very inexpensive technique that can be routinely applied on any oriented core.

4.8 Coring-Induced Fractures

4.8.1. Concept

Coring-induced fractures have recently become a reliable source of information on the orientation of the *in situ* stress field (Lorenz et al.[45]). There are two important aspects to the use of coring-induced fractures for stress information. First, the coring-induced fracture must be distinguished from natural fractures, and second, a clear understanding of the fracture, its source, and its relation to drilling parameters must be made. The morphology and orientation of two types of mechanically induced fractures (scribe-line and petal fractures) will be discussed here for the determination of the *in situ* stress orientations.

4.8.1.1. Petal and petal-centerline fractures

Petal fractures are short fractures that extend from the outer edge of the core towards the center, curving to align with the core axis as the center of the core is approached. Petal-centerline fractures are petal fractures that, upon reaching the center (or near center) of the core, continue in a plane aligned with the core axis for an extended distance. Kulander et al.[46] suggested that petal and petal-centerline fractures form in advance of the core bit in response to the induced stress field around the bit superimposed on the *in situ* stress field. The mechanism is inferred to be one wherein compression of the rock by the bit weight causes strain-induced fractures along a plane parallel to the bit-induced maximum stress. Extension (minimal, as indicated by the commonly incomplete rock separation) occurs normal to this plane. The geometry of the petal fractures is parallel to lines of the principal stress trajectories below the bit, as depicted in Figure 53. These trajectories are those produced solely by the weight of the bit. When the bit-induced stresses are added to the *in situ* stresses (where the overburden is generally the greatest compressive stress) , the resultant stress trajectories will become somewhat steeper.

The application of coring-induced fracture parameters for stress information becomes apparent when an anisotropic stress field is superimposed on the stress due to the bit. Anisotropy of the horizontal *in situ* stresses effectively alters the circular plan-view stress pattern below the core bit into an elliptical distribution. Petal fractures form along planes defined by σ_1 and σ_2, (normal to σ_3), where σ_1 is the combination of overburden stress and stress from the weight on bit, σ_2 is the maximum *in situ* horizontal stress, and σ_3 is the least horizontal stress. This situation is shown in Figure 54. Thus the strike of the petal fracture can be used to determine the orientation of the stress field.

Petal fractures tend to occur in swarms with a regular spacing between individual fractures. It is likely that each petal fracture is initiated by an increase in bit stress, caused by a sudden increase of the weight on bit (as may occur with a sudden release of the draw-works by the driller or automatic driller). Alternatively, the formation of a petal fracture may relieve the stresses in the rock over a certain area, such that another fracture cannot form in the immediate vicinity, and thus the size of the zone of stress relief, or the fortuitous

occurrences of flaws in the rock, may control the spacing of petal fractures. Although these may be contributing factors to spacing, the range of actual spacings is probably greater than the range of sizes of stress-relief zones, and therefore abrupt changes in weight are inferred to be the dominant factor.

4.8.1.2. Scribe-knife fractures

Scribe-line fractures commonly originate from badly scarred scribe lines (knife-edge spalls of Kulander et al[46]), and are inferred to have resulted from the extra stresses associated with dull scribing knives. Dull knives would impart more stress to the rock as the knife is dragged along the core rather than cutting it cleanly. Scribe-line fractures in sandstones and siltstones originate at scribe-line grooves and are preferentially oriented, approximately parallel to the maximum *in situ* horizontal stress where stresses are anisotropic (Figure 55). They appear to maintain this orientation despite variations in penetration rate (shear stress) that may have rotated nearby petal fractures (Lorenz et al.[45]) as described below.

Whereas petal fractures are formed in the rock mass below the bit, scribe-line fractures are created in the core several inches above the bit face as the scribe knives and core barrel are forced over the core several minutes after the core has been cut from the rock mass Where visible, fracture surface ornamentation indicates that the origin of these fractures migrated, corresponding to the relative motion between the knife and the core (Kulander et al[47]). If the coring equipment is working properly and the scribe lines are straight, the rotating bit does not add shear stress to the core at the point where the scribe-line fractures form. However, this core is still under the influence of the *in situ* stress regime since the core has not undergone complete strain relaxation, and the rock retains a "memory" of the stress state for several hours after the core is cut (Teufel[3]). Thus the *in situ* stress dictates the orientation of the developing scribe-line fractures, unless the initial stress state is isotropic in the plane perpendicular to the axis of the core.

Scribe-line fractures initiate in a vertical plane because they originate at a linear, vertical scribe line, and because the minimum stress is initially horizontal. However, they commonly curve and become irregular in inclination as they propagate into the core. This may be because the lithostatic overburden has been removed and vertical expansion of the core is taking place, and thus the minimum stress becomes vertical before the core is entirely removed from the influence of the horizontal stresses in the rock mass below the bit face.

4.8.2. Data Acquisition

Data for this technique are acquired from oriented core and require a very careful layout and examination of the core (Lorenz and Hill[48] and Lorenz[49]). Indicators of petal fracturing, such as the regular spacing and the characteristic petal shape should be carefully noted. Anomalies in the orientation data should be compared with the drilling geolograph data, as torque, penetration, or other drilling factors may reorient petal fractures.

All scribe marks should be searched for any fractures entering the core. These can usually be most easily seen at mechanical breaks, where the plane perpendicular to the axis of the core is in full view.

The criteria for the distinction between artificial and natural fractures in core are not always obvious, and the possible mechanisms for the formation of many types of artificial fractures are poorly understood. Kulander et al.[46] and Pendexter and Rohn[50] listed recognition characteristics that differentiate induced fractures from natural fractures in core, and a new and comprehensive volume on the identification and logging of core fractures is now available (Kulander et al.[47]). Kulander et al.[46,47] determined that induced fractures are extensional in origin, and describe several types of induced fractures in core. Only petal/petal-centerline and scribe-line fractures are appropriate here.

Other than a capability to measure angles of fractures within the core, no special instrumentation is required.

4.8.3. Data Analysis

There is no special data analysis for the interpretation of coring-induced fractures, however, it is always worthwhile to correlate these results with lithology and drilling information.

4.8.4. Application Example

4.8.4.1 MWX

A large population of coring induced fractures was found in both oriented and unoriented core from the Mesaverde group at the Multiwell experiment (Lorenz et al[45]). This experiment was located in the Piceance basin of western Colorado near the town of Rifle. Data were obtained in three wells, from depths of 4000-8000 ft, and stress orientation was compared with many available techniques.

4.8.4.1.1. Petal and petal-centerline fractures

Petal fractures in MWX core range from closely spaced, 1-in long petals (Figure 56) to rarer, well-developed centerline fractures over 6 ft long with ancillary petal fractures (Figure 57). The surfaces of the MWX petal fractures do not display systematic markings. The fracture surfaces of MWX petal fractures commonly contain coatings of drilling mud (identified by X-ray diffractometry) and, less commonly, small patches of white powder. This powder has a microbrecciated texture and is inferred to be powdered rock created by the drilling process. Scanning electron microscope (SEM) photography of the fracture surfaces that are clean of drilling mud or rock powder show fresh, conchoidally-broken mineral grains with no crystalline overgrowths or mineralization.

Many of the MWX petal fractures consist of multiple anastamosed fracture planes, and in such cases, the separation of the rock across the fracture is incomplete. The anastamosed character and incomplete separation, coupled with the rock powder patches that macroscopically resemble mineralization, can lead to the erroneous conclusion that such fractures are natural fractures.

MWX petal fractures commonly occur in swarms (up to 10 individual fractures), spaced 1 to 6 in apart vertically, and overlapping where closely spaced. All fractures in a swarm have the same strike, and they may either occur all on one side of the core or may occur irregularly on opposite sides of the core, dipping toward the core centerline. In a few cases, they occur as pairs at the same depth on opposite sides of the core. In heterogeneous rock they may terminate at lithologic boundaries, but in homogeneous rock there is commonly no apparent lithologic cause for termination. Few of the petal fractures in MWX core extend into centerline fractures; most extend downward a few inches at most, and penetrate only about one-fourth to one-third of the 4-in core diameter.

A third of the petal fractures in MWX core decrease in dip as they penetrate the core (slightly "concave up"), and a third increase in dip (slightly "concave down"). The last third display no apparent change in dip angle over their 1- to 2-in. length. The concave-up fractures predominate at the shallower depths (4500 to 6000 ft) whereas concave-down petal fractures predominate deeper in the well (7800 to 8000 ft) (Figure 58). For unknown reasons, few petal fractures formed outside of these two intervals. Constant-angle petal fractures first appear at intermediate depths and occur mixed with the other types at greater depths.

Petal fractures occur predominantly in siltstones, none being recorded from the interbedded mudstones, shales, or coals. The siltstones have a significantly higher Young's modulus than other lithologies, indirectly implying a greater susceptibility to fracturing. In the one zone where petal fractures occur commonly in sandstones (the lowermost zone, Figure 58), the Young's moduli of the sandstones and siltstones are about equal.

Adjacent petal fractures have parallel strikes, and strikes are generally consistent over tens of feet of core. Most MWX petal fractures strike west-northwest, parallel to the maximum *in situ* horizontal stress at MWX measured by Teufel[3] and Warpinski and Teufel.[24]

Although it is apparent that the *in situ* horizontal stresses control the strike of most MWX petal fractures, there are anomalous petal fracture orientations. These anomalies seem to be caused by high shear stresses added to the total stress system by drag of the rotating core bit on the rock. The magnitude of such shear stresses is a function of lithology, bit type, bit condition, bit rotation speed, and weight on bit. Unfortunately, there are no foot-by-foot records of these factors in the MWX data base. The available detailed record that is most similar to measurements of shear is the foot-by-foot penetration rate. No torque log is available.

At MWX, one section of relatively homogeneous sandstone was cored in both MWX-1 and MWX-2 (wells offset by only 125 ft), and numerous petal fractures were observed (Figure 59). This is a zone of significant overpressurization of the formation (gradient 0.80 psi/ft, almost twice normal), where high pore pressures create lower effective stresses, and thus the zone is relatively susceptible to a reorientation of the *in situ* stresses. Whereas petal fractures in MWX-1 strike consistently west-northwest, petal fractures in MWX-2 in this same lithologic and stress regime strike more north-northwest, exhibiting clockwise strike rotation of 15° to 20°. The petals all occur in a homogeneous sandstone bed, and the only apparent difference between the two wells is in the average core-bit penetration rate (18 vs 24 ft per minute) over the cored interval. Therefore there was presumably a difference in the shear stress that was imparted to the rock mass below the bit in the two wells. Lower penetration rates imply a greater difficulty in cutting through the rock, and therefore that more shear stress existed between the turning bit and the rock. Such increased shear stress, imparted in the clockwise sense of rotation of the bit, will significantly rotate the *in situ* stress field in the immediate vicinity of the bit and account for these anomalies in orientation.

There is evidence that supports this idea. The orientation of the strike of individual petal fractures in the interval shown in Figure 59 correlates with the rate of penetration for the foot in which the fracture occurs. Further support for this correlation is provided by a few instances where drill-string penetration rate decreased abruptly to 40 or 50 minutes per foot just prior to a jamming of the core barrel, high sheer (rotational) stress, and the premature end of a core run. In these instances, the strikes of associated petal fractures in the core are rotated up to 60 degrees clockwise from the normal west-northwest trend (see Figure 59, base of MWX-2 core, for one example).

Finally, the dip angles of the petal fractures are roughly segregated by well in this interval: "unrotated" petal fractures in MWX-1 core generally dip 50 degrees or less, whereas rotated petal fractures in MWX-2 core dip between 55 degrees and 85 degrees. This suggests that the MWX-2 petal fractures were aligned with a steeper stress array caused by increased weight on bit, which in turn created greater shear stress on the rock and rotated petal-fracture strikes.

4.8.4.1.2. Scribe-line fractures

Knife-edge spalls are present in the brittle, well-cemented sandstones and siltstones of MWX core. Scribe-line fractures are found where the spalls are especially well developed (i.e., where the scribe line is particularly badly marred, indicating excessive stress imparted to the core, probably by dulled scribe knives). These fractures originate within the scribe-line groove, and, in siltstones and sandstones, penetrate into the core less than half of the core diameter. Because they are narrow, are obscured by the groove, and commonly do not completely penetrate the core, these fractures are difficult to detect. They are more apparent when the core is slabbed. Only 16 scribe-line fractures were observed in the MWX core.

Scribe-line fractures are usually short (1 to 3 in. in length) and irregular. They initiate as vertical fractures, parallel to the vertical scribe-line groove, but most of them curve and become irregular as they penetrate the core. These fractures occur sporadically, rather than in groups as is common with petal fractures. All scribe-line fractures observed in oriented sandstone and siltstone core from MWX strike west-northwest, as seen in Figure 60. This orientation is consistent with the anisotropic *in situ* horizontal stress field in these lithologies (Warpinski and Teufel, 1989). On the other hand, the orientations of scribe-line fractures in core of mudstone and carbonaceous mudstone are variable, and fractures have been noted that cut across core to connect scribe grooves. In several examples, two perpendicular scribe-line fractures--originating from different scribe-line grooves at the same depth--occur in the same piece of mudstone core. Mudstone cores tested for anelastic strain recovery were found to exhibit horizontally isotropic strain behavior (Warpinski and Teufel[24]), which is consistent with the absence of a preferred strike for scribe-line fractures observed in these lithologies.

4.8.4.2. Travis Peak

Data from the lower Cretaceous Travis Peak consisted of 101 oriented petal and petal-centerline fractures found in seven different wells in northeast Texas (Laubach and Monson[51]). Petal-centerline and petal fractures were found to be common in the Travis Peak core, and they occurred in both sandstones and mudstones. A frequency of 3-5 petals per foot of core is common, as shown in Figure 61. Widths of intact petal and petal-centerline fractures were found to be typically 0.009 in or less, with lengths generally less than 5 in. The surfaces of the coring-induced fractures are generally smooth in the Travis Peak, with few arrest lines or plumose structures (occasionally in the mudstones).

As shown in Figure 62, the petal and petal-centerline fractures in the Travis Peak strike predominantly east-northeast, with little difference between petal and petal-centerline fractures and a relatively small dispersion about the mean. Within intact core, petal and petal-centerline fractures are usually precisely parallel. The stress azimuth determined from the coring-induced fractures is in agreement with other orientation techniques used in this area (Laubach and Monson[51]).

4.8.5. Discussion

The significance of coring- and drilling-induced fractures lies primarily in the relationship of their orientation to the *in situ* horizontal stresses. If induced fractures are found in oriented core, the true orientation of the *in situ* stresses can usually be determined. If induced fractures are found in unoriented core but in conjunction with natural fractures, at least the relative angle between the natural fracture trend and a hydraulic stimulation fracture can be determined. However, petal fractures can be reoriented by core-bit shear stress, and should be studied carefully before conclusions of stress orientation are drawn. Scribe-line fractures

in sandstone and siltstone lithologies at MWX, however, seem to be unaffected by such torque, and they more consistently reflect the measured *in situ* horizontal stress orientation.

Lee[52] and GangaRao et al.[53] suggest that the initial dip angle of petal fractures (the tangent to the curved fracture plane near the outer core surface) is directly controlled by, and may be used to calculate, the magnitudes of the *in situ* stresses if stress ratios are known or can be reasonably estimated. In MWX core, however, the initial dip angles for petal fractures are scattered (Fig. 58), and do not support precise calculations based on this theoretical suggestion, although the maximum dip angle observed in petal fractures from any horizon does increase irregularly downhole.

Petal and petal-centerline fractures are formed below the bit, and might form whether or not the hole is being cored. The stress lines followed by petal fractures curve in toward the center of the wellbore as well as away from it, and it is conceivable that when the vertical stress is not significantly greater than the horizontal stress, "inverse" petal fractures are created beyond the wellbore (along lines d, e, Fig. 53). It is more likely, however, for the internal fracture planes associated with stress trajectories a, b, and c to extend beyond the wellbore. These fractures would extend the effective wellbore radius and provide excellent communication between the formation and the well. However, they may also allow deep penetration of drilling fluids into the formation, resulting in extensive formation damage. Kulander et al (1979) show a photograph of a petal-centerline fracture in an uncored roadcut drill hole, the wings of which extend at least three wellbore diameters on either side of the hole. Unpublished laboratory measurements of restored-state permeabilities along seven petal fractures in sandstones in MWX core show permeability enhancements of more than two orders of magnitude compared to the measured permeabilities of similar matrix rock.

Finally, these two types of induced fractures are commonly very small and therefore may be unnoticed or ignored. They will, however, produce spurious results if they are present in plugs taken from cores for measurements of rock properties. Certain pieces of MWX core showing anomalous velocity anisotropy test results were carefully inspected after testing and found to contain induced fractures that overshadowed the effects of microcracks that were being tested.

5.0 CONCLUSIONS

There are a number of core-based measurement techniques that are available to assess the *in situ* stress state at depth in a reservoir. However, all of these techniques require oriented core that is in relatively good condition. This aspect of these techniques is probably the single biggest drawback. However, if oriented core is obtained, then there are many techniques for measuring the stress azimuth, and several that can be used to estimate the stress magnitudes. In addition, some of these techniques are self-diagnosing and it is possible to discern if fabric problems are present.

Two good techniques for diagnosing fabric are petrographic examination and circumferential velocity analysis. CVA generally is well fit by the theoretical distribution if fabric is not present, but the shape of the velocity curve vs orientation is often blocky is fabric is involved. Natural fractures also significantly change the shape of the distribution. Petrographic examination is the surest way to find tectonic microcracks. These features are the most difficult type of fabric to assess.

The best way to use these core-based techniques is in tandem, as discrepancies in two or more techniques are often the best flag for alerting the analyst of possible problems. Because there is a wide range of methods, it is possible to begin with simple techniques where good statistics can be obtained, and then move to more sophisticated ones if problems develop or additional data are needed.

While all of these methods can provide accurate, reliable data, there are many precautions that must be taken, and the data must be carefully scrutinized. The service company will typically report all of the data, and it is up to the operator to determine which data are good and which are inaccurate.

The one core-based method that is not influenced by fabric of any kind is the analysis of coring induced fractures. As such, this is a powerful technique for corroborating other data. However, coring induced fractures are only occasionally found, and they may be re-oriented by weight on bit and other factors. Nevertheless, whenever oriented core is obtained, one should make an effort to search for these features.

Only ASR, DSCA, DWVA, and the Kaiser effect provide any possibility of estimating the magnitudes of the horizontal stresses. These methods occasionally provide accurate data, but there are many difficulties and uncertainties in these measurements. However, since there is a growing need for measurement of the maximum horizontal stress (for wellbore stability, production geomechanics, etc.), there is need for further development of these procedures, as there is currently no other good method for obtaining this parameter.

6.0 REFERENCES

1. Friedman, M., "Residual Elastic Strains in Rocks," *Tectonophysics*, Vol. 15, pp. 297-330, 1972.
2. Emery, C.L., "Strain Energy in Rocks," in **State of Stress in the Earth's Crust**, W.R. Judd (ed.), Elsevier, NY, pp. 235-280, 1964.
3. Teufel, L.W., "Determination of In Situ Stress from Anelastic Strain Recovery Measurements of Oriented Core," SPE 11649, Proc. SPE Symposium on Low Permeability Reservoirs, Denver, CO., pp. 421-430, March 13-16, 1983a.
4. Teufel, L.W., "Determination of the Principal Horizontal In Situ Stress Directions from Anelastic Strain Recovery Measurements of Oriented Cores from Deep Wells: Application to the Cotton Valley Formation of East Texas," Proc. ASME Symposium on Geomechanics, Houston, Texas, pp. 55-63, June 20-22, 1983b.
5. Teufel, L. W. and Warpinski, N. R., "Determination of In Situ Stress from Anelastic Strain Recovery of Oriented Core: Comparison to Hydraulic Fracture Stress Measurements," Proceedings, 25th U.S. Symposium on Rock Mechanics, Evanston, IL, pp. 176-185, 1984.
6. Smith, M.B., Ren, N.K., Sorrells, G.G. and Teufel, L.W., "A Comprehensive Fracture Diagnostics Experiment: Comparison of Seven Fracture Azimuth Measurements," *SPE Production Engineering*, Vol. 2, pp. 423-432, November 1986
7. Warpinski, N.R. and Teufel, L.W., "A Viscoelastic Constitutive Model for Determining In Situ Stress Magnitudes from Anelastic Strain Recovery of Core," *SPE Production Engineering*, Vol. 4, pp. 272-280, August 1989b.
8. Teufel, L.W., "Acoustic Emissions during Anelastic Strain Recovery of Cores from Deep Boreholes," Proc. 30th U.S. Symposium on Rock Mechanics, Morgantown, WV, pp. 269-276, June 1989.
9. Walsh, J.B., "The Effect of Cracks on the Compressibility of Rock," *J. of Geophys. Res.*, Vol. 70, No. 2, pp. 381-389, January 15, 1965.
10. Garbin, H.D. and Knopoff, L., "The Compressional Modulus of a Material Permeated by a Random Distribution of Free Circular Cracks," *Q. of Appl. Math.*, Vol. 30, pp. 453-464, 1973.
11. Ostensen, R.W., "The Effect of Stress-Dependent Permeability on Gas Production and Well Testing," *SPE Formation Evaluation*, Vol. 1, No. 3, pp. 227-235, June 1986.
12. Ingraffea, A.R. and Schmidt, R.A., "Experimental Verification of a Fracture Mechanics Model for Tensile Strength Prediction of Indiana Limestone," Proc. 19th U.S. Symposium on Rock Mechanics, Lake Tahoe, NV, pp. 247-253, June 1978.
13. Logan, J.M and Teufel, L.W., "The Prediction of Massive Hydraulic Fracturing from Analyses of Oriented Cores," 19th U.S. Symposium on Rock Mechanics, Lake Tahoe, CA, pp. 340-347, May 1-3,1978.

14. Nelson, R.A, Lennox, L.C. and Ward, B.J., "Oriented Core: Its Use, Error and Uncertainty," *AAPG Bulletin*, Vol. 71, No. 4, pp. 357-367, April 1987.

15. Bleakly, D.C., Van Alstine, D.R. and Packer, D.R., "Controlling Errors Minimizes Risk and Cost in Core Orientation," *Oil and Gas Journal*, pp. 103-109, Dec. 2, 1985.

16. Bleakly, D.C., Van Alstine, D.R. and Packer, D.R., "How to Evaluate Orientation Data Quality Control," *Oil and Gas Journal*, pp. 46-52, Dec. 9, 1985.

17. Nur, A. and Simmons, G., "Stress-Induced Velocity Anisotropy in Rock: An Experimental Study," *J. of Geophys. Res.*, Vol. 74, No. 27, pp. 6667-6674, December 15, 1969.

18. Warpinski, N.R. and Teufel, L.W., "Determination of the Effective Stress Law for Permeability and Deformation in Low-Permeability Rocks," *SPE Formation Evaluation*, Vol. 7, No. 2, pp. 123-131, June 1992.

19. Miller, W. K., Peterson, R.E., Stevens, J.E., Lackey, C.B. and Harrison, C.W., "In Situ Stress Profiling and Prediction of Hydraulic Fracture Azimuth for the Canyon Sands Formation, Sonora and Sawyer Fields, Sutton County, Texas," SPE 21848, proceedings SPE Rocky Mountain Regional/Low Permeability Reservoirs Symposium, pp. 445-456, Denver, Colorado, April 15-17, 1991.

20. Walls, J.D., Packwood, J., Hyman, L., Malek, D. and Admire, C., "Improvements of Formation Evaluation and Reservoir Engineering in Tight Gas Sands through Selected Core Analysis Procedures," GRI-92/0080, GRI Topical Report, December 1991.

21. Plumb, R., Engelder, T. and Yale, D., "Near-Surface In Situ Stress: 3. Correlation with Microcrack Fabric within the New Hampshire Granites," *J. of Geophys. Res.*, Vol. 89, No. B11, pp. 9350-9364, October 10, 1984.

22. Sayers, C.M., "Stress-Induced Ultrasonic Wave Velocity Anisotropy in Fractured Rock," *Ultrasonics*, Vol. 26, pp. 311-317, November 1988.

23. Laubach, S.E., Clift, S.J., Hill, R.E. and Fix, J., "Stress Directions in Cretaceous Frontier Formation, Green River Basin, Wyoming," **Wyoming Geol. Assoc. Guidebook**, 1992.

24. Warpinski, N.R. and Teufel, L.W., "In Situ Stresses in Low-Permeability Nonmarine Rocks," *J. of Pet. Tech.*, Vol. 41, No. 4, pp. 405-414, April 1989a.

25. Lorenz, J.C., Warpinski, N.R., Sattler, A.R. and D.A. Northrop, "Fractures and Stresses in the Bone Spring Sandstones, 1989 Annual Report," SAND90-2068, Sandia National Laboratories Report, September 1990.

26. Voight, B., " Determination of the Virgin State of Stress in the Vicinity of a borehole from Measurements of a Partial Anelastic Strain Tensor in Drill Cores, " *Felsmechanik V. Ingenieureol*, Vol. 6, pp. 201-215, 1968.

27. Teufel, L.W., "Prediction of Hydraulic Fracture Azimuth from Anelastic Strain Recovery Measurements of Oriented Core," 23rd U.S. Symposium on Rock Mechanics, Berkeley, CA, pp. 238-246, June 1982.

28. Lacy, L.L., "Comparison of Hydraulic-Fracture Orientation Techniques," *SPE Formation Evaluation*, Vol. 2, No. 1, pp. 66-76, March 1987.

29. Blanton, T. L., "The Relation between Recovery Deformation and In Situ Stress Magnitudes," SPE 11624, presented at 1983 SPE/DOE Symposium on Low Permeability Gas Reservoirs, Denver, CO, March 14-16, 1983.

30. Holcomb, D.J. and McNamee, M.J., "Displacement Gauge for the Rock Mechanics Laboratory," Sandia National Laboratories Report, SAND84-0651, 1984.

31. Obert, L. and Duvall, W. E., "Rock Mechanics and the Design of Structures in Rock," Wiley, New York, 558 p. (1967).

32. Warpinski, N.R., "ASR4: A Computer Code for Fitting and Processing 4-Gage Anelastic Strain Recovery Data," Sandia National Laboratories Report, SAND89-0484, May 1989.

33. Teufel, L.W. and Warpinski, N.R., "Determination of *In Situ* Stress from Anelastic Strain Recovery Measurements of Oriented Core: Comparison to Hydraulic Fracture Stress Measurements in the Rollins Sandstone, Piceance Basin, Colorado," Proc., 25th U.S. Symposium on Rock Mechanics, Northwestern University, Evanston, IL, June 25-27, 1984.

34. Strickland, F.G. and Ren, N-K., "Predicting the In-Situ Stress for Deep Wells Using Differential Strain Curve Analysis," SPE 8954, Proc. 1980 Symposium on Unconventional Reservoirs, Pittsburgh, PA, pp. 251-255, May 18-21, 1980.

35. Ren, N-K. and Roegiers, J.-C., "Differential Strain Curve Analysis - A New Method for Determining the Pre-Existing In Situ Stress State from Rock Core Measurements," 5th Congress of the International Society for Rock Mechanics, Melbourne, Australia, pp. F117-F127, 1983.

36. Ren, N-K. and Hudson, P.J., "Predicting the In-Situ State of Stress Using Differential Wave Velocity Analysis," Proc. 26th U.S. Symposium on Rock Mechanics, Rapid City, SD, pp. 1235-1244, June 26-28, 1985.

37. Holcomb, D.J., :"General Theory of the Kaiser Effect," *Int. J. Rock Mech. Min. Sci. & GeoPhys. Abstr.*, in press.

38. Holcomb, D.J. "Observations of the Kaiser Effect under Multiaxial Stress States: Implications for Its Use in Determining In Situ Stress," *Geophys. Res. Lett.* in press.

39. Momayez, M. and Hassani, F.P., "Application of Kaiser Effect to Measure In Situ Stresses in Underground Mines," 33rd U.S. Symposium on Rock Mechanics, Santa Fe, NM, pp. 979-988, June 3-5, 1992.

40. Gregg, W.J., "Mechanical Fabric and In Situ Stress Orientations in the Devonian Gas Shales of the Appalachian Basin," 27th U.S. Symposium on Rock Mechanics, Tuscaloosa AL, pp. 709-715, 1986.

41. Clift, S.J., Laubach, S.E. and Holder, J., "Strength Anisotropy in Low-Permeability Sandstone Gas Reservoirs: Application of Axial Point Load Test," *Gulf Coast Association of Geological Societies, Transactions*, Vol. 42, 1992.

42. Gies, R.M., "An Improved Method for Viewing Micropore Systems in Rocks with the Polarizing Microscope," *SPE Formation Evaluation*, Vol. 2, pp. 209-214, June 1987.

43. Soeder, D.J., "Applications of Fluorescence Microscopy to the Study of Pores in Tight Rocks," *AAPG Bulletin*, Vol. 74, pp. 30-40, January 1990.

44. Hoskins, E.R. and Russel, J.E., "The Origin of Measured Residual Strains in Crystalline Rocks," in **Mechanical Behavior of Crustal Rocks (The Handin Volume)**, Geophysical Monograph 24, AGU, Washington, D.C., pp. 187-198, 1981.

45. Lorenz, J.C., Finley, S.J. and Warpinski, N.R., "Significance of Coring Induced Fractures in Mesaverde Core, Northwestern, Colorado," *AAPG Bulletin*, Vol. 74, pp. 1017-1029, July 1990.

46. Kulander, B. R., Barton, C. C. and Dean, S. L., "The Application of Fractography to Core and Outcrop Fractures Investigations," METC/SP-79/3, U.S. DOE, Morgantown Energy Technology Center, 174 p., 1979.

47. Kulander, B. R., Dean, S. L., and Ward, B. J. Jr., 1990, Interpretation and Logging of Natural and Induced Fractures in Core," AAPG, 1990.

48. Lorenz, J.C. and Hill, R.E., "Measurements and Analysis of Fractures in Core," in *Geological Studies Relevant to Horizontal Drilling: Examples from Western North America*", J.W. Schumaker, E.B. Coalson and C.A. Brown, eds., Rocky Mt. Assoc. Geol., pp. 47-59, 1992.

49. Lorenz, J.C., "Lithology, The Missing Ingredient in Core Fracture Analysis," in *New Technology for the Independent Producer*, NIPER/DOE, Bartlesville, OK, pp. 61-67, 1993.

50. Pendexter, C., and R. E. Rohn, Fractures Induced During Drilling," *J. of Pet. Tech.*, March 1954, pp. 15 and 49, 1954.

51. Laubach, S. E., and Monson, E. R., "Coring-Induced Fractures: Indicators of Hydraulic Fracture Propagation in a Naturally Fractured Reservoir," SPE 18164, in Proceedings of the 63rd Annual Technical Conference and Exhibition of the Society of Petroleum Engineers, Houston TX, October 2-5, pp. 587-596, 1988.

52. Lee, S-C., "Investigation of Stress and Fracture Responses Associated with Coring Operations," B.Sc. Thesis, West Virginia University, p. 111, 1978.

53. GangaRao, H. V. S., Advani, S. H., Chang, P., Lee, S. C., and Dean, C. S., "In Situ Stress Determination Based on Fracture Responses Associated with Coring

Operations," 20th U.S. Symposium on Rock Mechanics, Austin, TX, pp. 683-690, 1979.

7.0 ADDITIONAL BIBLIOGRAPHY

Avasthi, J.M., Nolen-Hoeksema, R.C., El Rabaa, A.W.M. and Wilson, L.E., "In Situ Stress Evaluation in the McElroy Field, West Texas," SPE 20105, Procs., Permian Basin Oil and Gas Recovery Conference, Midland, TX, pp. 177-188, March 8-9, 1990.

Charlez, Ph., Hamamdjian, C. and Despax, D., "Is the Microcracking of a Rock a Memory of its Initial State of Stress," Procs., International Symposium on rock Stress and Rock Stress Measurements, Stockholm, pp. 341-350, Sept. 1-3, 1986.

Deflandre, J-P. and Sarda, J-P., "Core Relaxation Measurements on Compacted Sedimentary Formations (Well Ba 1)," Procs., 33rd U.S. Symposium on Rock Mechanics, Santa Fe, NM, pp. 49-57, June 3-5, 1992.

El Rabaa, A.W.M. and Meadows, D.L., "Laboratory and Field Applications of the Strain Relaxation Method," SPE 15072, Procs., 56th California Regional Mtg, Oakland, CA., pp. 259-265, April 2-4, 1986.

El Rabaa, A.W., "Determination of the Stress Field and Fracture Direction in the Danian Chalk," **Rock at Great Depth**, Maury and Fourmaintraux (eds.), Balkema, Rotterdam, pp. 1017-1024, 1989.

Griffin, K.W., "Induced Fracture Orientation Determination in the Kuparuk Reservoir," SPE 14261, Procs., SPE 60th Annual Tech. Conf., Las Vegas, NV, Sept. 22-25, 1985.

Hardy, H.R., Zhang, D. and Zelanko, J.C., "Recent Studies of the Kaiser Effect in Geologic Materials," Procs., Fourth Conference on Acoustic Emission/Microseismic Activity in Geologic Structures and Materials, Trans Tech Publications, (H.R. Hardy, ed.), pp. 27-55, 1989.

Hyman, L.A., Malek, D.J., Admire, C.A. and Walls, J.D., "The Effects of Microfractures on Directional Permeability in Tight Gas Sands," SPE 21878, Procs., Rocky Mt. Regional Mtg. and Low-Permeability Reservoirs Symposium, Denver, CO., April 15-17, 1991.

Kanagawa, T., Hayashi, M. and Nakasa, H., "Estimation of Spatial Geo-Stress Components in Rock Samples Using the Kaiser Effects of Acoustic Emission," Procs., Third Acoustic Emission Symposium, Tokyo, pp. 229-248, 1976.

Kanagawa, T., Hayashi, M. and Kitahara, Y., "Acoustic Emission and Over Coring Methods for Measuring Tectonic Stresses," Procs., International Symposium on Weak Rocks, Tokyo, pp. 1205-1210, 1981.

Montgomery, C.T. and Ren, N.K., "Differential Strain Curve Analysis: Does It Work?" Procs., Workshop on Hydraulic Fracturing Stress Measurements, National Academy Press, Monterey, CA, pp. 239-245, Dec. 2-5, 1981.

Perreau, P., Heugas, O. and Santarelli, F.J., "Tests of ASR, DSCA, and Core Discing Analyses to Evaluate In Situ Stresses," SPE 17960, Procs., Middle East Oil Technical Conf., Manama, Bahrain, March 11-14, 1989.

Ramos, G.G. and Rathmell, J.J., "Effects of Mechanical Anisotropy on Core Strain Measurements for In Situ Stress Determination," SCA 8909, Society of Core Analysts Annual Tech. Conf., New Orleans, LA, 1989.

Thiercelin, M.J. and Plumb, R.A., "A Core-Based Prediction of Lithologic Stress Contrasts in East Texas Formations," SPE 21847, Procs., Rocky Mt. Regional Mtg. and Low-Permeability Reservoirs Symposium, Denver, CO., pp. 429-444, April 15-17, 1991.

Tullis, T.E., "Reflections on Measurement of Residual Stress in Rock," *Pageophysics*, Vol. 115, pp. 57-68, 1977.

Warpinski, N.R. and Lorenz, J.C., "Development of Stimulation Diagnostic Technology," Annual Report GRI-92/0116, Gas Research Institute, February 1992.

Warpinski, N.R., Lorenz, J.C., Sleefe, G.E. and Engler, B.P., "Development of Stimulation Diagnostic Technology," Annual Report GRI-93/0119, Gas Research Institute, February 1993.

Yale, D.P. and Sprunt, E.S., "Prediction of Fracture Direction using Shear Acoustic Anisotropy," *The Log Analyst*, pp. 65-70, March-April, 1989.

Yale, D.P., Strubhar, M.K. and El Rabaa, A.W., "A Field Comparison of Techniques for Determining the Direction of Hydraulic Fractures," Procs., 33rd U.S. Symposium on Rock Mechanics, Santa Fe, NM, pp. 89-98, June 3-5, 1992.

APPENDIX A

This appendix contains a simple program for fitting a theoretical model to circumferential velocity anisotropy data.

```
      PROGRAM VELANIS
      CHARACTER*1 INPUTQ,IPLOT,IQUIT,IMORE,ITYPE
      CHARACTER*15 AFILE,OUTFIL
      CHARACTER*50 DEFCHAR
      DIMENSION THET(51),VELOC(51),SUM(16),TFIT(101),VFIT(101),
     1        VPERT(51),RES(51)
      WRITE(*,199)
  199 FORMAT(10X,'*********************************************'/
     1      10X,'*              VANISO                 */
     2      10X,'*  ANALYSIS OF VELOCITY ANISOTROPY CORE DATA  */
     3      10X,'*         WRITTEN BY: N. R. WARPINSKI      */
     4      10X,'*         SANDIA NATIONAL LABORATORIES     */
     5      10X,'*              MAY, 1989                   */
     6      10X,'*            OPEN INFORMATION              */
     7      10X,'*        WRITTEN USING PLOT88 SOFTWARE     */
     8      10x,'*     COMPILED USING RYAN-MCFARLAND FORTRAN  */
     9      10X,'*********************************************'/)
      PI=3.141592654
C  INPUT VELOCITY VS ANGLE DATA
  900 WRITE(*,200)
  200 FORMAT(' DO YOU WANT DATA INPUT BY HAND(H) OR FILE(F): ')
      READ(*,100) INPUTQ
  100 FORMAT (A1)
      IF (INPUTQ .EQ. 'H' .OR. INPUTQ .EQ. 'h') THEN
        WRITE(*,201)
  201   FORMAT(' INPUT DATA IN THE FOLLOWING FORMAT'/
     1  ' ANGLE IN DEGREES, VELOCITY IN ANY UNIT: '
     2  /10X,' INPUT -999.0 FOR ANGLE TO END')
        I=1
   10   WRITE(*,203) I
  203   FORMAT(' DATA POINT # ',I3,': ')
        READ(*,*,ERR=11,END=11) THET(I),VELOC(I)
        IF(THET(I) .EQ. -999.0) GO TO 11
        I=I+1
        GO TO 10
   11   WRITE(*,204)
        M=I-1
  204   FORMAT(' THESE DATA WILL BE WRITTEN TO A FILE FOR LATER USE'/
     1  ' INPUT THE NAME OF THE FILE (1-15 CHARACTERS): ')
        READ(*,101) AFILE
  101   FORMAT(A15)
        OPEN (13,FILE=AFILE)
        REWIND 13
        WRITE(13,*) M
        DO 12 I=1,M
   12   WRITE(13,*) THET(I),VELOC(I)
        CLOSE (13)
      ELSE
        WRITE(*,207)
```

```
 207   FORMAT(' INPUT THE NAME OF THE FILE: ')
       READ(*,101) AFILE
       OPEN(14,FILE=AFILE)
       REWIND 14
       READ(14,*) M
       DO 13 I=1,M
  13   READ(14,*) THET(I),VELOC(I)
     CLOSE (14)
     ENDIF
     WRITE(*,281) M
 281 FORMAT('*****   NUMBER OF TIME STEPS = ',I3,'   *****')
     WRITE(*,210) (THET(I),VELOC(I),I=1,M)
 210 FORMAT(' THET=',F10.2,' VELOC=',F15.5)
C  OPEN UP AN OUTPUT FILE
     PRINT*,' WHAT NAME FOR THE OUTPUT FILE OF DATA: '
     READ(*,101) OUTFIL
     OPEN(11,FILE=OUTFIL)
     REWIND 11
     WRITE(11,554) AFILE
 554 FORMAT('   INPUT FILE NAME = ',A15)
     WRITE(11,555) M
     WRITE(11,588) OUTFIL
 588 FORMAT(/'   OUTPUT FILE NAME = ',A15)
 555 FORMAT(2X,I4,' DATA POINTS')
     WRITE(11,281) M
     WRITE(11,210) (THET(J),VELOC(J),J=1,M)
C
C    PICK THE TYPE OF FIT DESIRED
C
     PRINT*,' CHOOSE A*COS(2*THET) ------------------------ 1'
     PRINT*,'    OR A*COS(2*THET)+B*COS(4*THET) ----------- 2:  '
     READ(*,100) ITYPE
C
C    START CALCULATIONS
C
     DPHI=PI/12.0
     PHI=0.0
     J=0
     KCHECK=0
  20 J=J+1
C
C    GET SUMS
C
     DO 30 I=1,16
  30   SUM(I)=0.0
     IF(ITYPE .EQ. '1') THEN
C
C    COS(2*THET) FIT
C
C    GET DATA SUMS
C
       DO 40 N=1,M
         ANG=THET(N)*PI/180.
         ANG2=2.*(ANG+PHI)
         SUM(1)=SUM(1)+VELOC(N)
```

```
          SUM(2)=SUM(2)+VELOC(N)*COS(ANG2)
          SUM(3)=SUM(3)+COS(ANG2)
          SUM(4)=SUM(4)+COS(ANG2)**2
          SUM(5)=SUM(5)+VELOC(N)*SIN(ANG2)
          SUM(6)=SUM(6)+SIN(ANG2)
   40     SUM(7)=SUM(7)+SIN(ANG2)*COS(ANG2)
        DET=FLOAT(M)*SUM(4)-SUM(3)**2
        VAVG=(SUM(1)*SUM(4)-SUM(2)*SUM(3))/DET
        A=(FLOAT(M)*SUM(2)-SUM(1)*SUM(3))/DET
        F=SUM(5)-VAVG*SUM(6)-A*SUM(7)
      ELSE
C
C   COS(2*THET)+COS(4*THET) FIT
C
      DO 65 N=1,M
        ANG=THET(N)*PI/180.0
        ANG2=2.*(ANG+PHI)
        ANG4=4.*(ANG+PHI)
        SUM(1)=SUM(1)+VELOC(N)
        SUM(2)=SUM(2)+VELOC(N)*COS(ANG2)
        SUM(3)=SUM(3)+VELOC(N)*COS(ANG4)
        SUM(4)=SUM(4)+COS(ANG2)
        SUM(5)=SUM(5)+COS(ANG4)
        SUM(6)=SUM(6)+COS(ANG2)**2
        SUM(7)=SUM(7)+COS(ANG4)**2
        SUM(8)=SUM(8)+COS(ANG2)*COS(ANG4)
        SUM(9)=SUM(9)+VELOC(N)*SIN(ANG2)
        SUM(10)=SUM(10)+VELOC(N)*SIN(ANG4)
        SUM(11)=SUM(11)+SIN(ANG2)
        SUM(12)=SUM(12)+SIN(ANG4)
        SUM(13)=SUM(13)+COS(ANG2)*SIN(ANG2)
        SUM(14)=SUM(14)+COS(ANG2)*SIN(ANG4)
        SUM(15)=SUM(15)+SIN(ANG2)*COS(ANG4)
   65   SUM(16)=SUM(16)+COS(ANG4)*SIN(ANG4)
C
C   GET A, B, AND VALUE OF FUNCTION(PHI)
C
      DET=FLOAT(M)*SUM(6)*SUM(7)+2.0*SUM(4)*SUM(5)*SUM(8)
     1   -SUM(6)*SUM(5)**2-SUM(4)**2*SUM(7)-FLOAT(M)*SUM(8)**2
      VAVG=(SUM(1)*SUM(6)*SUM(7)+SUM(3)*SUM(4)*SUM(8)
     1   +SUM(2)*SUM(5)*SUM(8)-SUM(3)*SUM(6)*SUM(5)
     2   -SUM(2)*SUM(4)*SUM(7)-SUM(1)*SUM(8)**2)/DET
      A   =(FLOAT(M)*SUM(2)*SUM(7)+SUM(1)*SUM(5)*SUM(8)
     1   +SUM(3)*SUM(4)*SUM(5)-SUM(2)*SUM(5)**2
     2   -SUM(1)*SUM(4)*SUM(7)-FLOAT(M)*SUM(3)*SUM(8))/DET
      B   =(FLOAT(M)*SUM(3)*SUM(6)+SUM(2)*SUM(4)*SUM(5)
     1   +SUM(1)*SUM(4)*SUM(8)-SUM(1)*SUM(6)*SUM(5)
     2   -FLOAT(M)*SUM(2)*SUM(8)-SUM(3)*SUM(4)**2)/DET
      F   =A*SUM(9)+2.0*B*SUM(10)-A*VAVG*SUM(11)-2.0*B*VAVG*SUM(12)
     1   -A*SUM(13)-2.0*A*B*SUM(14)-A*B*SUM(15)-2.0*B*B*SUM(16)
      ENDIF
C
C   CHECK AND ADJUST FOR CONVERGENCE ON ROOT OF F
C
      IF(J .EQ. 1) FOLD=F
```

```
      FTEST=F/FOLD
      PHIOLD=PHI
      IF(KCHECK .EQ. 0 .AND. FTEST .GT. 0.0) THEN
        PHI=PHI+DPHI
      ELSE IF(KCHECK .EQ. 0 .AND. FTEST .LT. 0.0) THEN
        IF(FOLD .LT. 0.0) THEN
          KCHECK=1
          DPHI=DPHI/2.0
          PHI=PHI-DPHI
        ELSE IF(FOLD .GT. 0.0) THEN
          PHI=PHI+DPHI
        ELSE
          GO TO 70
        ENDIF
      ELSE IF(KCHECK .EQ. 1) THEN
        DPHI=DPHI/2.0
        IF(F .GT. 0.0) PHI=PHI-DPHI
        IF(F .LT. 0.0) PHI=PHI+DPHI
      ELSE IF(KCHECK .EQ. 0 .AND. FTEST .EQ. 0.0) THEN
        GO TO 70
      ENDIF
      WRITE(*,320) J,PHIOLD,DPHI,F
      WRITE(11,320) J,PHIOLD,DPHI,F
  320 FORMAT(' J=',I4,'  PHI=',F10.5,'  DPHI=',F12.7,'  F=',E14.6)
      FOLD=F
      IF(DPHI .GT. 1.E-04) GO TO 20
C
C   CONVERGES
C
   70 WRITE(*,231) J,PHI,DPHI
      WRITE(11,231) J,PHI,DPHI
  231 FORMAT(' CONVERGES IN ',I3,' STEPS;  PHI=',F10.4,'  DPHI=',E12.4)
      IF(ITYPE .EQ. '1') THEN
        WRITE(*,327) VAVG,A
        WRITE(11,327) VAVG,A
      ELSE
        WRITE(*,321) VAVG,A,B
        WRITE(11,321) VAVG,A,B
      ENDIF
  321 FORMAT(' THE AVERAGE VELOCITY       =',F14.3/
     1       ' THE AMPLITUDE OF COS(2*THET) =',F14.3/
     2       ' THE AMPLITUDE OF COS(4*THET) =',F14.3)
  327 FORMAT(' THE AVERAGE VELOCITY       =',F14.3/
     1       ' THE AMPLITUDE OF COS(2*THET) =',F14.3)
C
C   GET RESIDUALS
C
      SUMRES=0.0
      SUMRES2=0.0
      DO 75 N=1,M
        ANG=THET(N)*PI/180.0+PHI
        IF(ITYPE .EQ. '1') THEN
          VFITR=A*COS(2.0*ANG)+VAVG
        ELSE
          VFITR=A*COS(2.0*ANG)+B*COS(4.0*ANG)+VAVG
```

```
      ENDIF
      RES(N)=VELOC(N)-VFITR
      SUMRES=SUMRES+RES(N)
   75   SUMRES2=SUMRES2+RES(N)**2
     RESAVG=SUMRES/FLOAT(M)
     RESSIG=SQRT((SUMRES2-2.0*RESAVG*SUMRES)/FLOAT(M)+RESAVG**2)
     WRITE(*,238) (THET(N),RES(N),N=1,M)
     WRITE(11,238) (THET(N),RES(N),N=1,M)
  238 FORMAT(' THET=',F6.1,'  RESIDUAL=',F12.3)
     WRITE(*,239) RESAVG,RESSIG
     WRITE(11,239) RESAVG,RESSIG
  239 FORMAT(' AVG RESIDUAL=',F12.4/' STANDARD DEV=',F12.4)
     PHMIN=(PI/2.0-PHI)*180.0/PI
     IF(A .LT. 0.0) PHMIN=PHMIN+90.0
   80 IF(PHMIN .GT. 180.0) PHMIN=PHMIN-180.0
     IF(PHMIN .LT. 0.0) PHMIN=PHMIN+180.0
     WRITE(*,233) PHMIN
     WRITE(11,233) PHMIN
  233 FORMAT(//' *****  THE MINIMUM VELOCITY AZIMUTH IS ',F10.4,
    1     ' DEG CW FROM SCRIBE  *****'//)
     PRINT*,' DO YOU WANT A PLOT OF THE FIT: '
     READ(*,100) IPLOT
     IF(IPLOT .EQ. 'Y' .OR. IPLOT .EQ. 'y') THEN
       PRINT*,' INPUT A DESCRIPTION OF THE SAMPLE (50 CHAR MAX) |'
       PRINT*,' '
       READ(*,105) DEFCHAR
  105   FORMAT(A50)
       WRITE(11,105) DEFCHAR
       DTFIT=180/100.
       TFIT(1)=0.0
       DO 90 I=1,101
         IF(I .NE. 1) TFIT(I)=TFIT(I-1)+DTFIT
         IF(ITYPE .EQ. '1') THEN
           VFIT(I)=A*COS(2.*TFIT(I)/180.0*PI+2.*PHI)+VAVG
         ELSE IF(ITYPE .EQ. '2') THEN
           VFIT(I)=A*COS(2.*TFIT(I)/180.0*PI+2.*PHI)+B*COS(4.*
    1          TFIT(I)/180.0*PI+4.*PHI)+VAVG
   90    ENDIF
C
C  CALL PLOTTING ROUTINE
C  YOU MUST HAVE PLOT88 SOFTWARE TO USE THIS PLOTTING ROUTINE
C
      CALL VELPLOT(101,TFIT,VFIT,THET,VELOC,M,DEFCHAR,PHMIN,ITYPE,
    1          VAVG,A,B)
     ENDIF
     CLOSE (11)
     PRINT*,' DO YOU WANT TO ANALYZE ANOTHER SET OF DATA: '
     READ(*,100) IMORE
     IF(IMORE .EQ. 'Y' .OR. IMORE .EQ. 'y') GO TO 900
     STOP
     END
C
C
C
     SUBROUTINE VELPLOT(N,TFIT,VFIT,THET,VELOC,M,DEFCHAR,PHMIN,ITYPE,
```

```
     1              VAVG,A,B)
C
C  THIS PROGRAM PLOTS THE DATA AND THE FIT
C  PLOT88 SOFTWARE IS USED FOR THIS APPLICATION
C  SUBROUTINES AXES AND SETUP ARE ALSO USED FOR PLOT PURPOSES
C
     DIMENSION TFIT(101),VFIT(101),THET(51),VELOC(51)
     CHARACTER*1 ICH,IPL,IRP,ITRUE,ATEST,ITYPE
     CHARACTER*2 CTEXT
     CHARACTER*7 TRUANG
     CHARACTER*10 VUNITS,LTEXT
     CHARACTER*20 LEGTEX
     CHARACTER*11 UTEXT
     CHARACTER*21 YLAB
     CHARACTER*50 DEFCHAR
     IOC=97
     IOPR=0
     MC=97
     MP=60
     PRINT*,' PLOTS ARE SETUP FOR IBM EGA AND LASERJET PRINTER'
     PRINT*,' DO YOU WANT TO CHANGE THESE? '
     READ(*,100) ICH
  100 FORMAT(A1)
     IF(ICH .EQ. 'Y' .OR. ICH .EQ. 'y') CALL SETUP(IOC,MC,IOPR,MP)
    1 IDEV=IOC
     JDEV=MC
     IPL='N'
     TSTART=0.0
     TSTEP=30.0
     TMAX=180.0
     TESTA=0.0
     TESTB=1.E+10
     DO 2 I=1,M
       IF(VELOC(I) .GT. TESTA) TESTA=VELOC(I)
    2  IF(VELOC(I) .LT. TESTB) TESTB=VELOC(I)
     DO 3 I=1,N
       IF(VFIT(I) .GT. TESTA) TESTA=VFIT(I)
    3  IF(VFIT(I) .LT. TESTB) TESTB=VFIT(I)
     WRITE(*,201) TESTB,TESTA
  201 FORMAT(' VMIN=',F10.2,' VMAX=',F10.2,' INPUT VO,VSTEP,',
     1'VMAX: ')
     READ(*,*) VELO,VELSTEP,VELMAX
     PRINT*,' INPUT VELOCITY UNITS FOR PLOT (10 CHAR MAX): '
     READ(*,110) VUNITS
  110 FORMAT(A10)
       DO 6 LL=1,10
         LM=11-LL
         ATEST=VUNITS(LM:LM)
    6    IF(ATEST .NE. ' ') GO TO 7
    7 UTEXT=VUNITS(1:LM)//')'
     YLAB='VELOCITY '//'('//UTEXT
     NLAB=11+LM
     PRINT*,' DO YOU WANT TO PUT TRUE ORIENTATION ON THE PLOT? '
     READ(*,100) ITRUE
     IF(ITRUE .EQ. 'Y') THEN
```

```
      PRINT*,' INPUT TRUE ORIENTATION (E.G., N103E): '
      READ(*,108) TRUANG
108   FORMAT(A7)
    ENDIF
 10 CALL PLOTS(0,IDEV,JDEV)
    XMAX=10.0
    YMAX=8.0
    CALL WINDOW(0.,0.,12.,10.)
    IF(IPL .EQ. 'Y' .OR. IPL .EQ. 'y') CALL FACTOR(0.68)
    OX=1.7
    OY=1.5
    IF(IPL .EQ. 'Y' .OR. IPL .EQ. 'y') THEN
      OX=2.0
      OY=2.0
      IF(MP .EQ. 62) CALL NEWPEN(2)
      IF(MP .EQ. 64) CALL NEWPEN(3)
    ENDIF
    CALL COLOR(11,IERR)
    CALL XAXIS(OX,OY,'ANGLE(DEG)',10,XMAX,TSTART,TSTEP,TMAX,0)
    CALL YAXIS(OX,OY,YLAB,NLAB,YMAX,VELO,VELSTEP,VELMAX,0)
      CALL COLOR(10,IERR)
      DO 15 I=1,M
        X=THET(I)/TMAX*XMAX+OX
        YP=(VELOC(I)-VELO)/(VELMAX-VELO)*YMAX+OY
 15     CALL SYMBOL(X,YP,0.14,CHAR(0),0.0,-1)
      DO 25 I=1,101
        X=TFIT(I)/TMAX*XMAX+OX
        YP=(VFIT(I)-VELO)/(VELMAX-VELO)*YMAX+OY
        IF(I .EQ. 1) CALL PLOT(X,YP,3)
 25     IF(I .GT. 1) CALL PLOT(X,YP,2)
 30   CONTINUE
    CALL COLOR(14,IERR)
    XP=OX+PHMIN/TMAX*XMAX
    YP=OY+5.0
    CALL PLOT(XP,YP,3)
    CALL PLOT(XP,YP+1.0,2)
    CALL GETNUM(PHMIN,1,LTEXT,NC)
    CALL GETWID(0.2222,LTEXT,NC,WID)
    CALL SYMBOL(XP-WID/2.0,YP-0.4,0.2222,LTEXT,0.,NC)
    IF(ITRUE .EQ. 'Y') THEN
      DO 33 LL=1,7
        LM=8-LL
        ATEST=TRUANG(LM:LM)
 33     IF(ATEST .NE. ' ') GO TO 34
 34   CALL GETWID(0.2222,TRUANG,LM,WID)
      CALL SYMBOL(XP-WID/2.0,YP+1.2,0.2222,TRUANG,0.,LM)
    ENDIF
    CALL COLOR(12,IERR)
    CALL SYMBOL(OX+0.2,YMAX+0.2+OY,0.2222,DEFCHAR,0.0,50)
    CALL COLOR(14,IERR)
    IF(ITYPE .EQ. '1') CALL SYMBOL(OX+5.8,OY+0.1,0.2222,
   1              'V=VAVG+A*COS(2*THET)',0.0,20)
    IF(ITYPE .EQ. '2') CALL SYMBOL(OX+3.5,OY+0.1,0.2222,
   1              'V=VAVG+A*COS(2*THET)+B*COS(4*THET)',0.0,34)
    IF((XP-OX) .GE. (XMAX/1.7)) THEN
```

```
      XP2=XP-XMAX/2.0
      IF(XP2 .LT. (OX+0.2)) XP2=OX+0.2
    ELSE
      XP2=XP+XMAX/2.0-1.2
      IF(XP2 .GT. (8.0+OX)) XP2=8.0+OX
    ENDIF
    CALL GETNUM(VAVG,0,LTEXT,NC)
    LEGTEX='VAVG='//LTEXT
    CALL SYMBOL(XP2,OY+2.2,0.2,LEGTEX,0.,NC+5)
    CALL GETNUM(A,1,LTEXT,NC)
    LEGTEX='  A='//LTEXT
    CALL SYMBOL(XP2,OY+1.9,0.2,LEGTEX,0.,NC+5)
    IF(ITYPE .EQ. '2') THEN
      CALL GETNUM(B,1,LTEXT,NC)
      LEGTEX='  B='//LTEXT
      CALL SYMBOL(XP2,OY+1.6,0.2,LEGTEX,0.,NC+5)
    ENDIF
    CALL PLOT(0.0,0.0,999)
    IF(IPL .EQ. 'Y' .OR. IPL .EQ. 'y') GO TO 90
    PRINT*,' DO YOU WANT A HARDCOPY OF THIS PLOT: '
    READ(*,100) IPL
    IF(IPL .EQ. 'Y' .OR. IPL .EQ. 'y') THEN
      PRINT*,' PLOTTING IN PROGRESS '
      IDEV=IOP
      JDEV=MP
      GO TO 10
    ENDIF
 90 CONTINUE
    PRINT*,' DO YOU WANT TO REPLOT THE VELOCITY DATA? '
    READ(*,100) IRP
    IF(IRP .EQ. 'Y' .OR. IRP .EQ. 'y') GO TO 1
    RETURN
    END
    SUBROUTINE XAXIS(XO,YA,LTEXT,NT,XMAX,XSTART,XINT,XEND,IDEC)
    CHARACTER*10 CTEXT
    CHARACTER*30 LTEXT
    YO=YA-0.025
    CALL PLOT(XO-0.025,YO,3)
    CALL PLOT(XO+XMAX,YO,2)
    XLAB=XSTART+XINT
    AY=(XEND-XSTART)/XINT
    IY=AINT(AY+0.0001)
    DX=XMAX/AY
    X=XO+DX
    IF(IDEC .EQ. 0) ID=-1
    IF(IDEC .GT. 0) ID=IDEC
    CALL GETNUM(XSTART,ID,CTEXT,NC)
    CALL GETWID(0.2222,CTEXT,NC,WID)
    XS=XO-WID/2.0
    YS=YO-0.4
    CALL SYMBOL(XS,YS,0.2222,CTEXT,0.,NC)
    DO 10 I=1,IY
      CALL PLOT(X,YO,3)
      CALL PLOT(X,YO-0.1,2)
      CALL GETNUM(XLAB,ID,CTEXT,NC)
```

```
      CALL GETWID(0.2222,CTEXT,NC,WID)
      XS=X-WID/2.0
      CALL SYMBOL(XS,YS,0.2222,CTEXT,0.,NC)
      XLAB=XLAB+XINT
   10 X=X+DX
    CALL GETWID(0.25,LTEXT,NT,WID)
    XS=XO+XMAX/2.0-WID/2.0
    YS=YO-0.85
    CALL SYMBOL(XS,YS,0.25,LTEXT,0.,NT)
    RETURN
    END
C
C
C
    SUBROUTINE YAXIS(XA,YO,LTEXT,NT,YMAX,YSTART,YINT,YEND,IDEC)
    CHARACTER*10 CTEXT
    CHARACTER*30 LTEXT
    XO=XA-0.025
    CALL PLOT(XO,YO-0.025,3)
    CALL PLOT(XO,YO+YMAX,2)
    YLAB=YSTART+YINT
    AY=(YEND-YSTART)/YINT
    IY=AINT(AY+0.0001)
    DY=YMAX/AY
    Y=YO+DY
    IF(IDEC .EQ. 0) ID=-1
    IF(IDEC .GT. 0) ID=IDEC
    CALL GETNUM(YSTART,ID,CTEXT,NC)
    CALL GETWID(0.2222,CTEXT,NC,WID)
    WIDMAX=WID
    XS=XO-0.15-WID
    YS=YO
    CALL SYMBOL(XS,YS,0.2222,CTEXT,0.,NC)
    DO 10 I=1,IY
      CALL PLOT(XO,Y,3)
      CALL PLOT(XO-0.1,Y,2)
      CALL GETNUM(YLAB,ID,CTEXT,NC)
      CALL GETWID(0.2222,CTEXT,NC,WID)
      IF(WID .GT. WIDMAX) WIDMAX=WID
      XS=XO-0.15-WID
      YS=Y-0.125
      CALL SYMBOL(XS,YS,0.2222,CTEXT,0.,NC)
      YLAB=YLAB+YINT
   10 Y=Y+DY
    CALL GETWID(0.25,LTEXT,NT,WID)
    XS=XO-0.35-WIDMAX
    YS=YO+YMAX/2.0-WID/2.0
    CALL SYMBOL(XS,YS,0.25,LTEXT,90.0,NT)
    RETURN
    END
    SUBROUTINE SETUP(IOPORC,MODELC,IOPORP,MODELP)
    CHARACTER*1 ITRUE
    PRINT*,' TO GET PLOT OUTPUT, CHOOSE OUTPUT PORT AND MODEL'
    PRINT*,' SEE PLOT88 MANUAL FOR DETAILED INFORMATION'
    PRINT*,' ************************************************'
```

```
      PRINT*,' FIRST CHOOSE THE CONSOLE VALUES'
      PRINT*,' ************************************************'
      PRINT*,' 99 ---- HERCULES GRAPHICS CARD'
      PRINT*,' 99 ---- IBM COLOR GRAPHICS ADAPTOR, 640X200 (COLOR OR
     1B & W)'
      PRINT*,'        IBM ENHANCED GRAPHICS ADAPTOR'
      PRINT*,' 94 ---- 64K, 320X200 (16 COLOR)'
      PRINT*,' 95 ---- 64K, 640X200 (16 COLOR)'
      PRINT*,' 99 ---- 64K, 640X200 (2 COLOR)'
      PRINT*,' 96 ---- 128K, 640X350 (4 COLOR-MONO)'
      PRINT*,' 99 ---- 64K, 640X200 (2 COLOR)'
      PRINT*,' 94 ---- 64K, 320X200 (16 COLOR)'
      PRINT*,' 95 ---- 64K, 640X200 (16 COLOR)'
      PRINT*,' 97 ---- 128K, 640X350 (16 COLOR)'
      PRINT*,' ************************************************'
      PRINT*,' INPUT THE CONSOLE VALUE: '
      READ(*,*) IOPORC
      MODELC=IOPORC
      PRINT*,' '
      PRINT*,' ************************************************'
      PRINT*,' NEXT CHOOSE THE PRINTER VALUE'
      PRINT*,' ASSUMES THE PRINTER PORT IS PRN OR LPT1; IS THIS TRUE? '
      READ(*,100) ITRUE
  100 FORMAT(A1)
      IOPORP=0
      IF(ITRUE .EQ. 'N' .OR. ITRUE .EQ. 'n') THEN
        PRINT*,' SEE PLOT88 MANUAL FOR DETAILED INFO'
        PRINT*,' INPUT CORRECT PRINTER PORT CODE: '
        READ(*,*) IOPORP
      ENDIF
      PRINT*,' NEXT CHOOSE PRINTER MODEL TYPE'
      PRINT*,' ************************************************'
      PRINT*,' 0 ---- EPSON FX-80, SINGLE DENSITY'
      PRINT*,' 1 ---------- DOUBLE DENSITY'
      PRINT*,' 2 ---------- DOUBLE SPEED, DUAL DENSITY'
      PRINT*,' 3 ---------- QUAD DENSITY'
      PRINT*,' 4 ---------- CRT GRAPHICS I'
      PRINT*,' 5 ---------- PLOTTER GRAPHICS'
      PRINT*,' 6 ---------- CRT GRAPHICS II'
      PRINT*,' 1 ---------- IBM GRAPHICS AND PROPRINTERS'
      PRINT*,' 60 --- HP LASERJET, 75 DOTS/INCH'
      PRINT*,' 62 ---------- 150 DOTS/INCH'
      PRINT*,' 64 ---------- 350 DOTS/INCH'
      PRINT*,' FOR OTHER PRINTERS, SEE PLOT88 MANUAL'
      PRINT*,' ************************************************'
      PRINT*,' INPUT PRINTER MODEL CODE: '
      READ(*,*) MODELP
      PRINT*,' ********** SETUP IS COMPLETE **********'
      RETURN
      END
```

Example input data set from a file (data can also be input by hand).
First line (number of points).
Succeeding lines give azimuth and velocity in any unit.

```
    13
 12.00000000  10023.00000000
 27.00000000   9830.00000000
 42.00000000   9888.00000000
 57.00000000  10176.00000000
 72.00000000  10581.00000000
 87.00000000  11112.00000000
102.00000000  11496.00000000
117.00000000  11637.00000000
132.00000000  11340.00000000
147.00000000  10965.00000000
162.00000000  10683.00000000
177.00000000  10286.00000000
177.00000000  10286.00000000
```

Example of output data file

```
  INPUT FILE NAME = SFE414.DAT
   13 DATA POINTS

  OUTPUT FILE NAME = SFE414.OUT
*****   NUMBER OF TIME STEPS =  13   *****
 THET=    12.00 VELOC=   10023.00000
 THET=    27.00 VELOC=    9830.00000
 THET=    42.00 VELOC=    9888.00000
 THET=    57.00 VELOC=   10176.00000
 THET=    72.00 VELOC=   10581.00000
 THET=    87.00 VELOC=   11112.00000
 THET=   102.00 VELOC=   11496.00000
 THET=   117.00 VELOC=   11637.00000
 THET=   132.00 VELOC=   11340.00000
 THET=   147.00 VELOC=   10965.00000
 THET=   162.00 VELOC=   10683.00000
 THET=   177.00 VELOC=   10286.00000
 THET=   177.00 VELOC=   10286.00000
J=  1 PHI=  0.00000 DPHI=  0.2617994 F= 0.209111E+07
```

```
J=  2 PHI=  0.26180 DPHI=  0.2617994 F= 0.554277E+06
J=  3 PHI=  0.52360 DPHI=  0.2617994 F=-0.146218E+07
J=  4 PHI=  0.78540 DPHI=  0.2617994 F=-0.230521E+07
J=  5 PHI=  1.04720 DPHI=  0.2617994 F=-0.724928E+06
J=  6 PHI=  1.30900 DPHI=  0.1308997 F= 0.137838E+07
J=  7 PHI=  1.17810 DPHI=  0.0654498 F= 0.405326E+06
J=  8 PHI=  1.11265 DPHI=  0.0327249 F=-0.152078E+06
J=  9 PHI=  1.14537 DPHI=  0.0163625 F= 0.130579E+06
J= 10 PHI=  1.12901 DPHI=  0.0081812 F=-0.996907E+04
J= 11 PHI=  1.13719 DPHI=  0.0040906 F= 0.605231E+05
J= 12 PHI=  1.13310 DPHI=  0.0020453 F= 0.253323E+05
J= 13 PHI=  1.13106 DPHI=  0.0010227 F= 0.768952E+04
J= 14 PHI=  1.13003 DPHI=  0.0005113 F=-0.113450E+04
J= 15 PHI=  1.13054 DPHI=  0.0002557 F= 0.328082E+04
J= 16 PHI=  1.13029 DPHI=  0.0001278 F= 0.107451E+04
J= 17 PHI=  1.13016 DPHI=  0.0000639 F=-0.333035E+02
CONVERGES IN  17 STEPS;  PHI=   1.1302  DPHI= 0.6392E-04
THE AVERAGE VELOCITY       =    10676.270
THE AMPLITUDE OF COS(2*THET) =     846.685
THE AMPLITUDE OF COS(4*THET) =      54.049
THET=  12.0  RESIDUAL=    72.003
THET=  27.0  RESIDUAL=   -54.819
THET=  42.0  RESIDUAL=  -103.440
THET=  57.0  RESIDUAL=   -90.119
THET=  72.0  RESIDUAL=   -93.524
THET=  87.0  RESIDUAL=   -10.667
THET= 102.0  RESIDUAL=    29.360
THET= 117.0  RESIDUAL=    61.994
THET= 132.0  RESIDUAL=   -63.287
THET= 147.0  RESIDUAL=   -56.322
THET= 162.0  RESIDUAL=   112.271
THET= 177.0  RESIDUAL=    98.316
THET= 177.0  RESIDUAL=    98.316
AVG RESIDUAL=     0.0063
STANDARD DEV=    78.2950


***** THE MINIMUM VELOCITY AZIMUTH IS   25.2429 DEG CW FROM
SCRIBE *****


SFE-4  ASR 14  7422.4-7422.8 FT
```

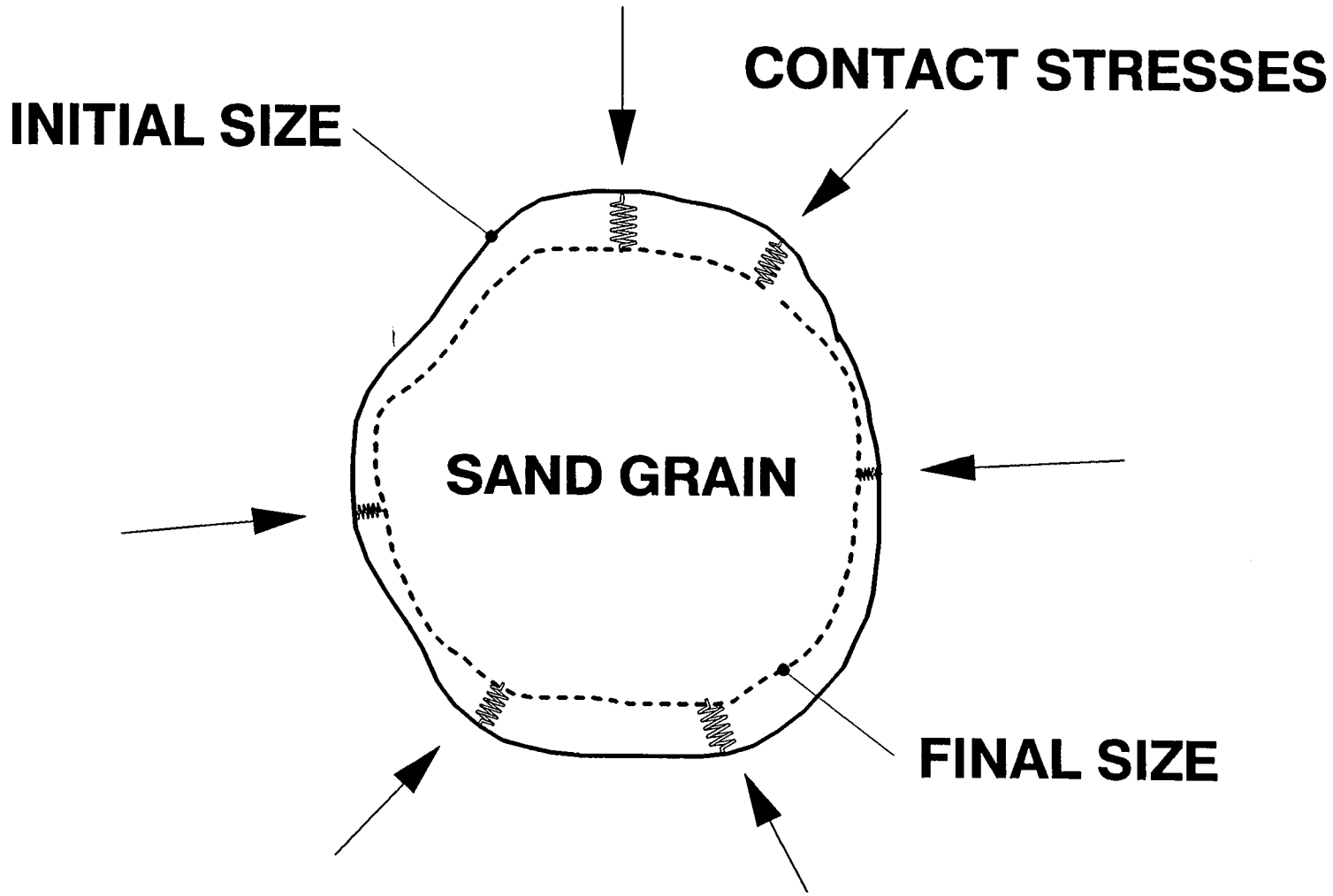

Figure 1. Schematic of stored energy with sand grain.

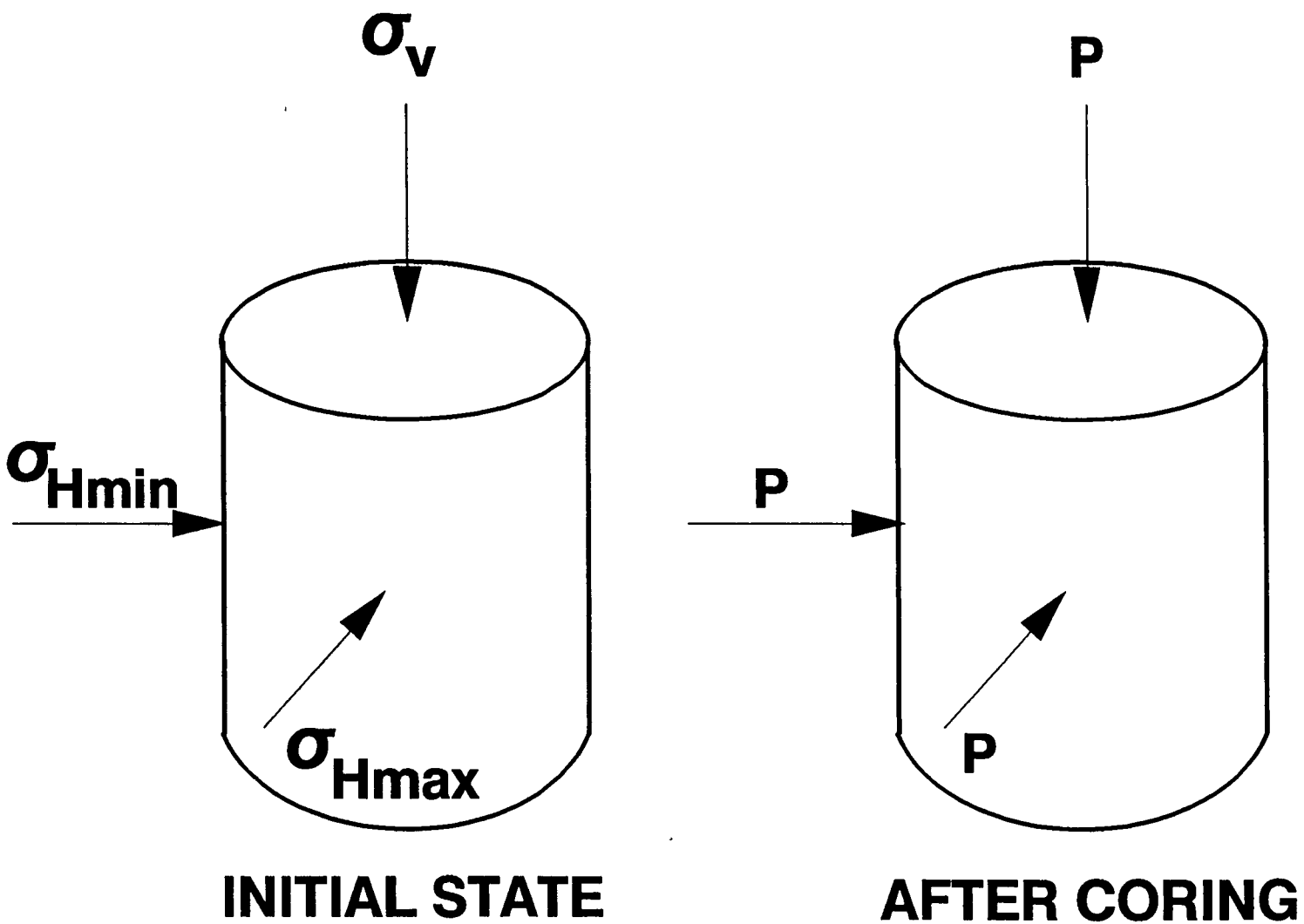

Figure 2. Stress state before and after coring.

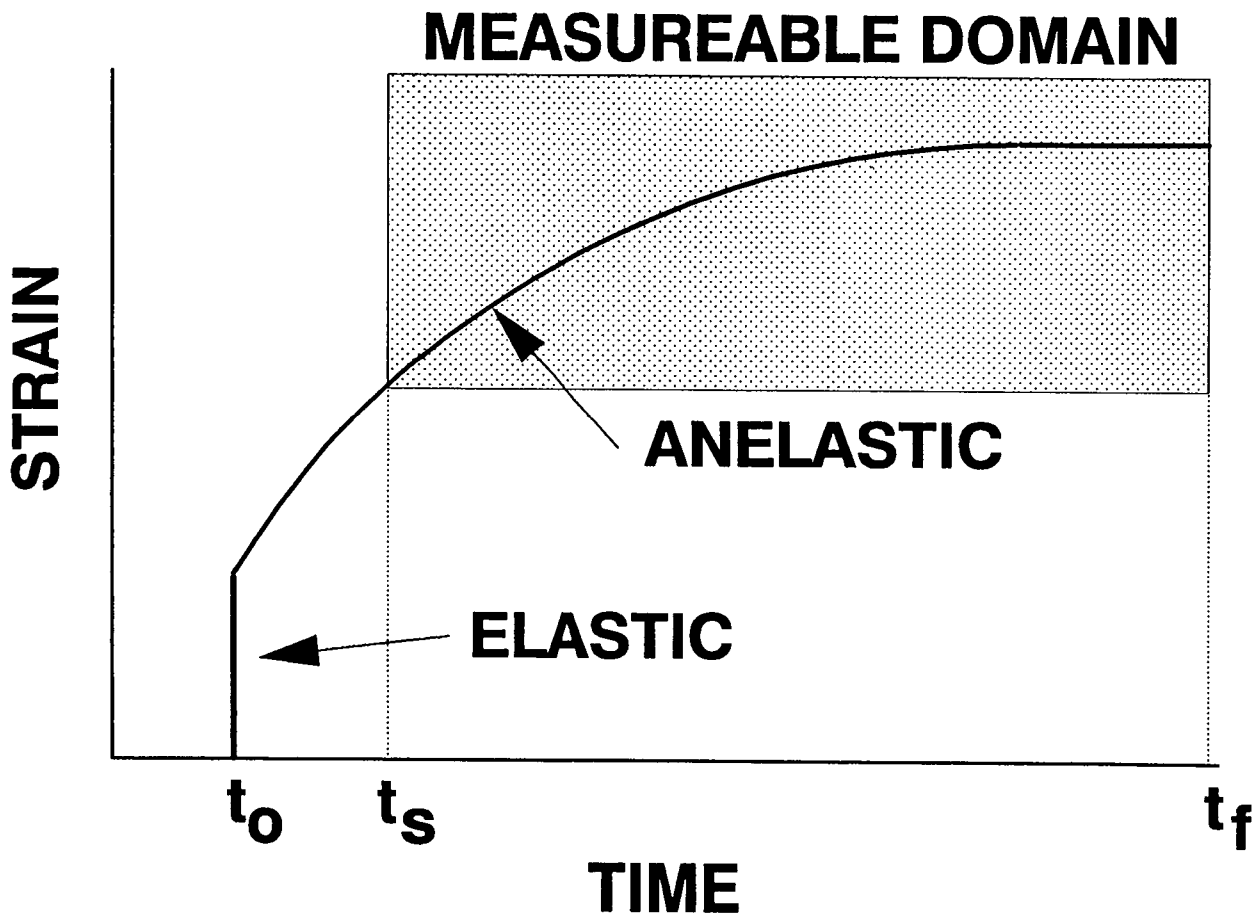

Figure 3. Time dependent strain recovery after coring.

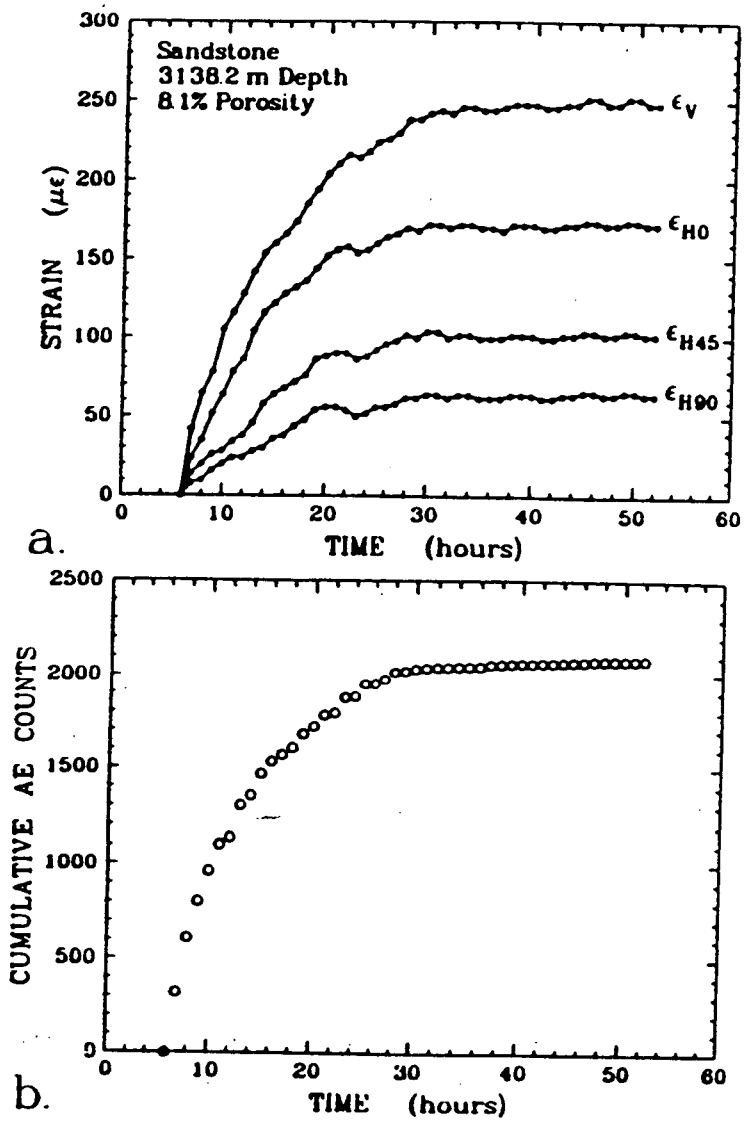

Figure 4. Correlation of strain and acoustic emissions after coring.[8]

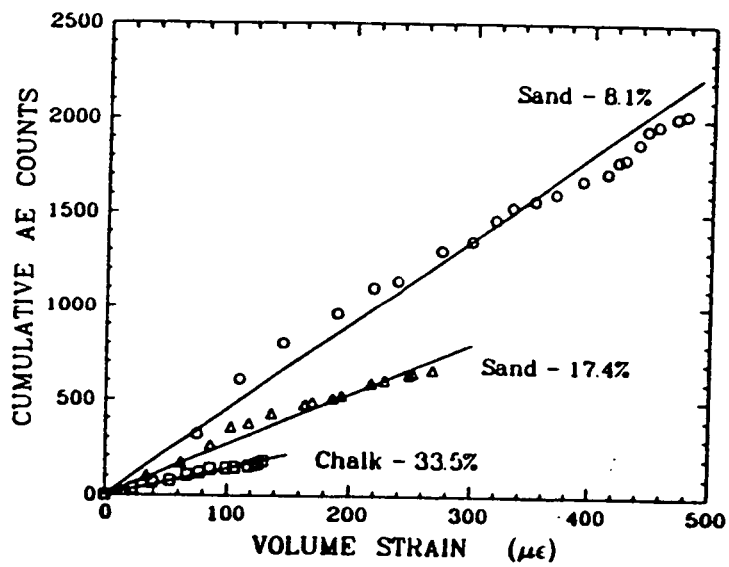

Figure 5. Correlation between acoustic emissions and volume strain.[8]

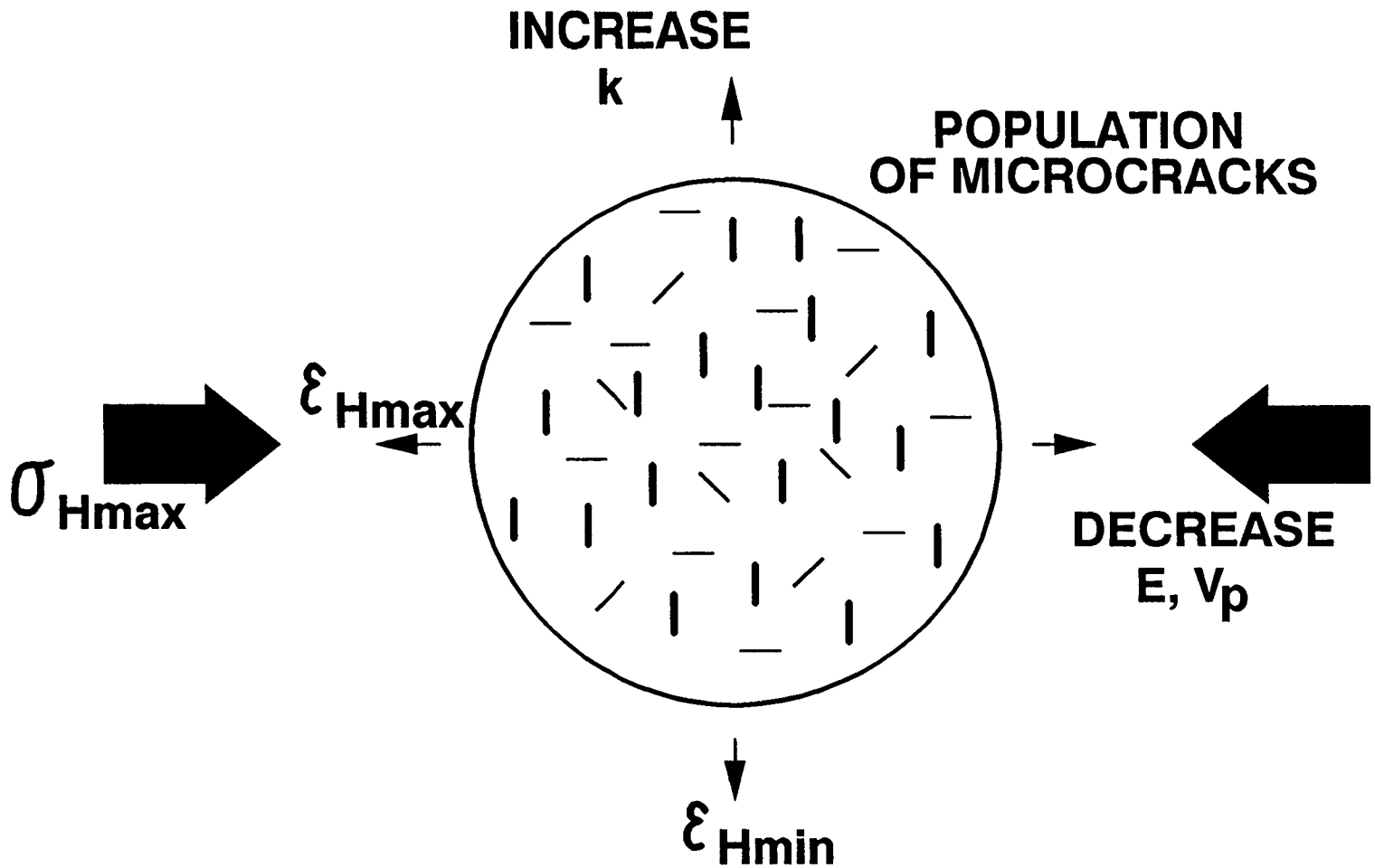

Figure 6. Schematic of microcrack effects.

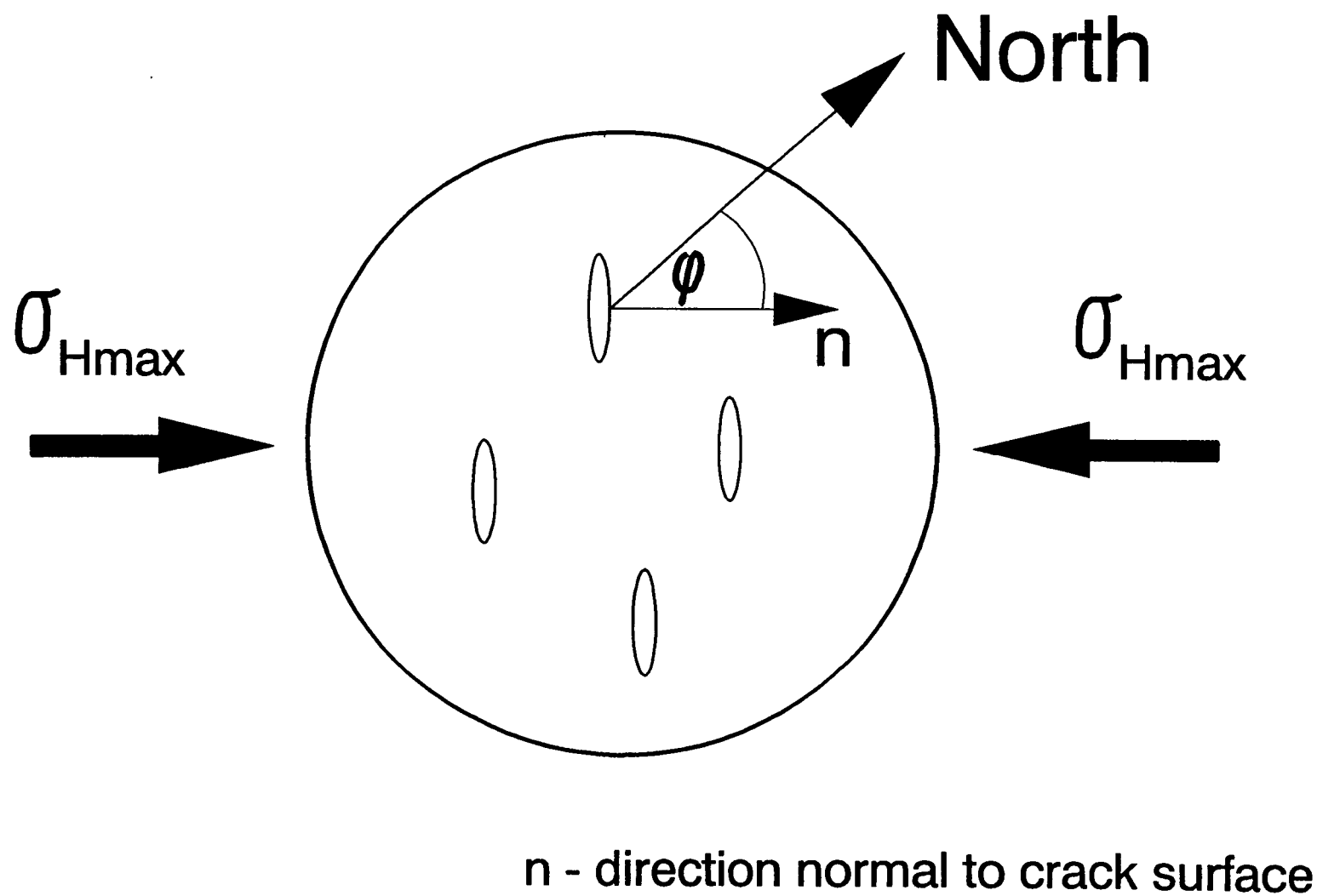

Figure 7. Geometry for preferrentially oriented microcracks.

Figure 8. Intragranular tectonic microcracks in sandstone.

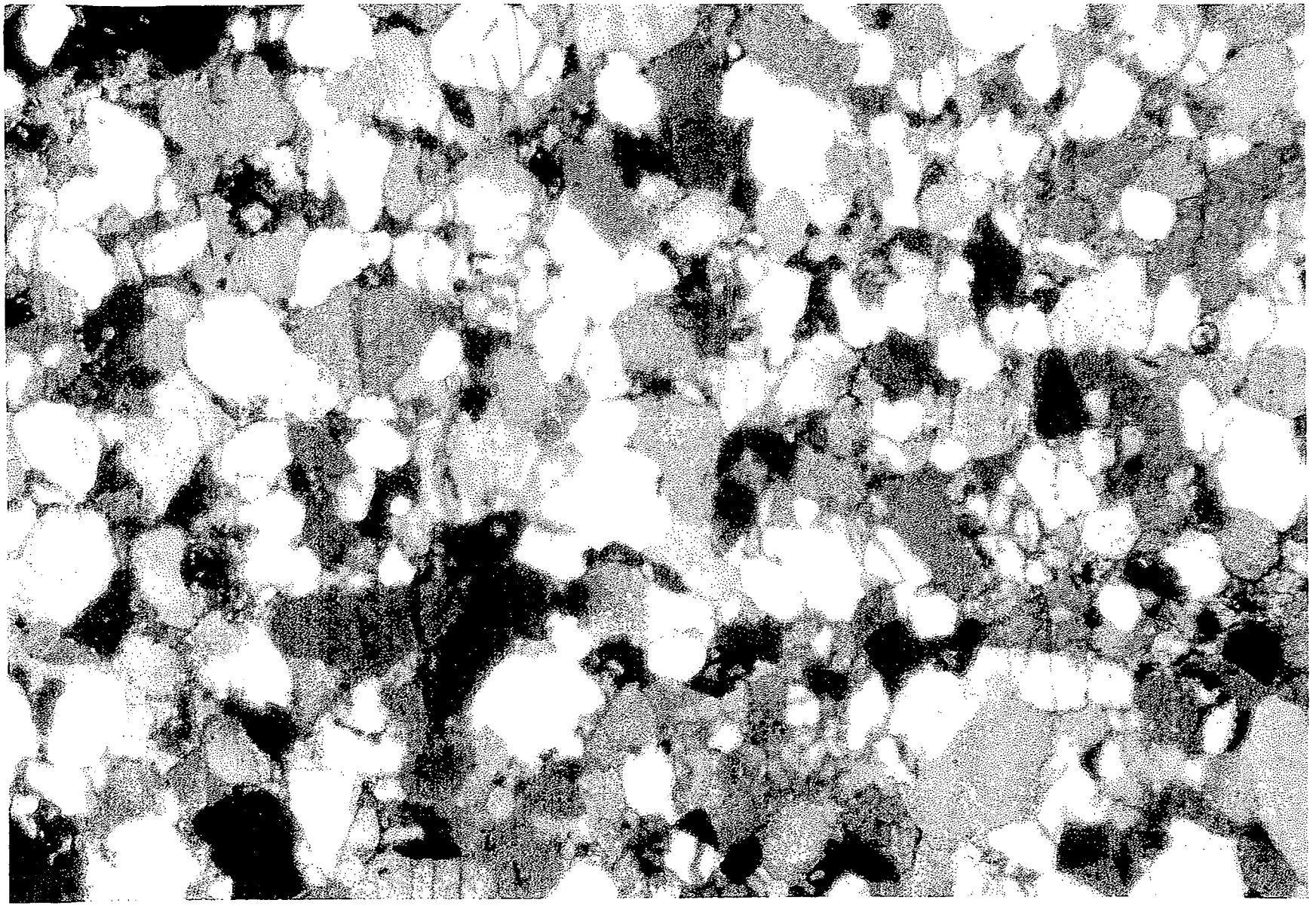

Figure 9. Zone of tectonic microcracks.

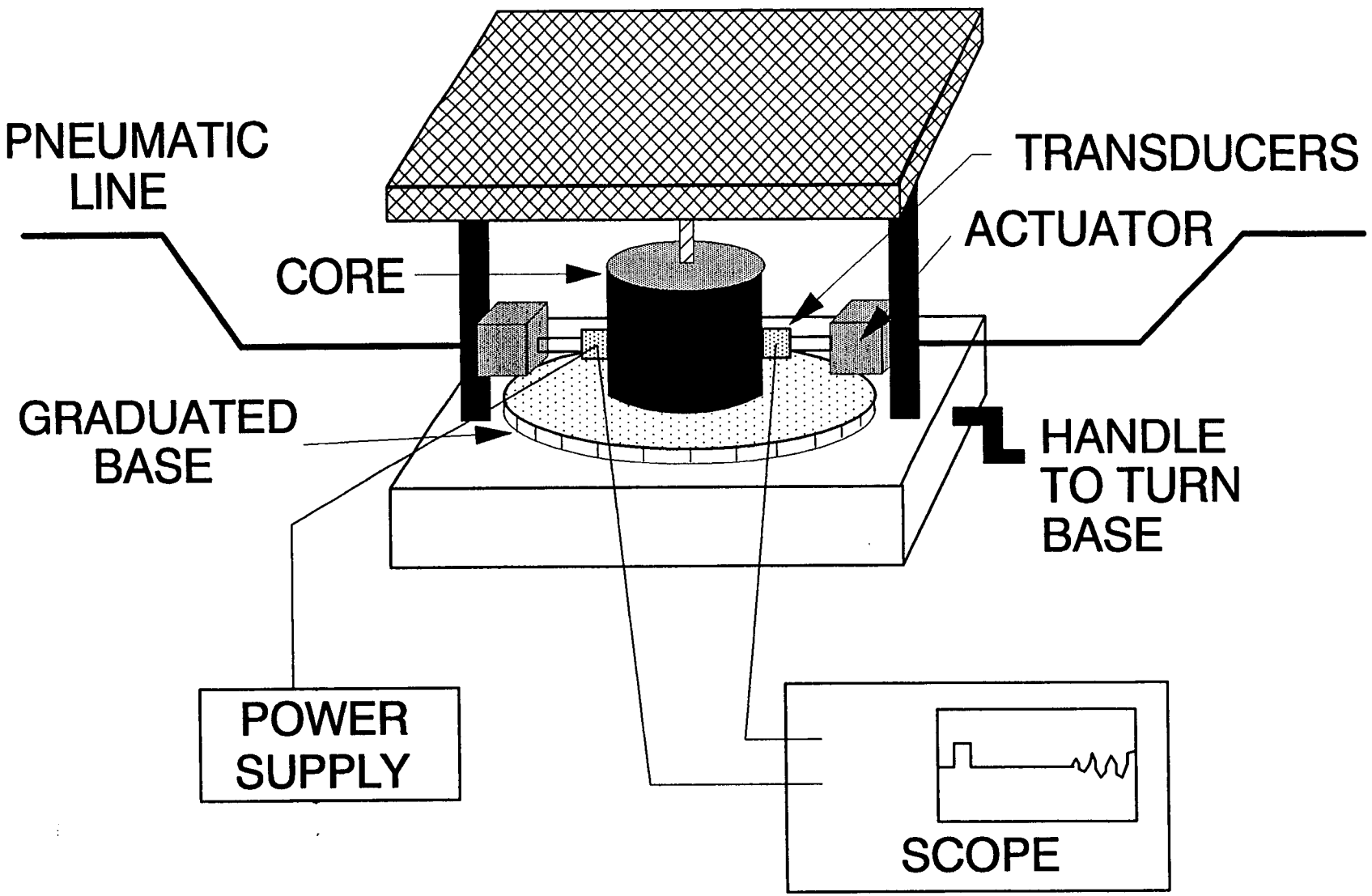

Figure 10. Schematic of circumferential velocity anisotropy apparatus.

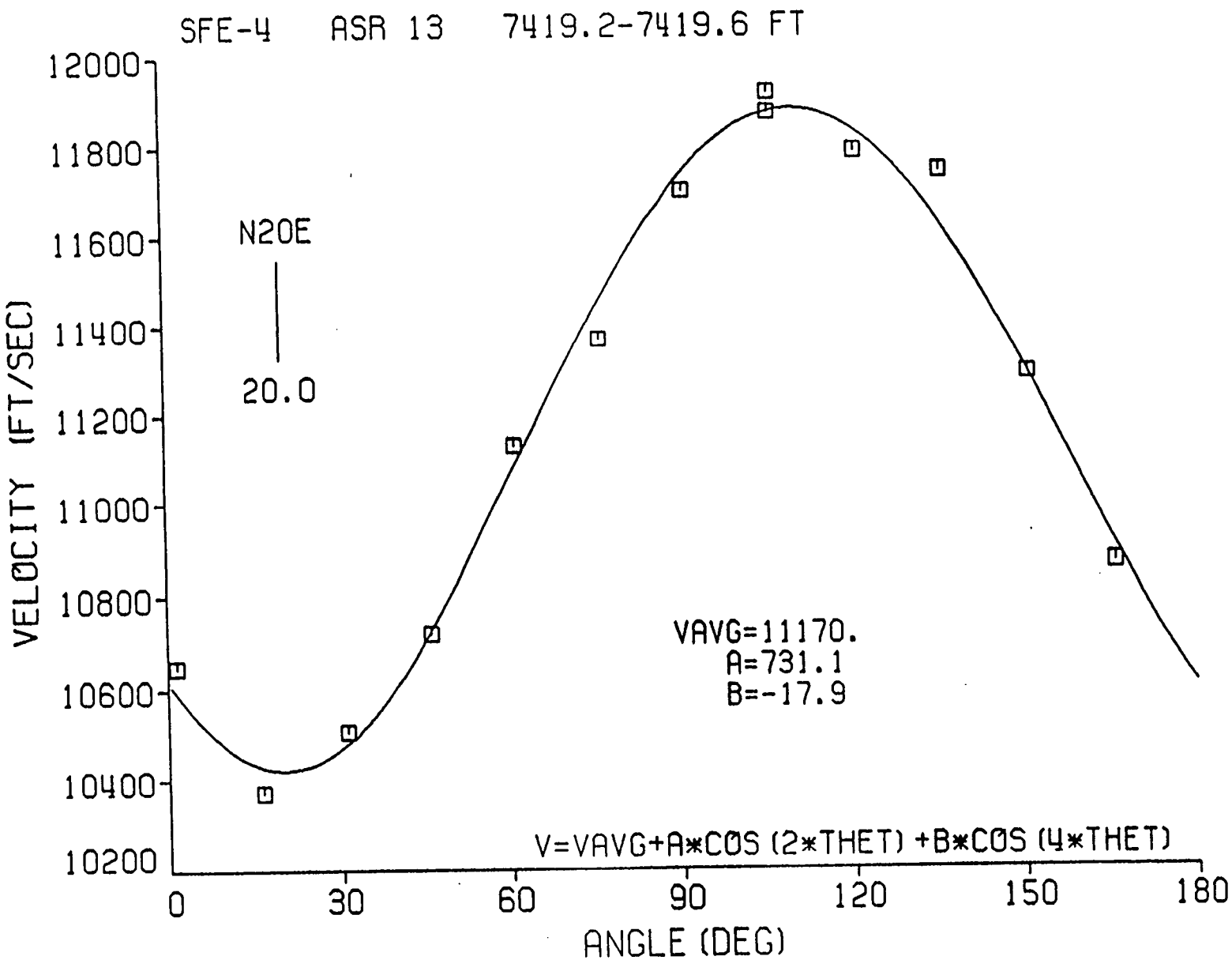

Figure 11. CVA data for SFE-4, ASR-13.

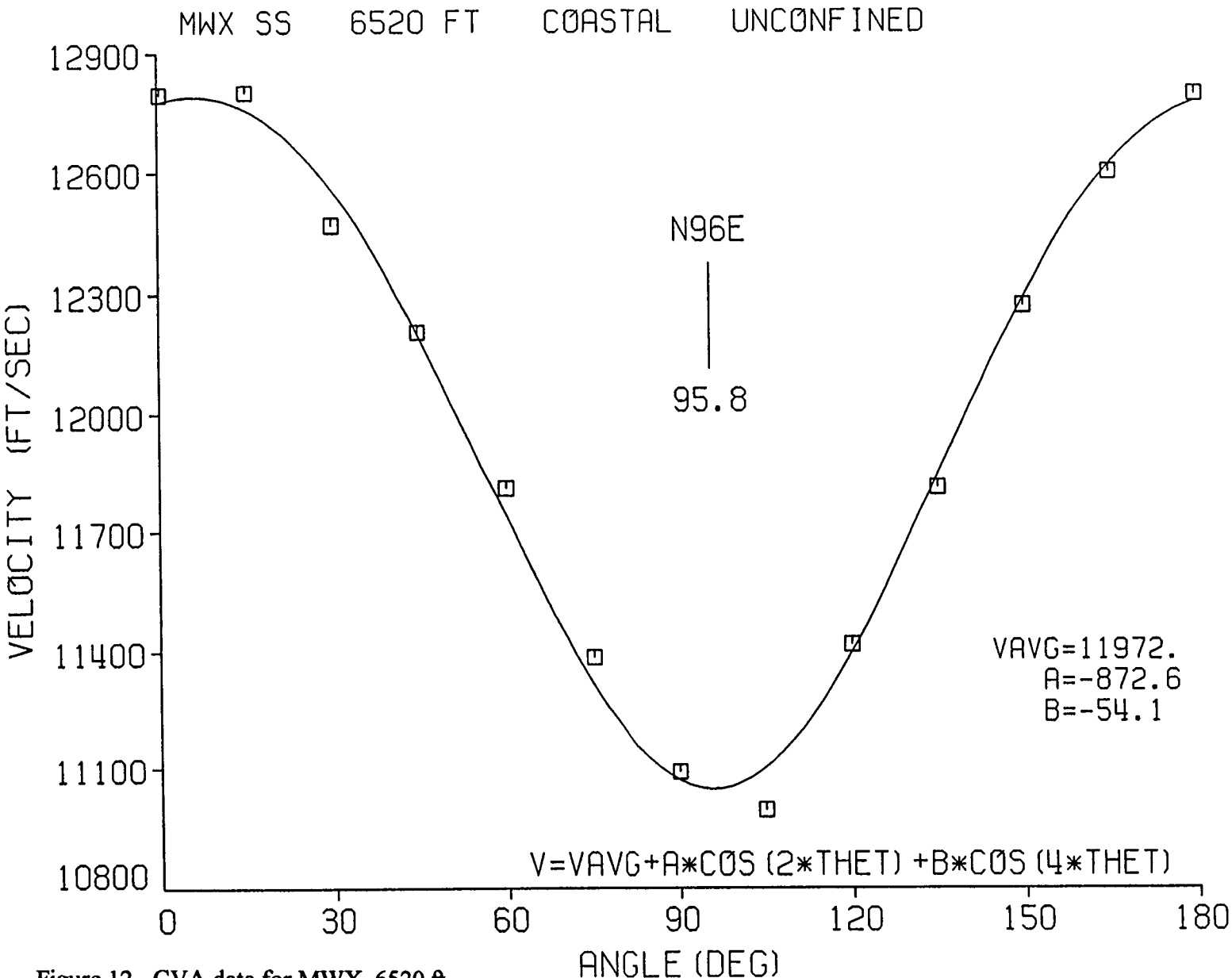

Figure 12. CVA data for MWX, 6520 ft.

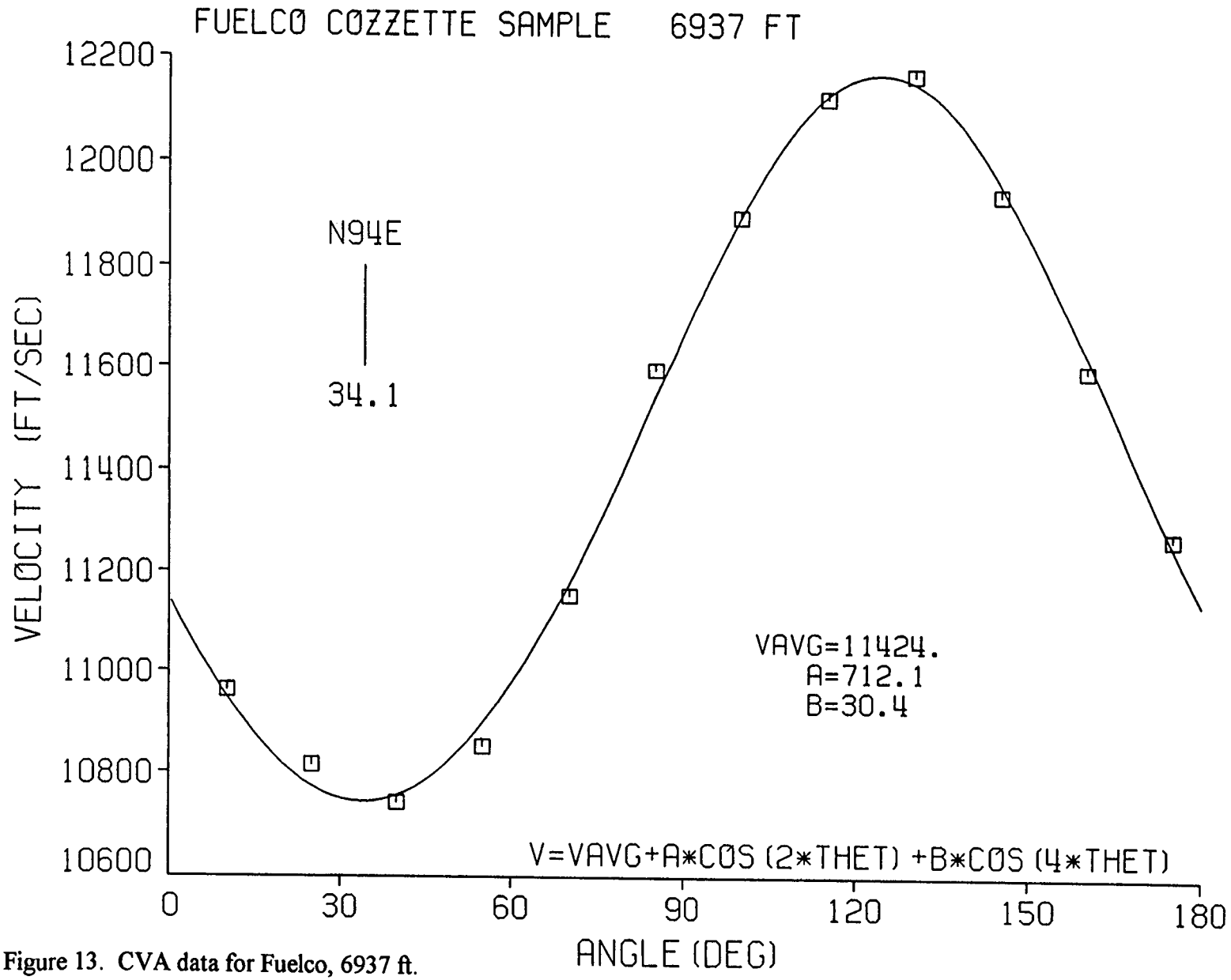

Figure 13. CVA data for Fuelco, 6937 ft.

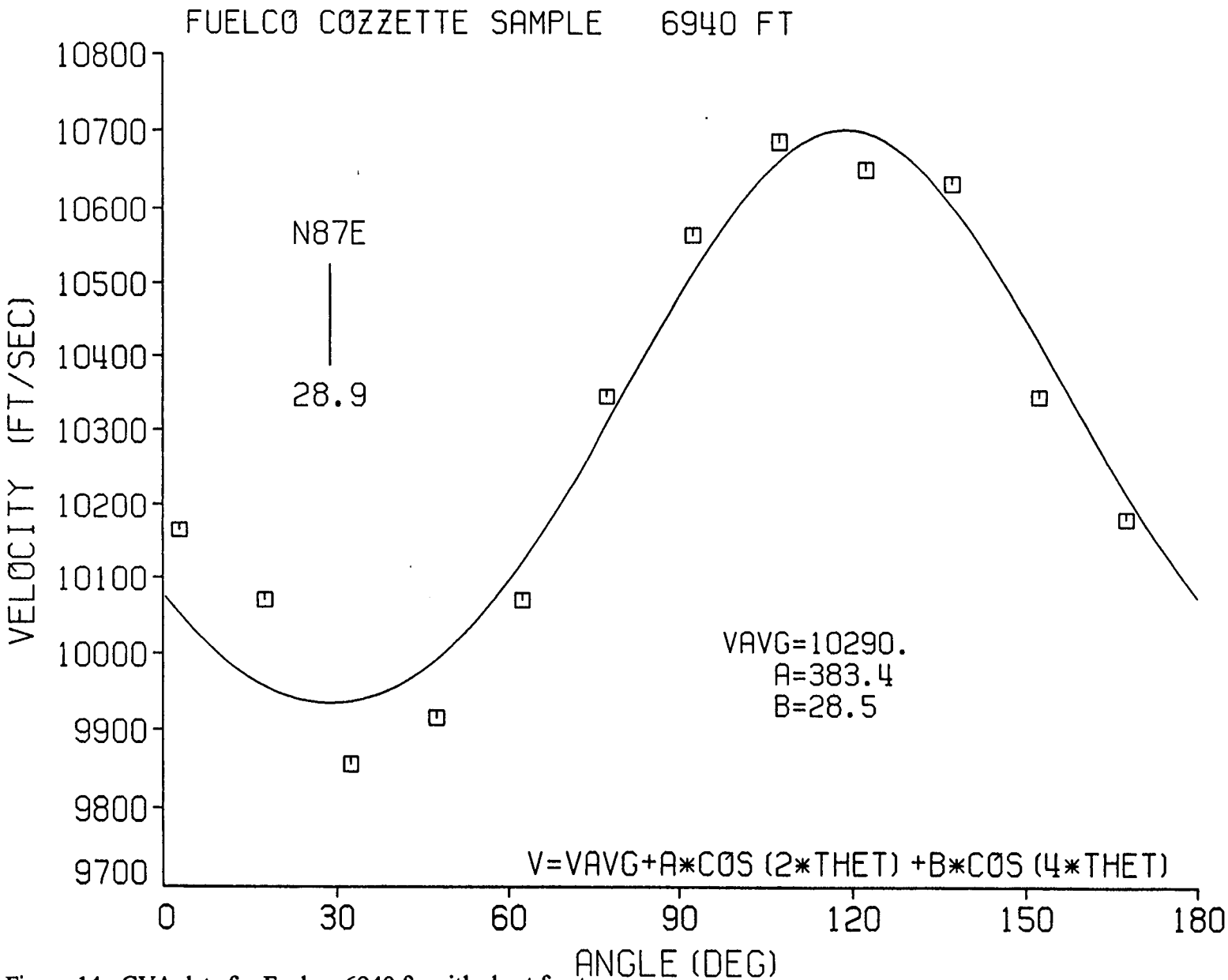

Figure 14. CVA data for Fuelco, 6940 ft, with short fracture.

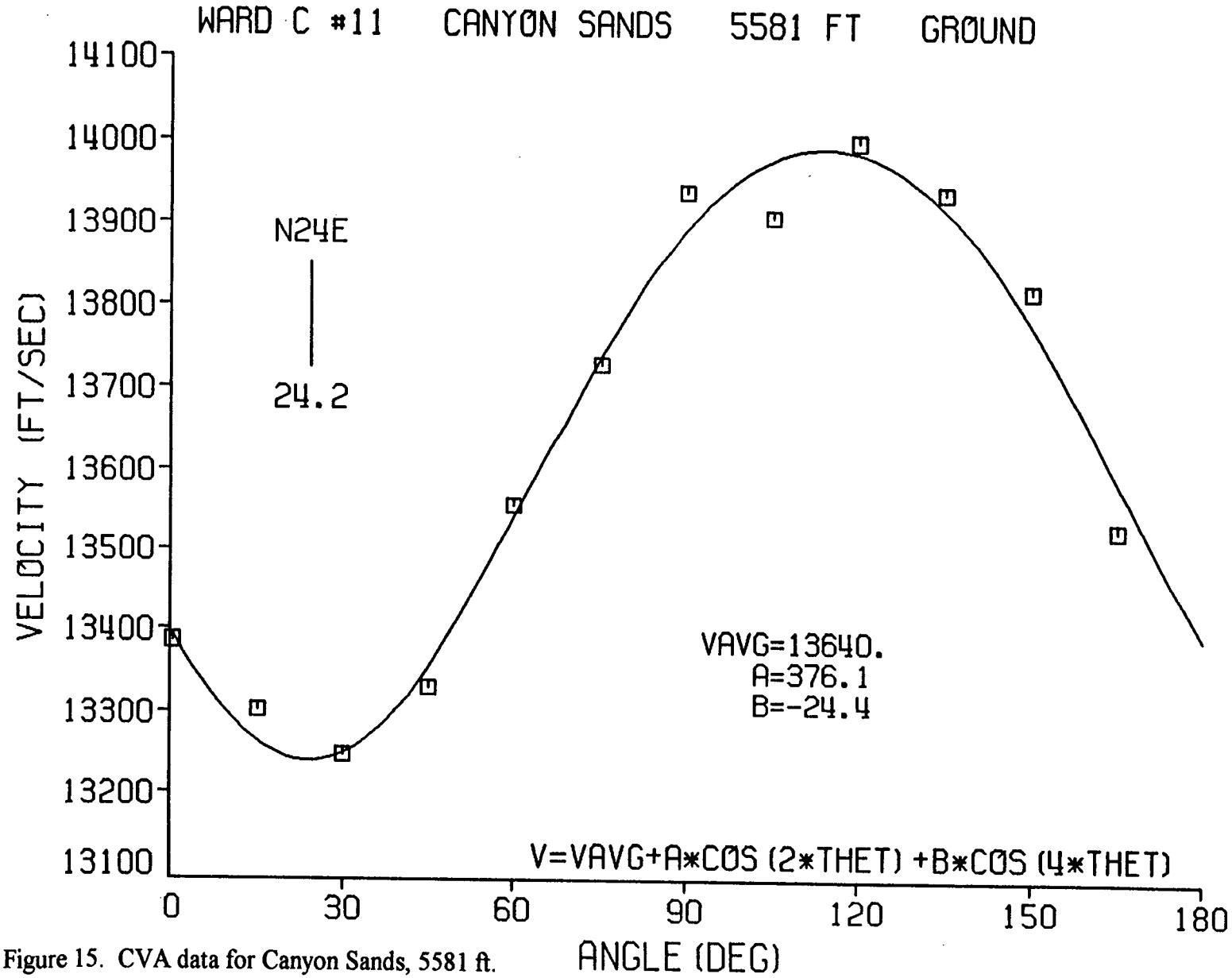

Figure 15. CVA data for Canyon Sands, 5581 ft.

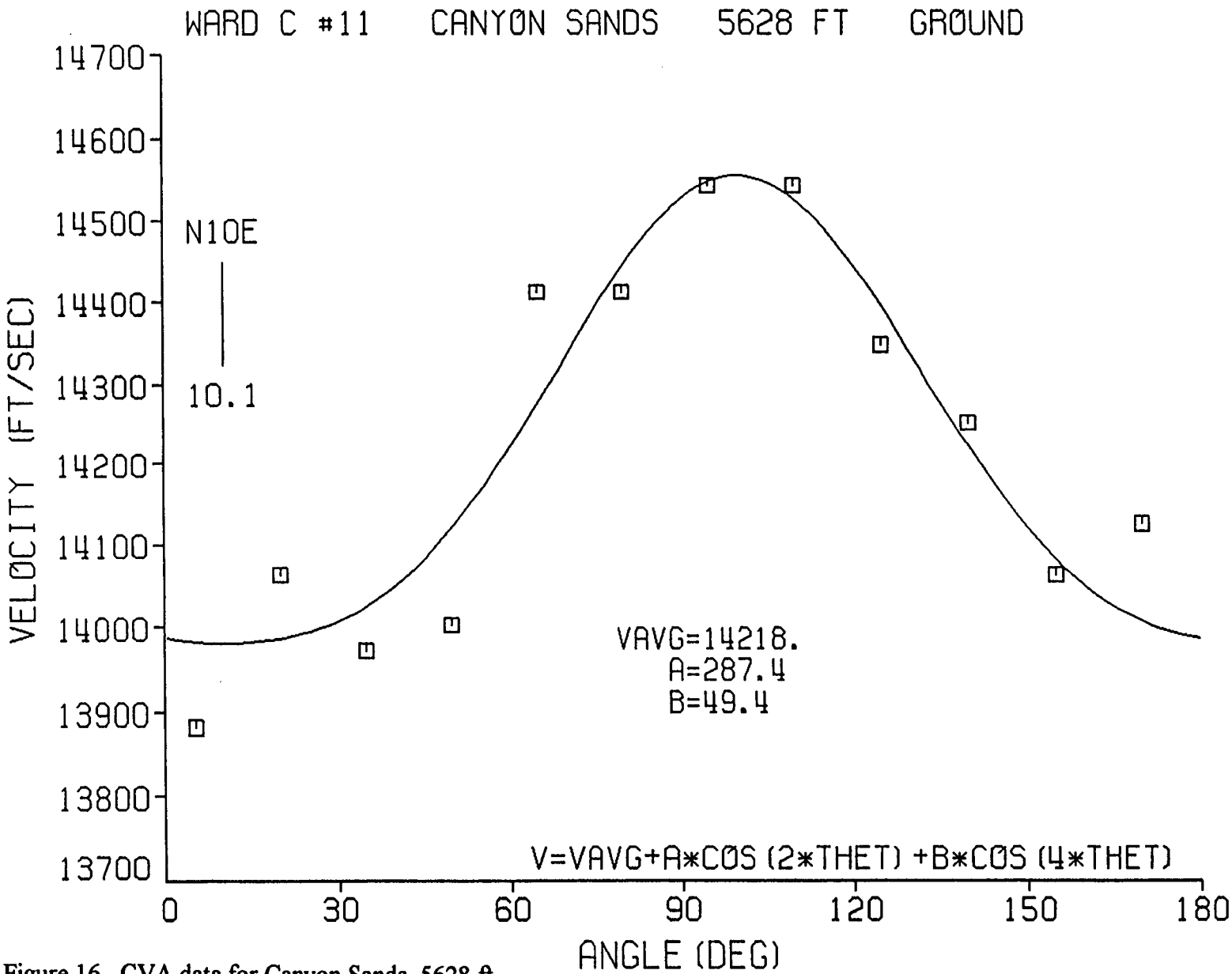

Figure 16. CVA data for Canyon Sands, 5628 ft.

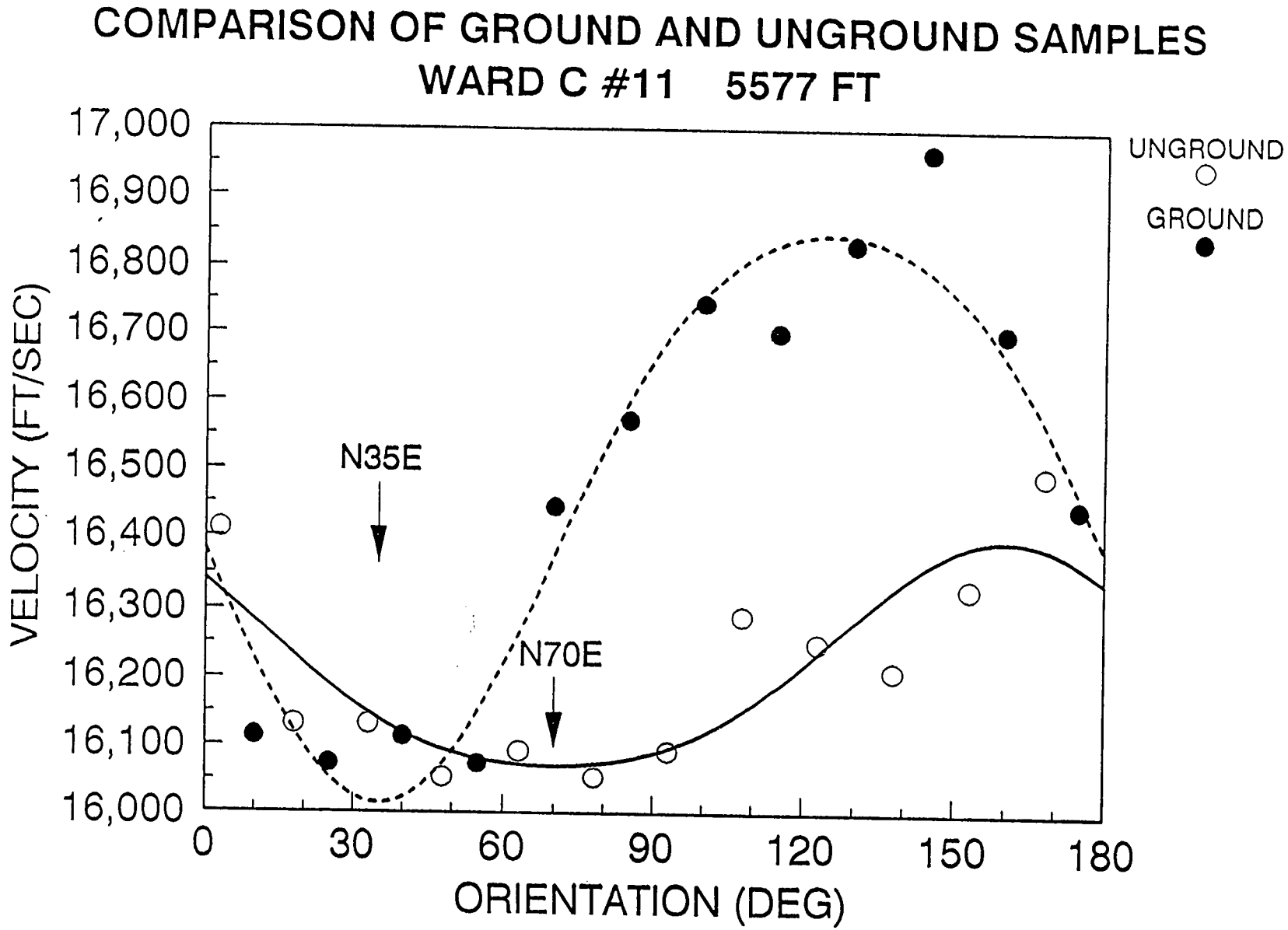

Figure 17. CVA data, as-received and ground, for Canyon Sands, 5577 ft.

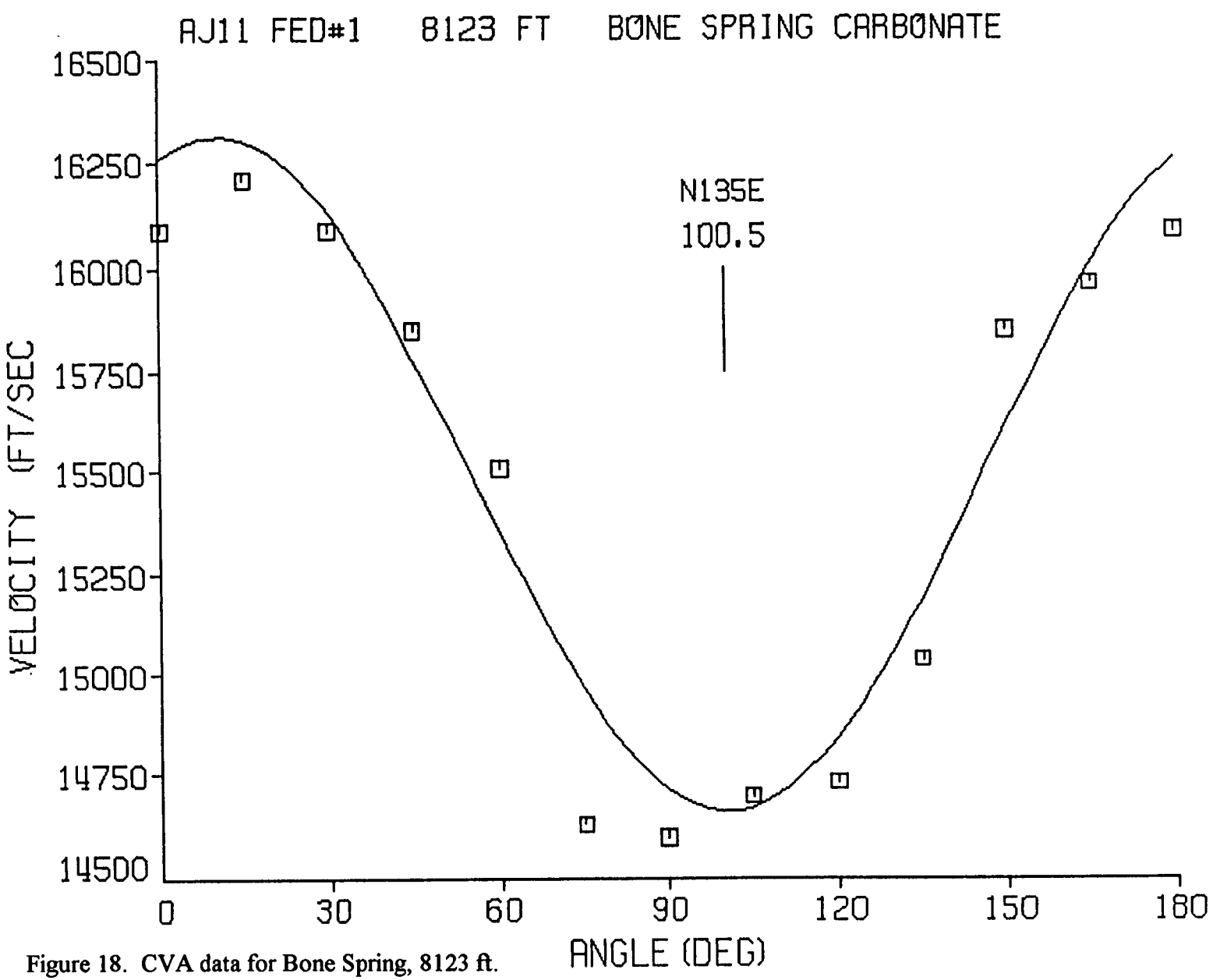

Figure 18. CVA data for Bone Spring, 8123 ft.

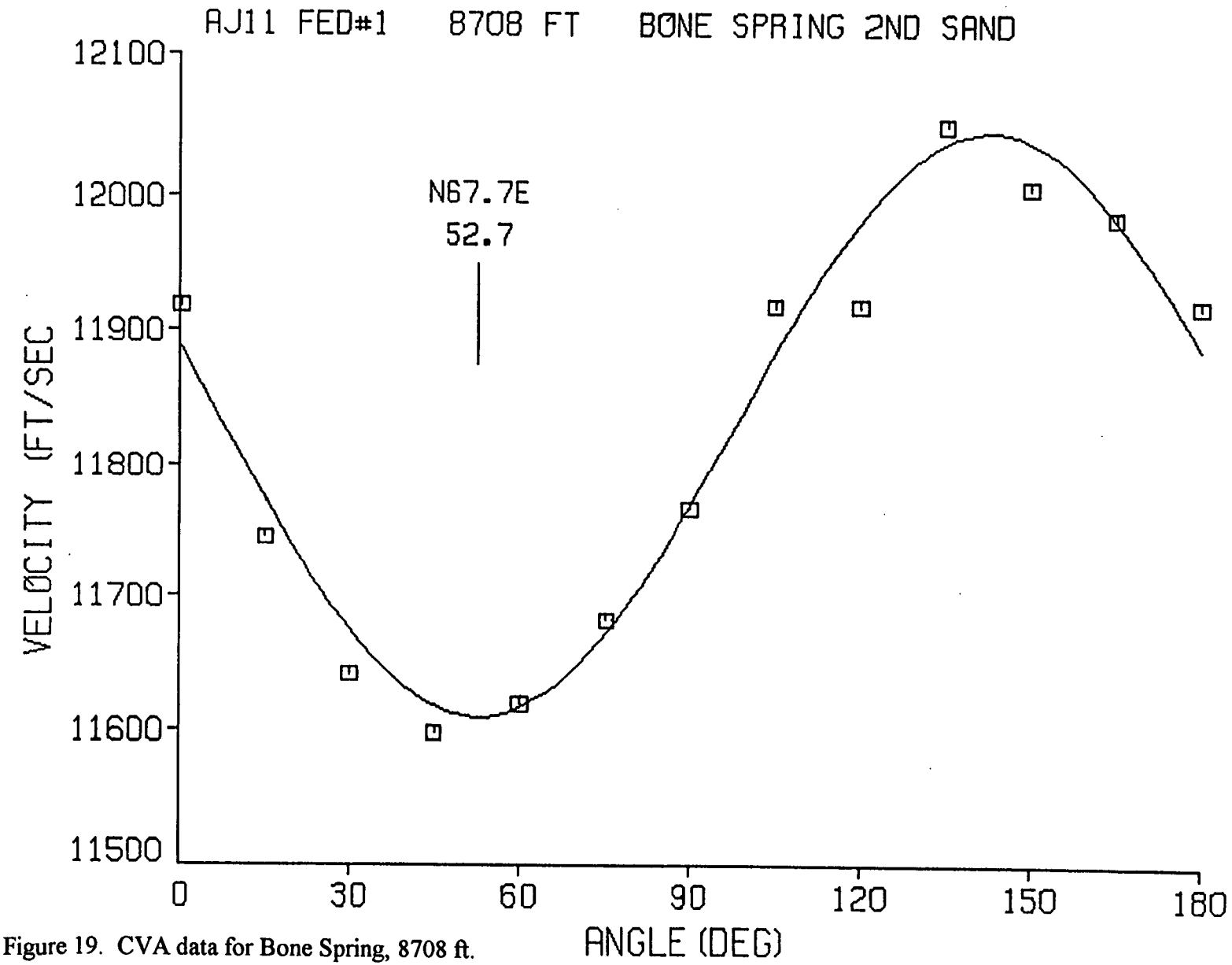

Figure 19. CVA data for Bone Spring, 8708 ft.

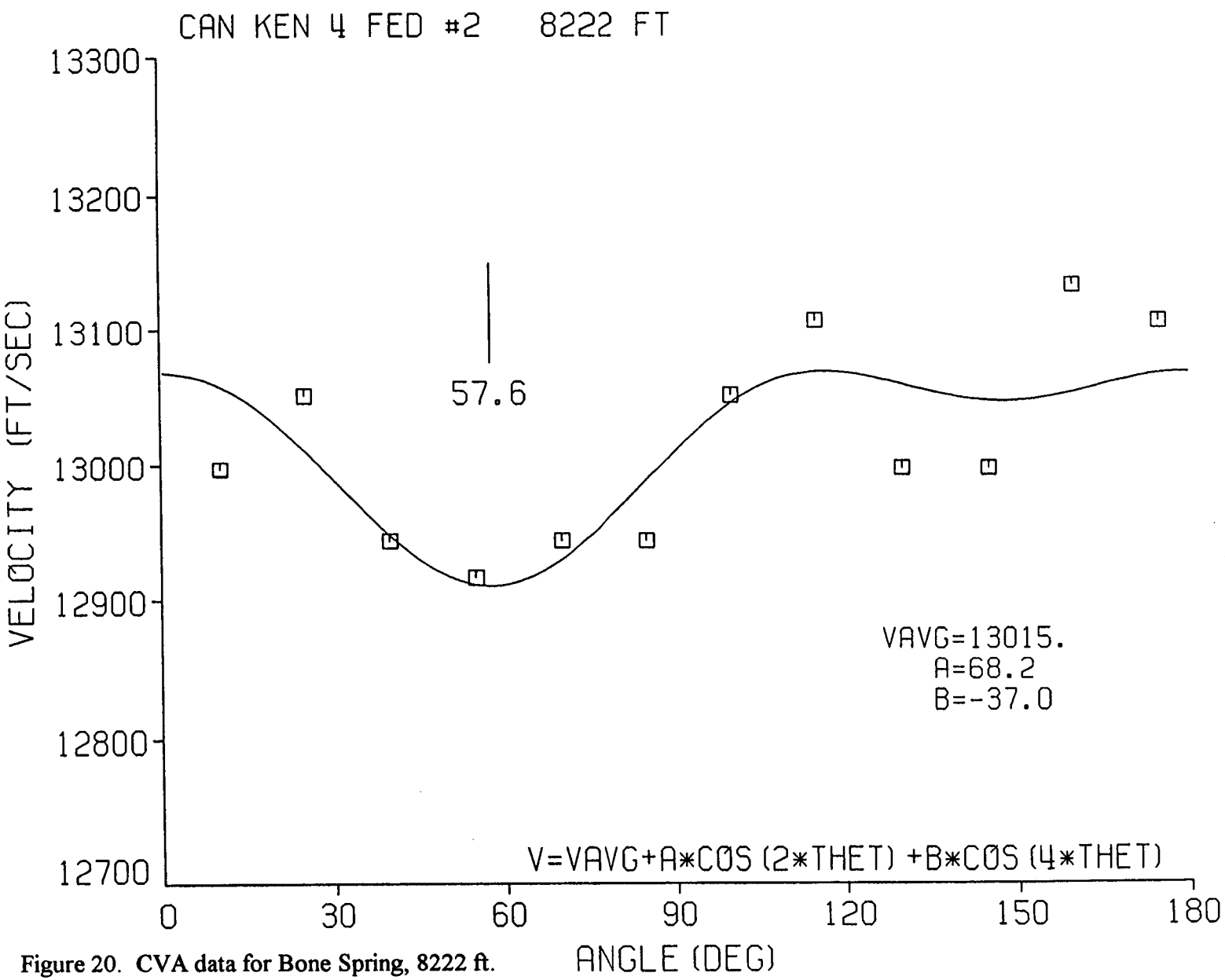

Figure 20. CVA data for Bone Spring, 8222 ft.

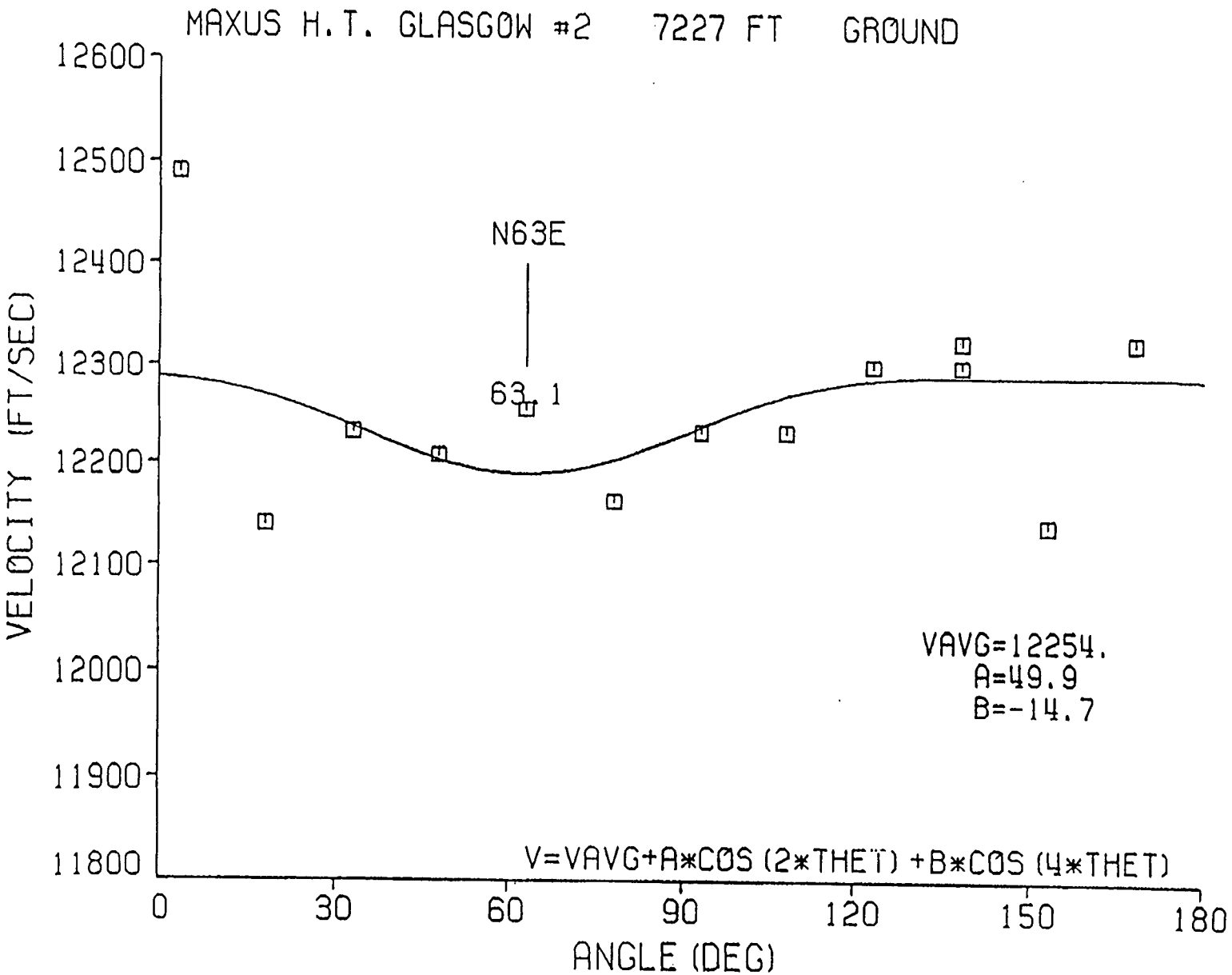

Figure 21. CVA data for Cleveland sandstone, 7227 ft.

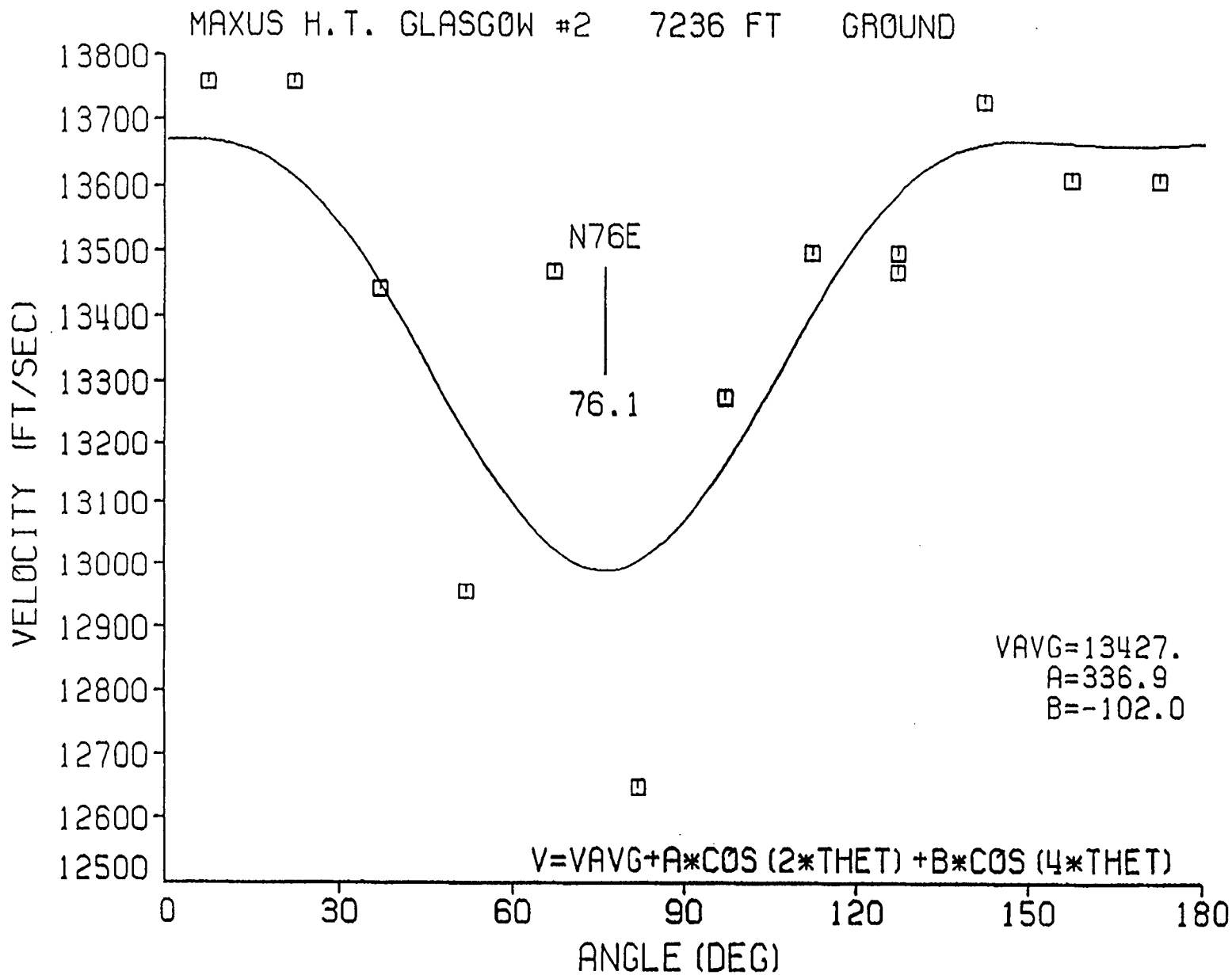

Figure 22. CVA data for Cleveland sandstone, 7236 ft.

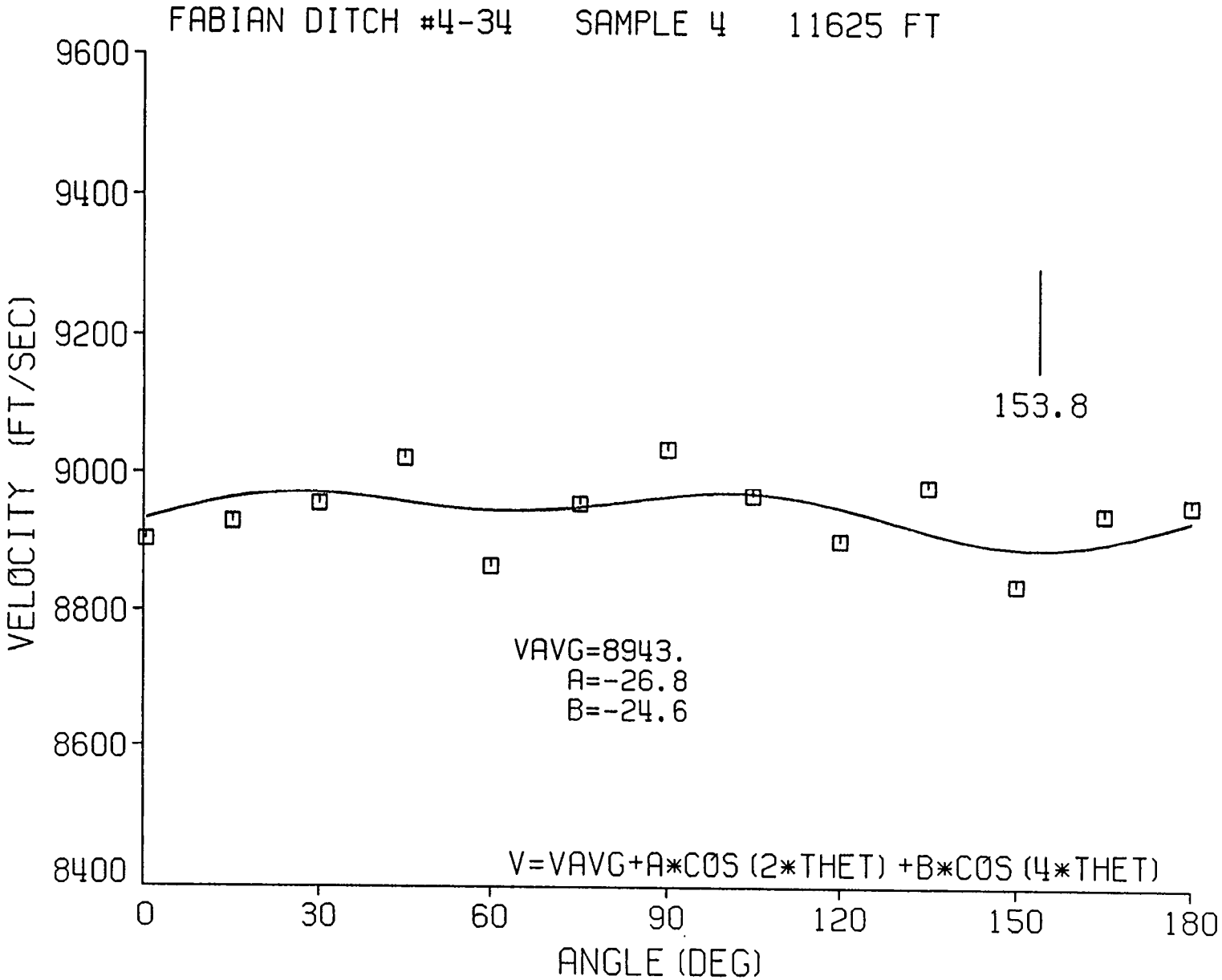

Figure 23. CVA data for Frontier sandstone, 11625 ft.

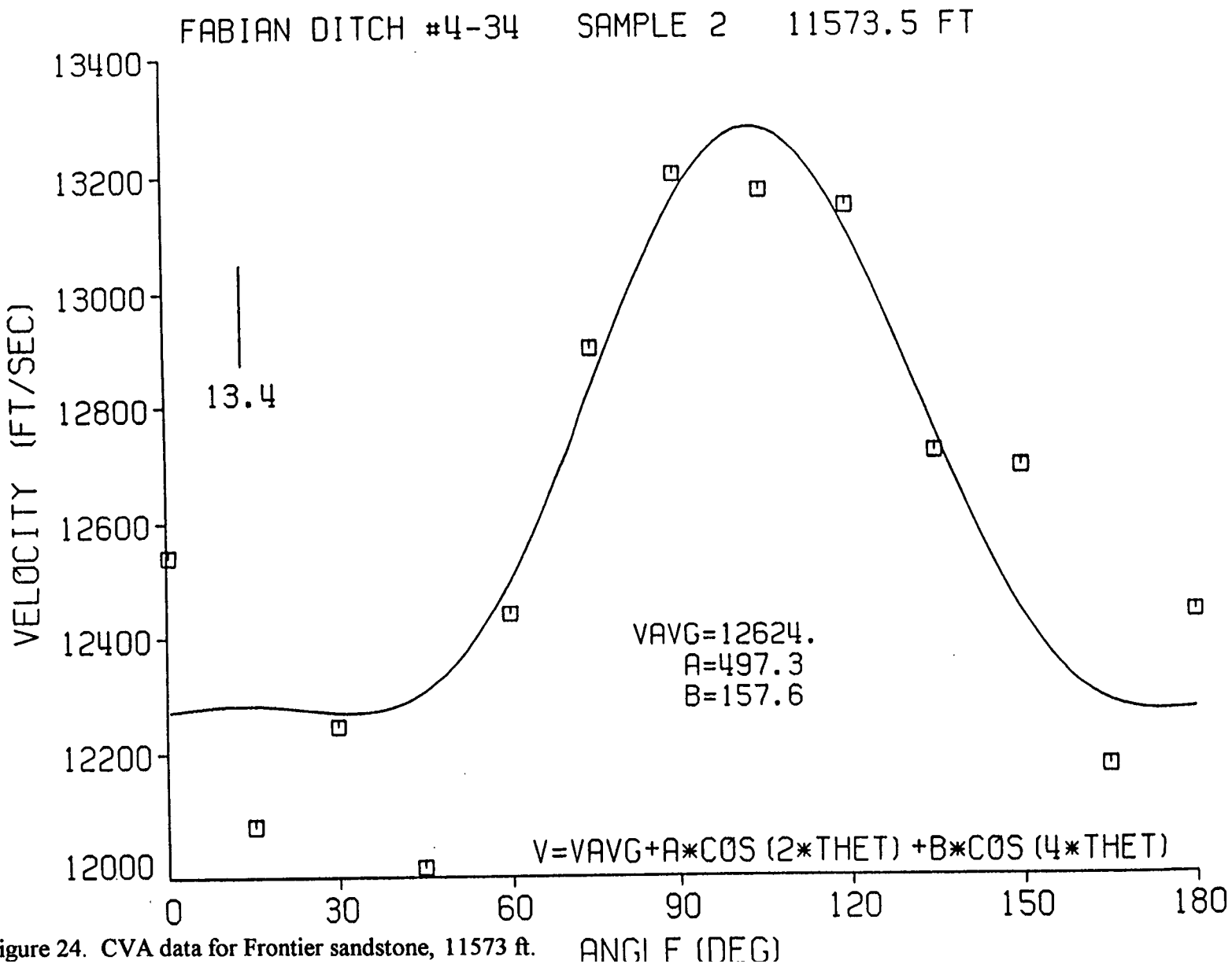

Figure 24. CVA data for Frontier sandstone, 11573 ft.

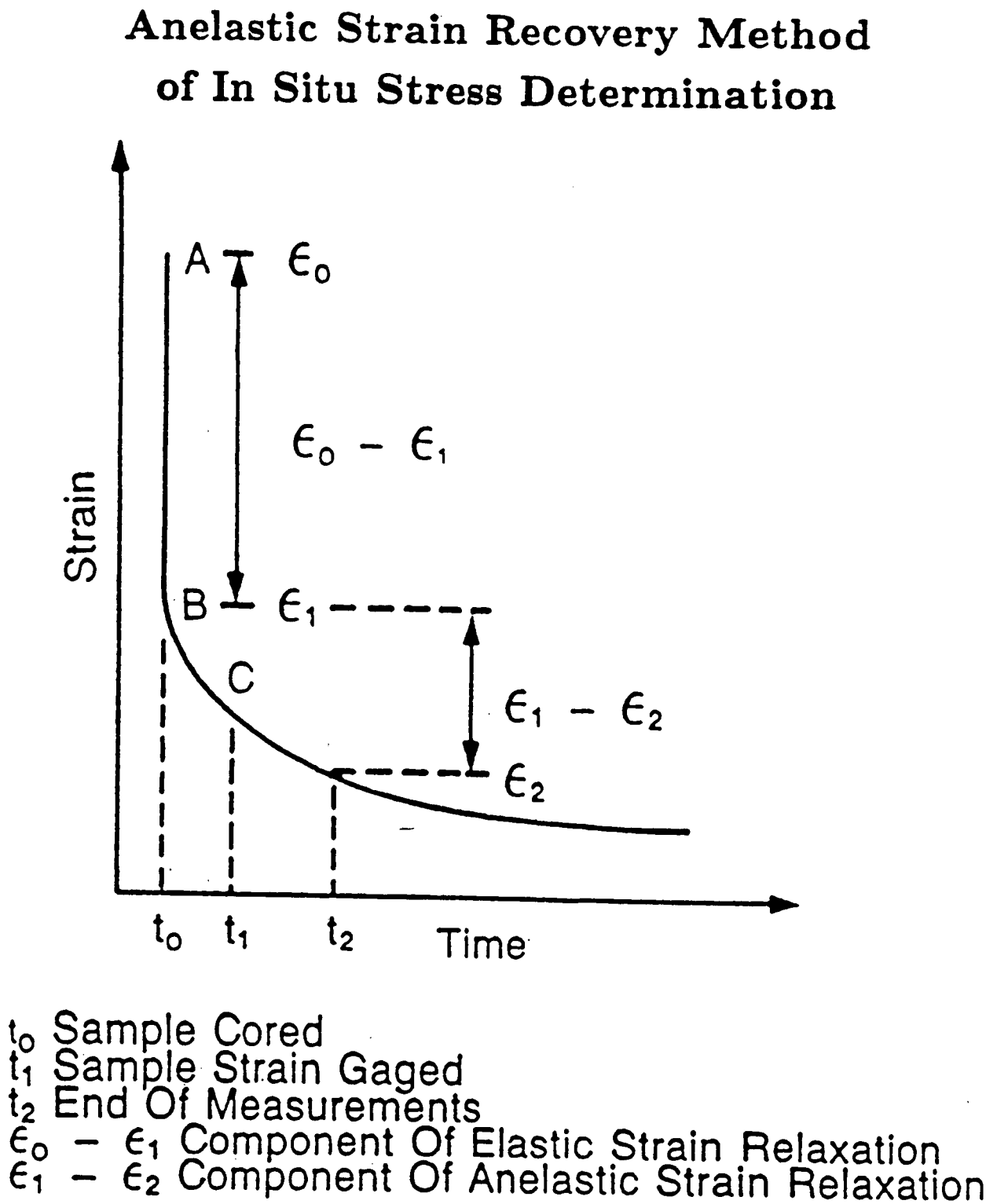

Figure 25. Strain recovery of a core sample.

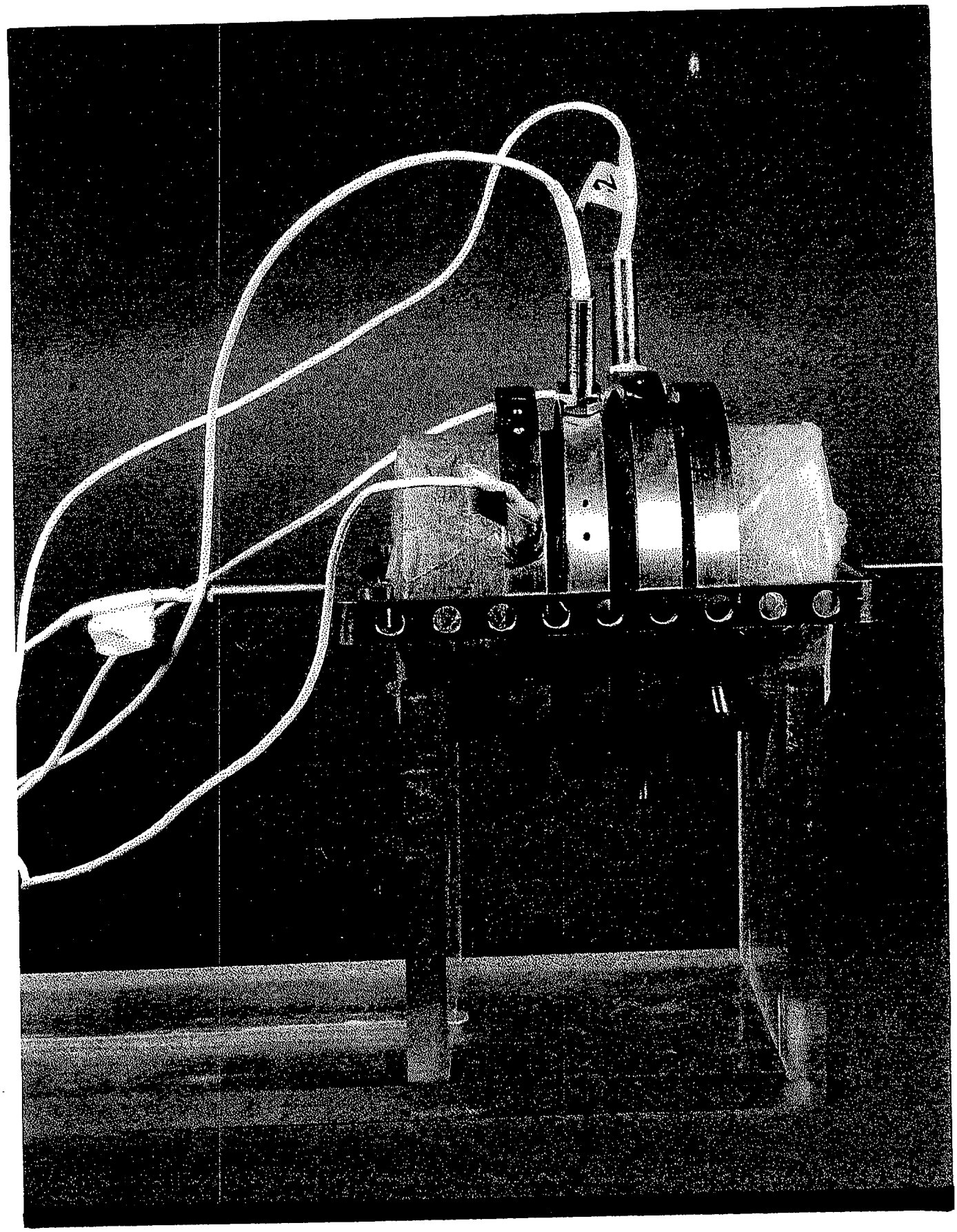

Figure 26. Photograph of ASR equipment.

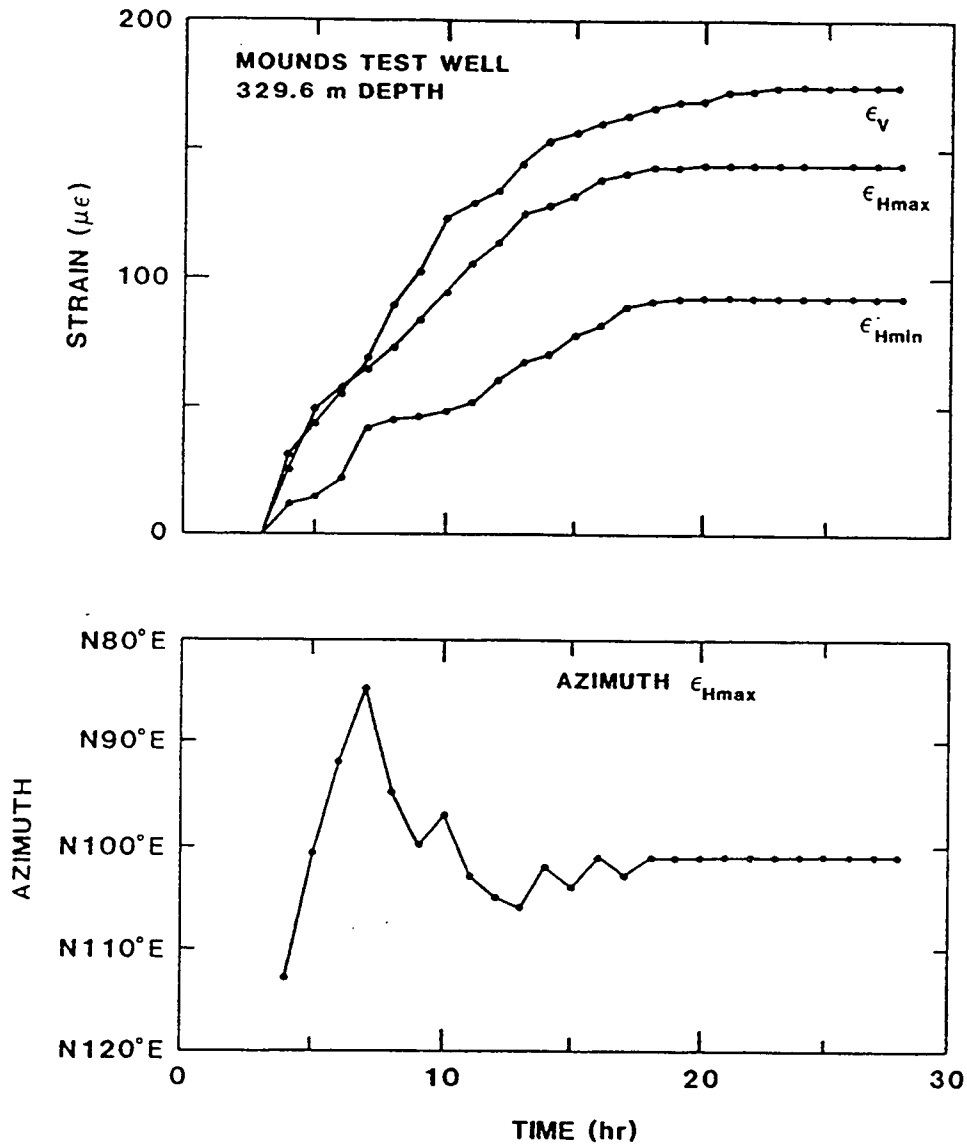

Figure 27. ASR results from Mounds experiment, 1081 ft.

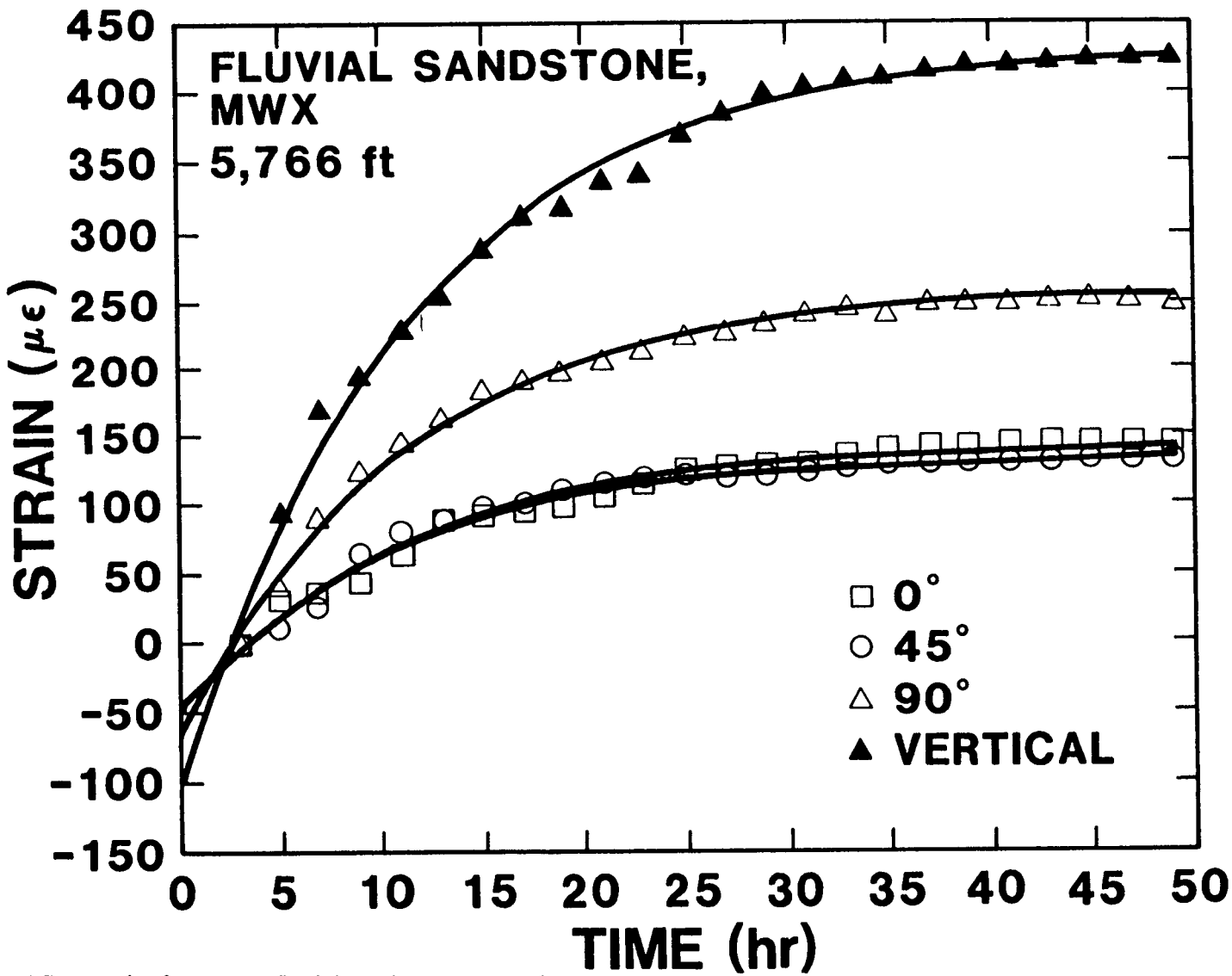

Figure 28. ASR results for MWX fluvial sandstone, 5766 ft.

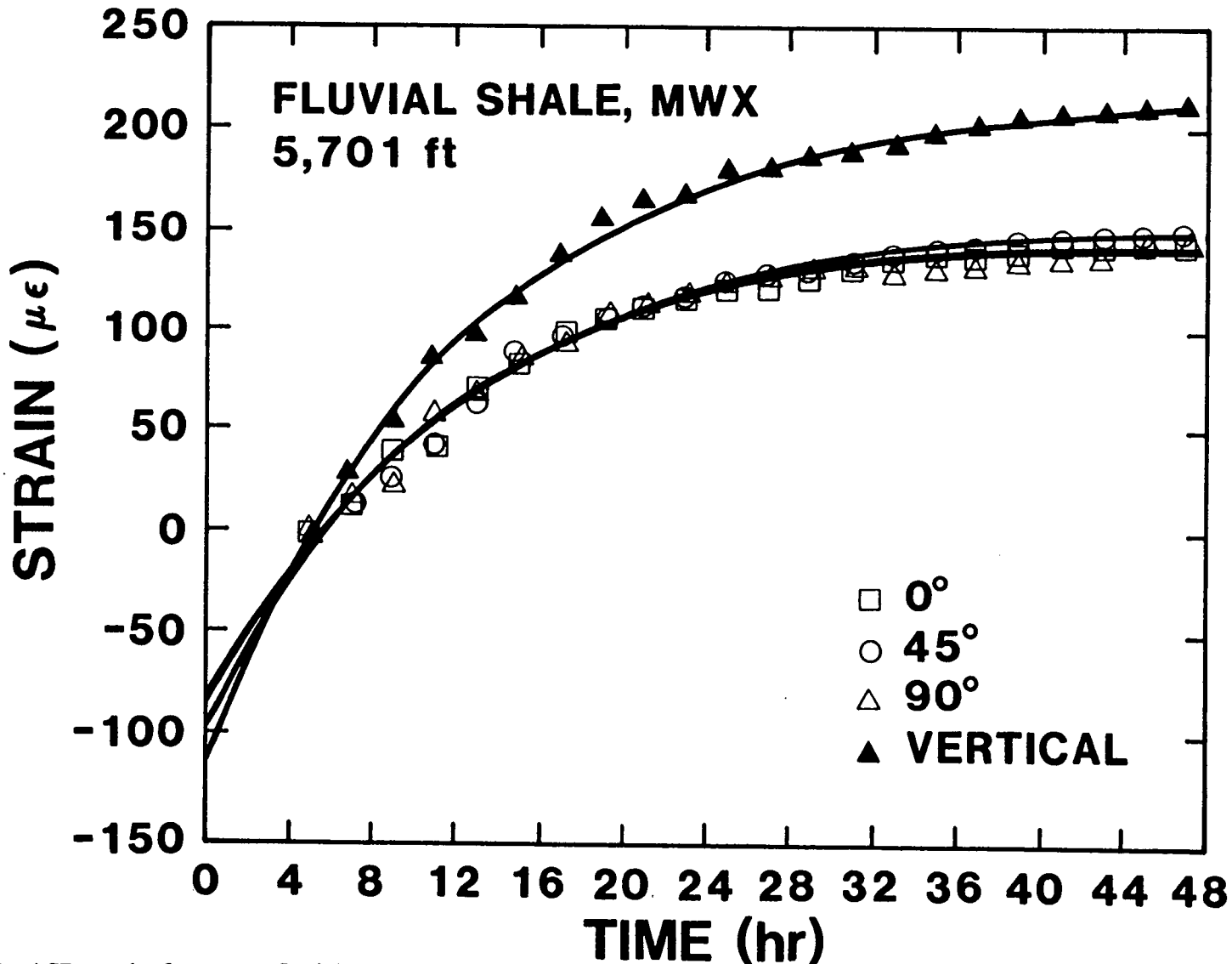

Figure 29. ASR results for MWX fluvial mudstone, 5701 ft.

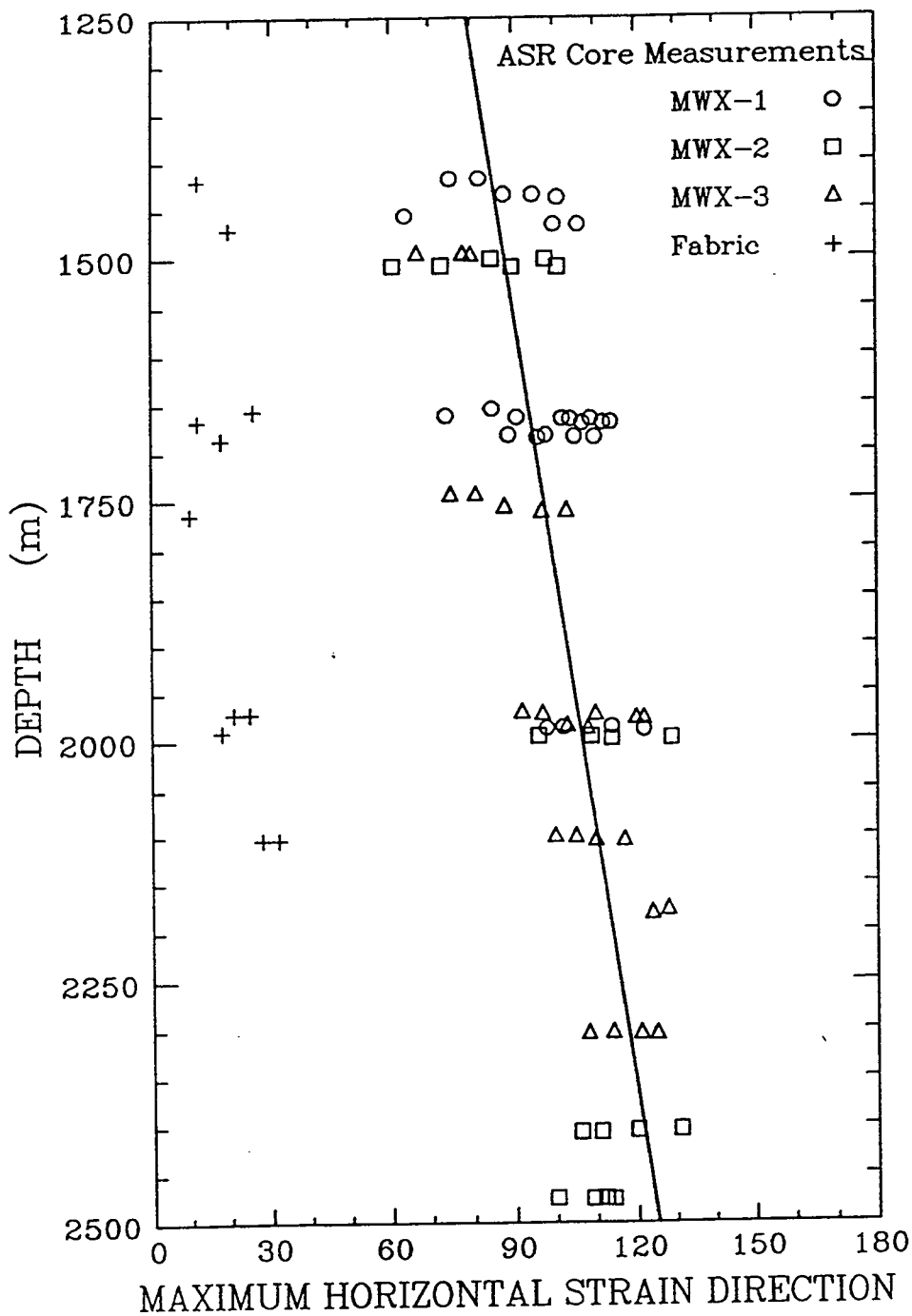

Figure 30. MWX azimuth results.

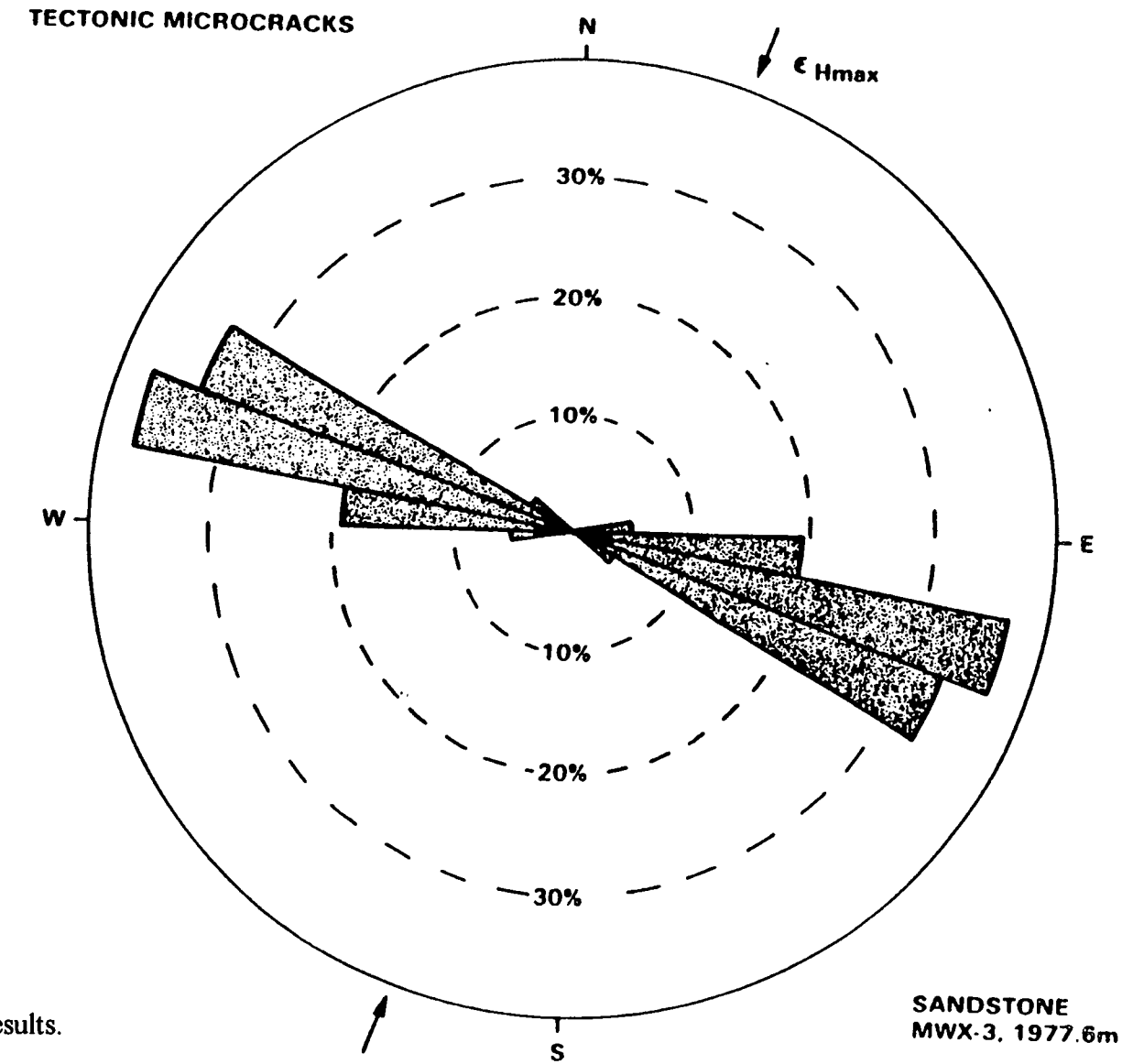

Figure 31. MWX fabric results.

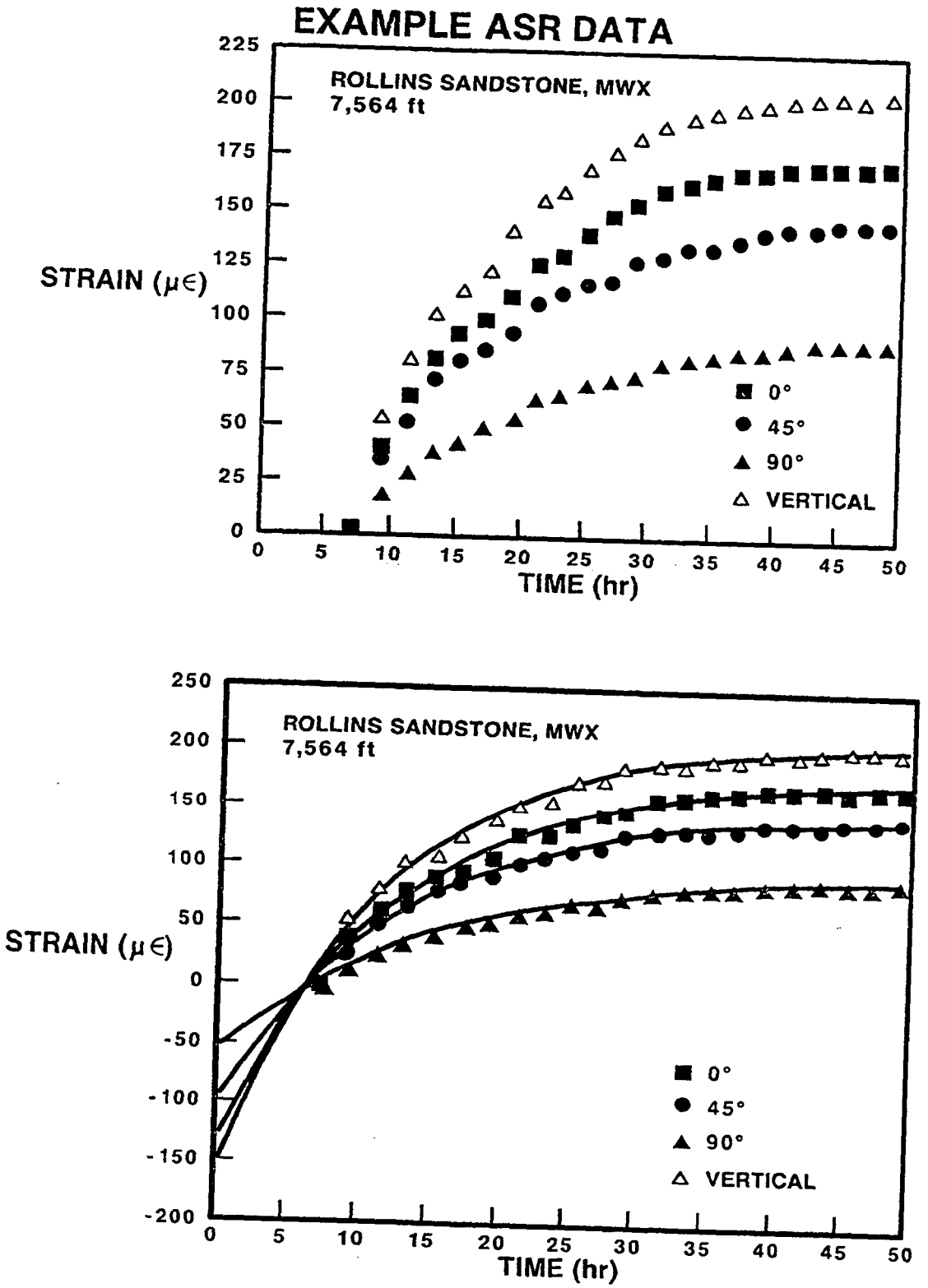

Figure 32. MWX ASR data for magnitude calculation.

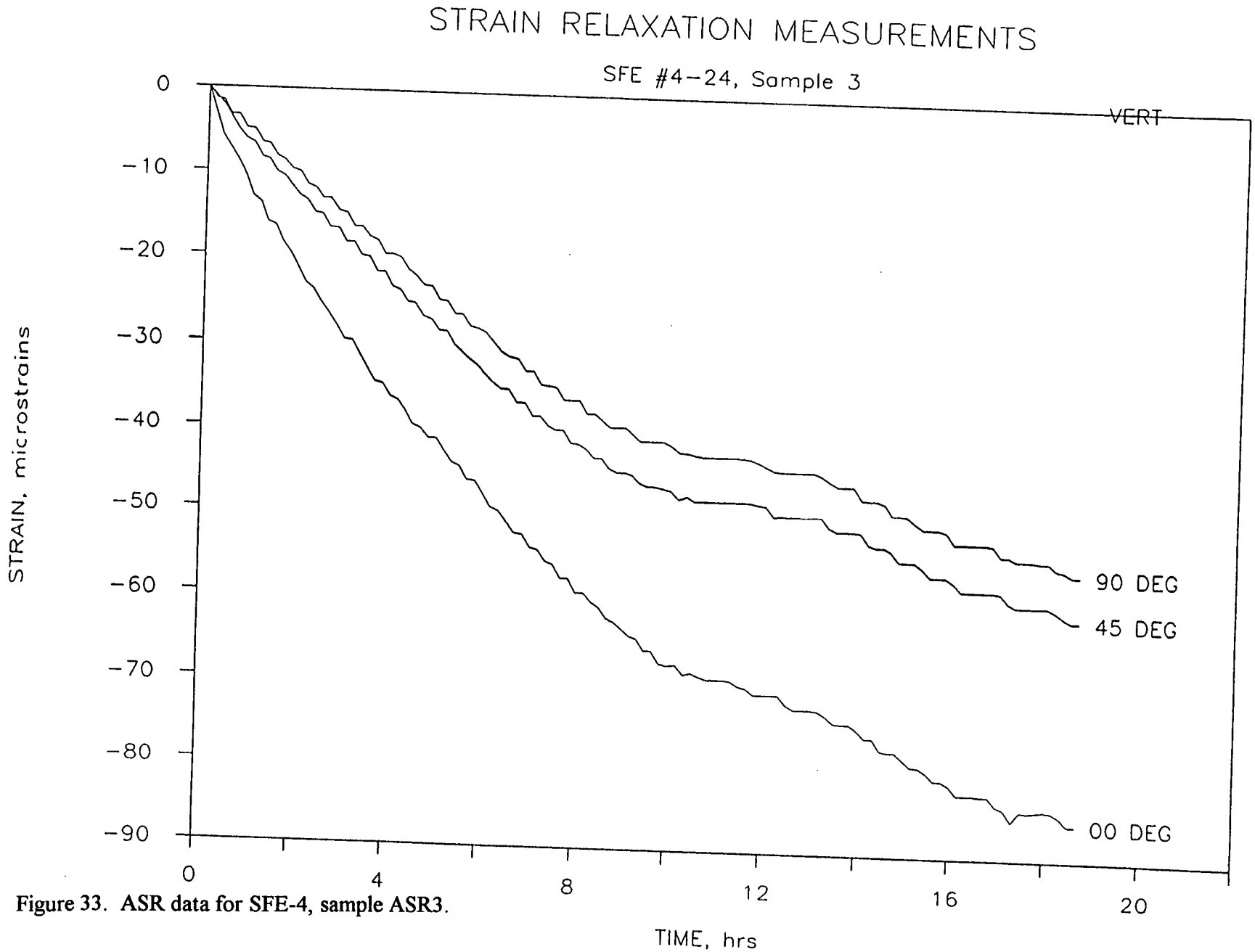

Figure 33. ASR data for SFE-4, sample ASR3.

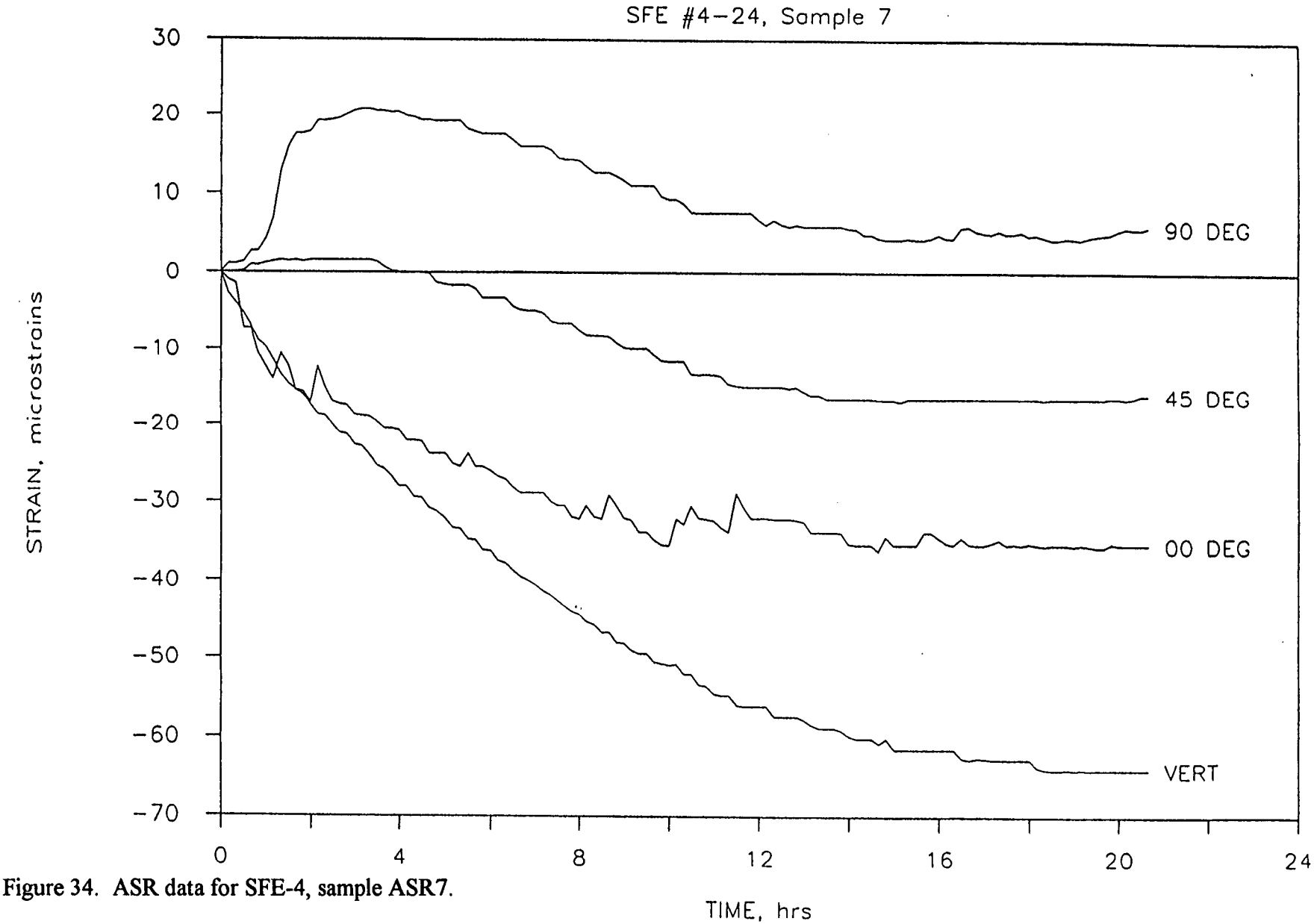

Figure 34. ASR data for SFE-4, sample ASR7.

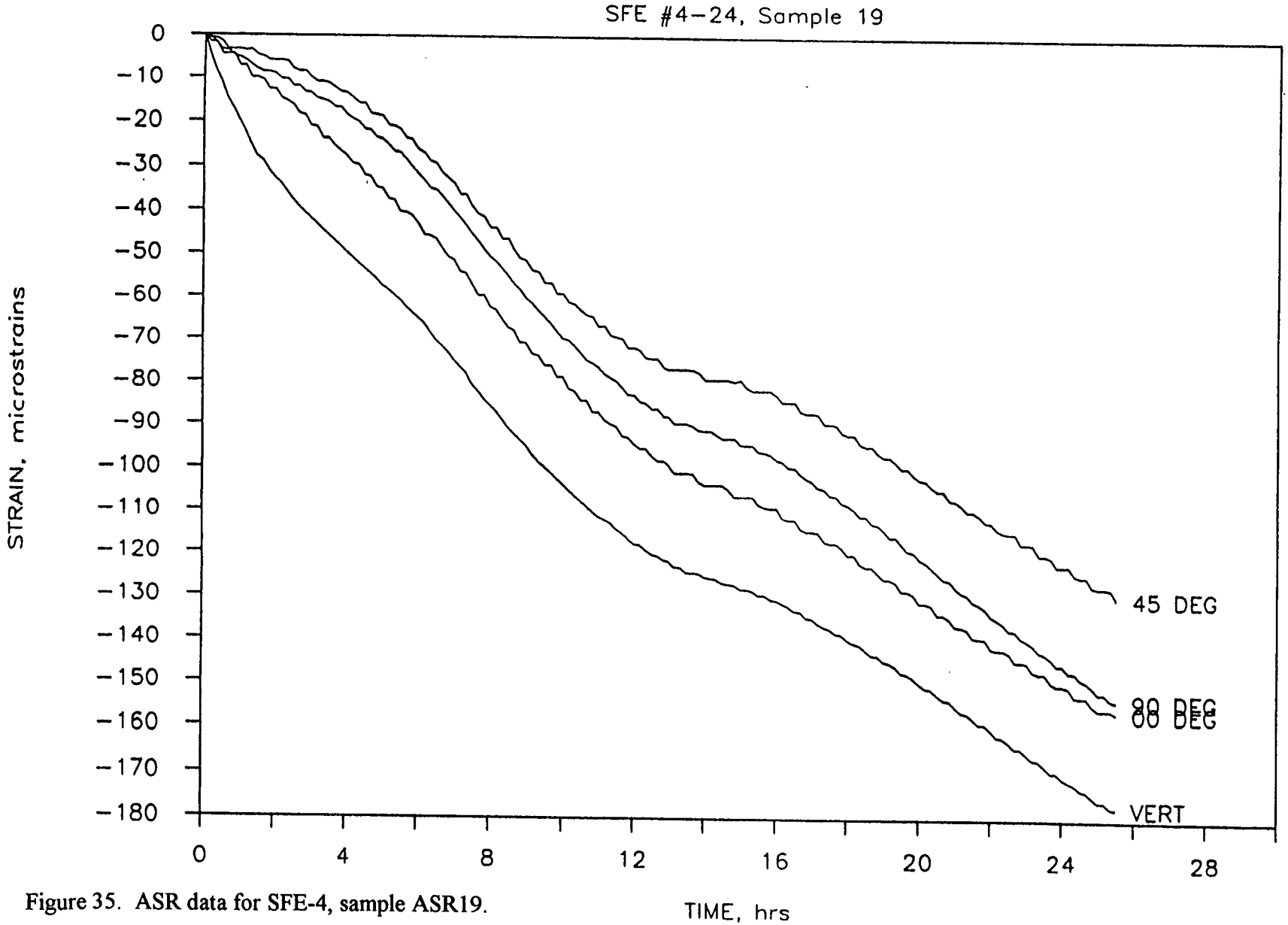

Figure 35. ASR data for SFE-4, sample ASR19.

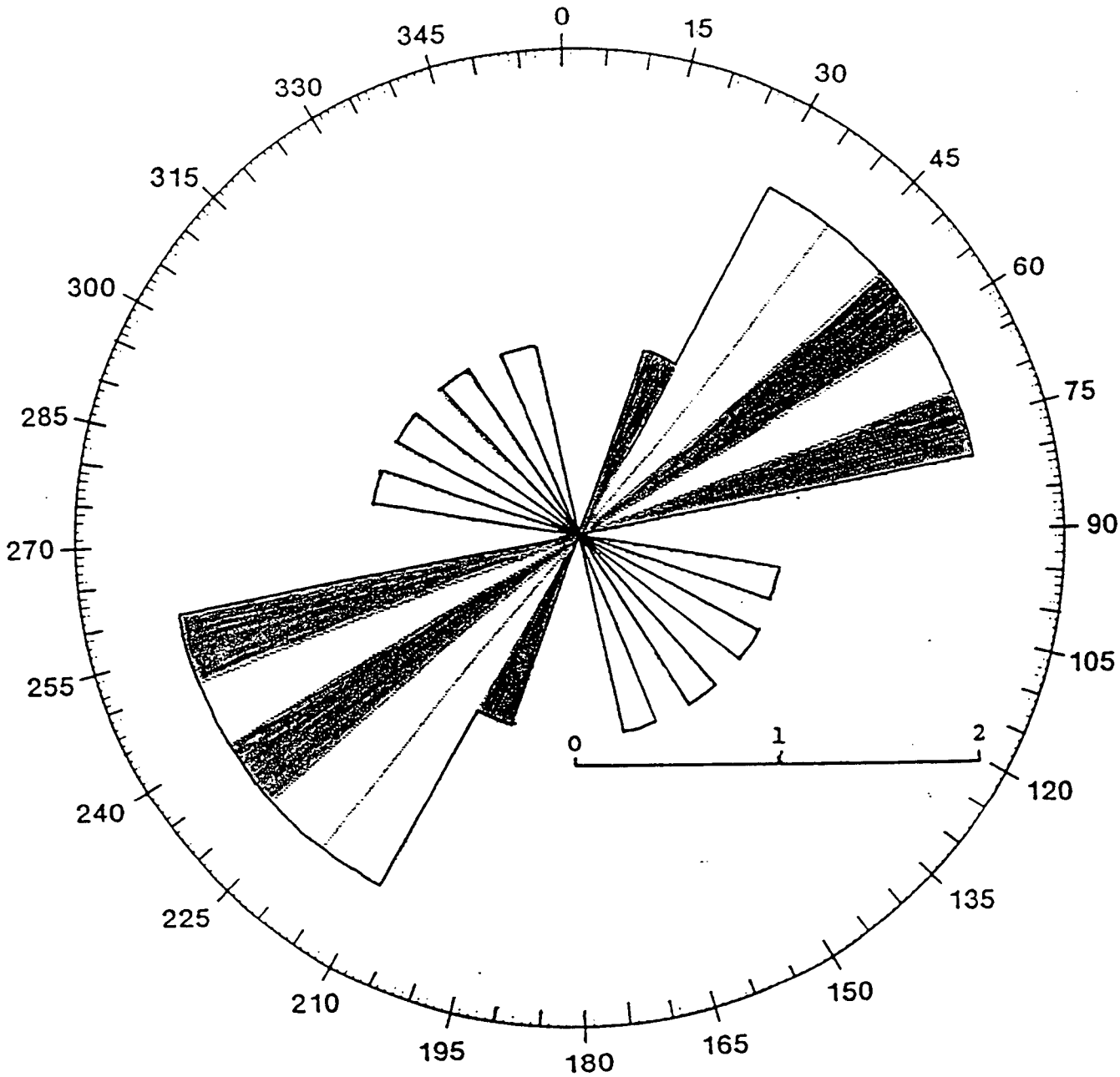

Figure 36. Results for SFE-4 ASR data.

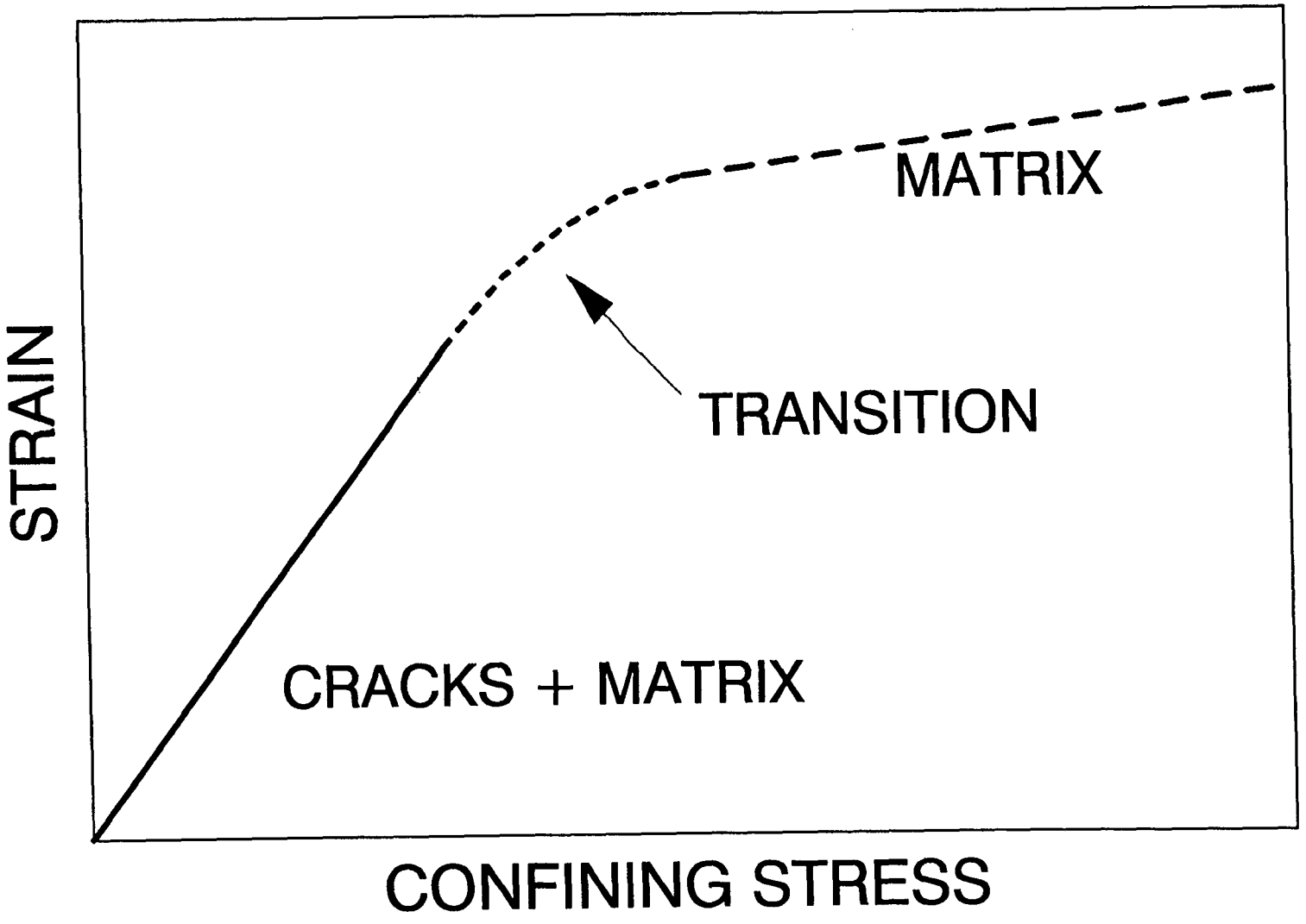

Figure 37. Schematic of differential strain behavior.

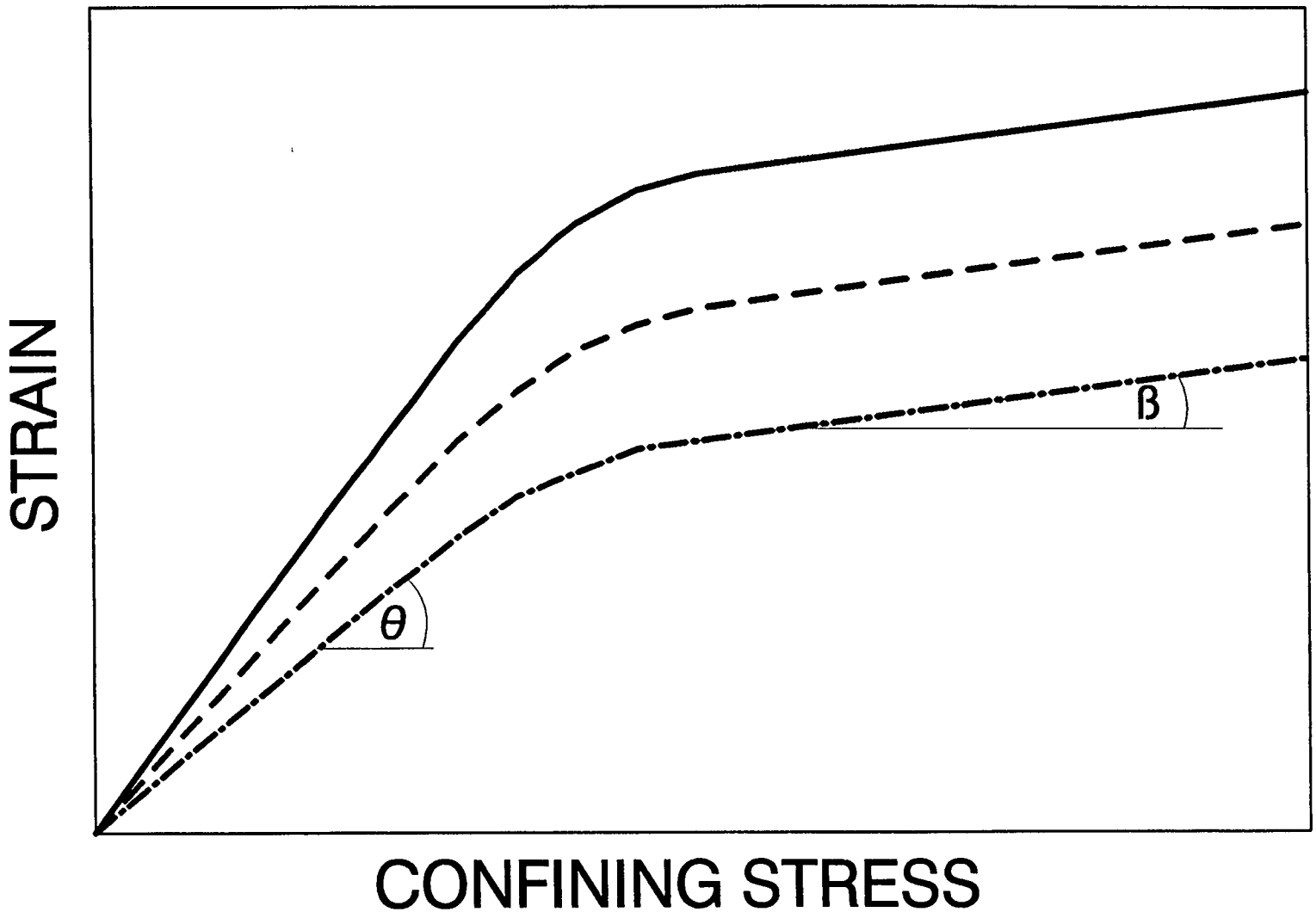

Figure 38. Differential strain behavior for three orientations.

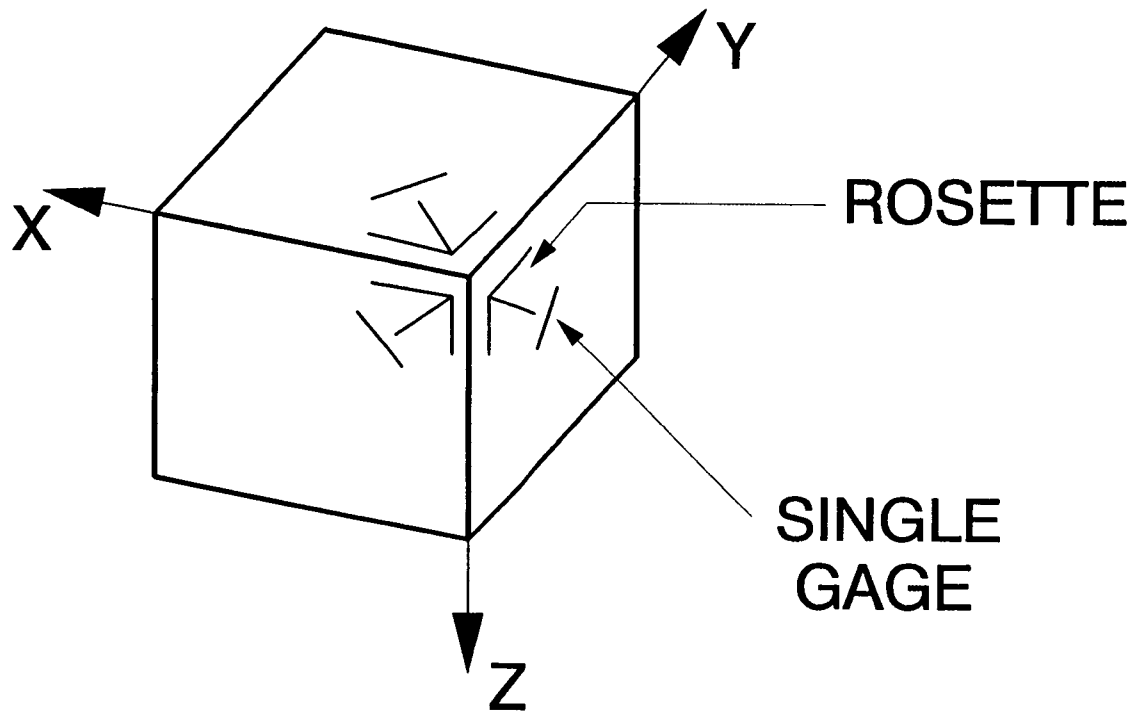

Figure 39. Core setup using cubical sample for DSCA.[34,35]

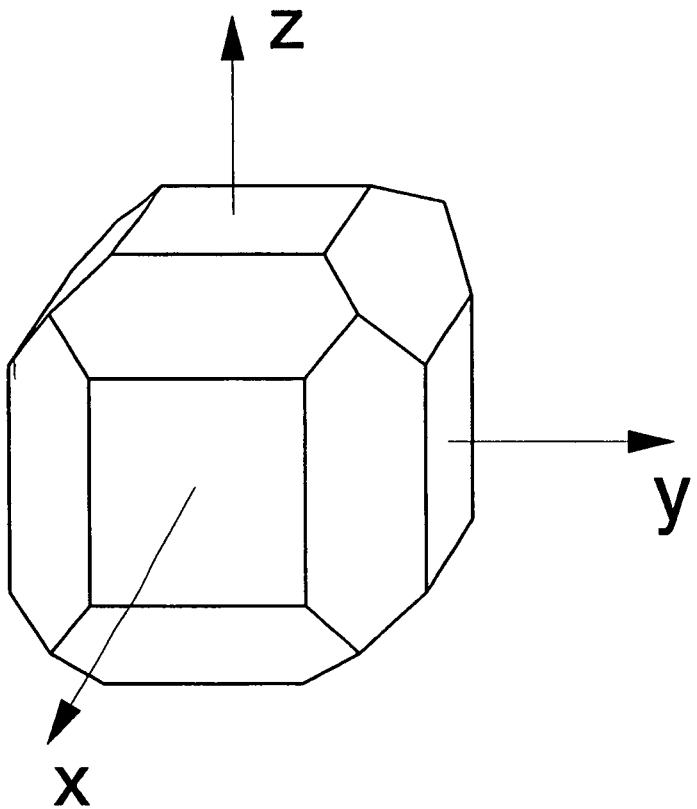

Figure 40. Core setup using 18 sided sample for DWVA.[36]

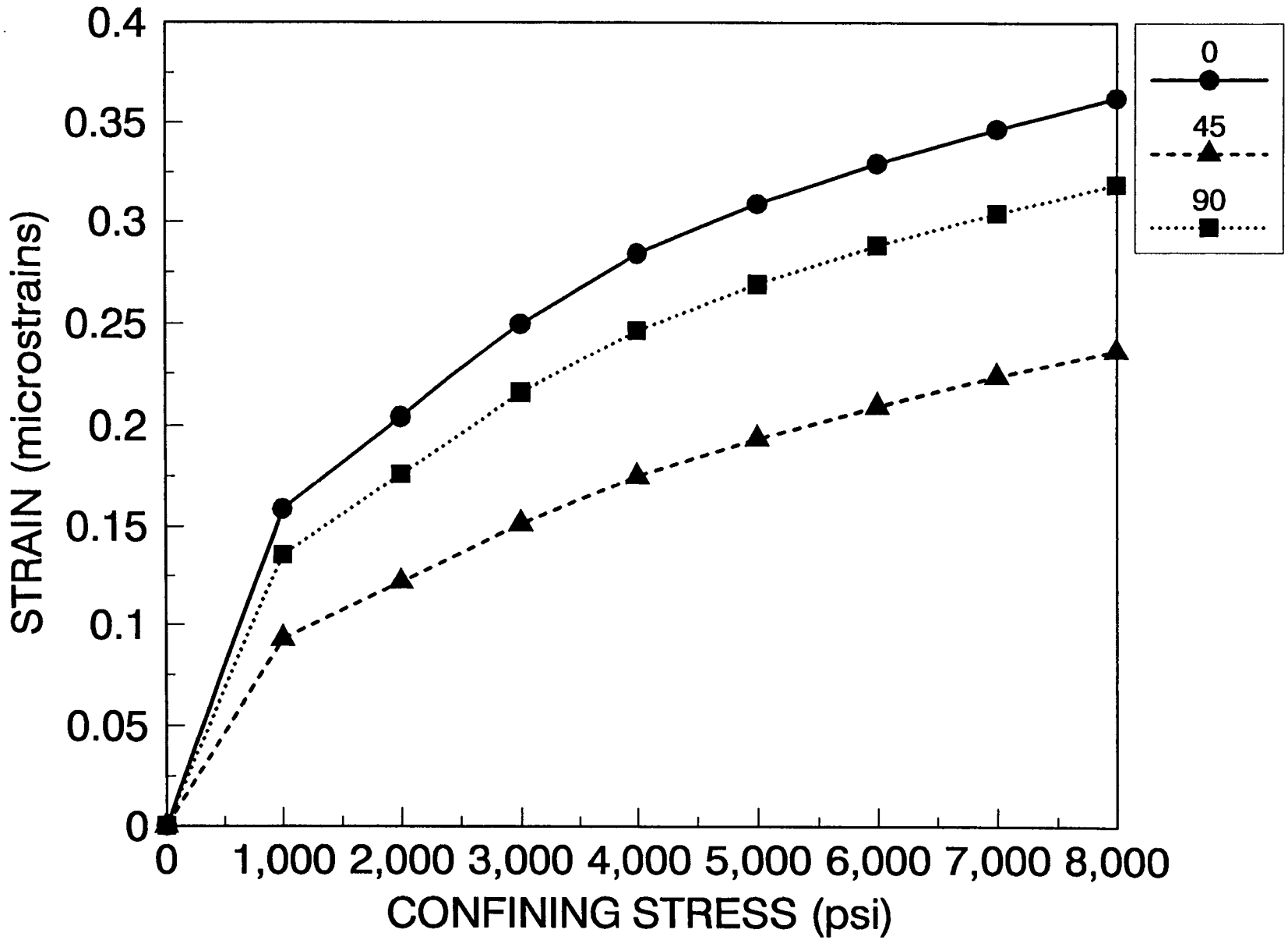

Figure 41. Example DSCA curves for MWX core, 6520 ft.

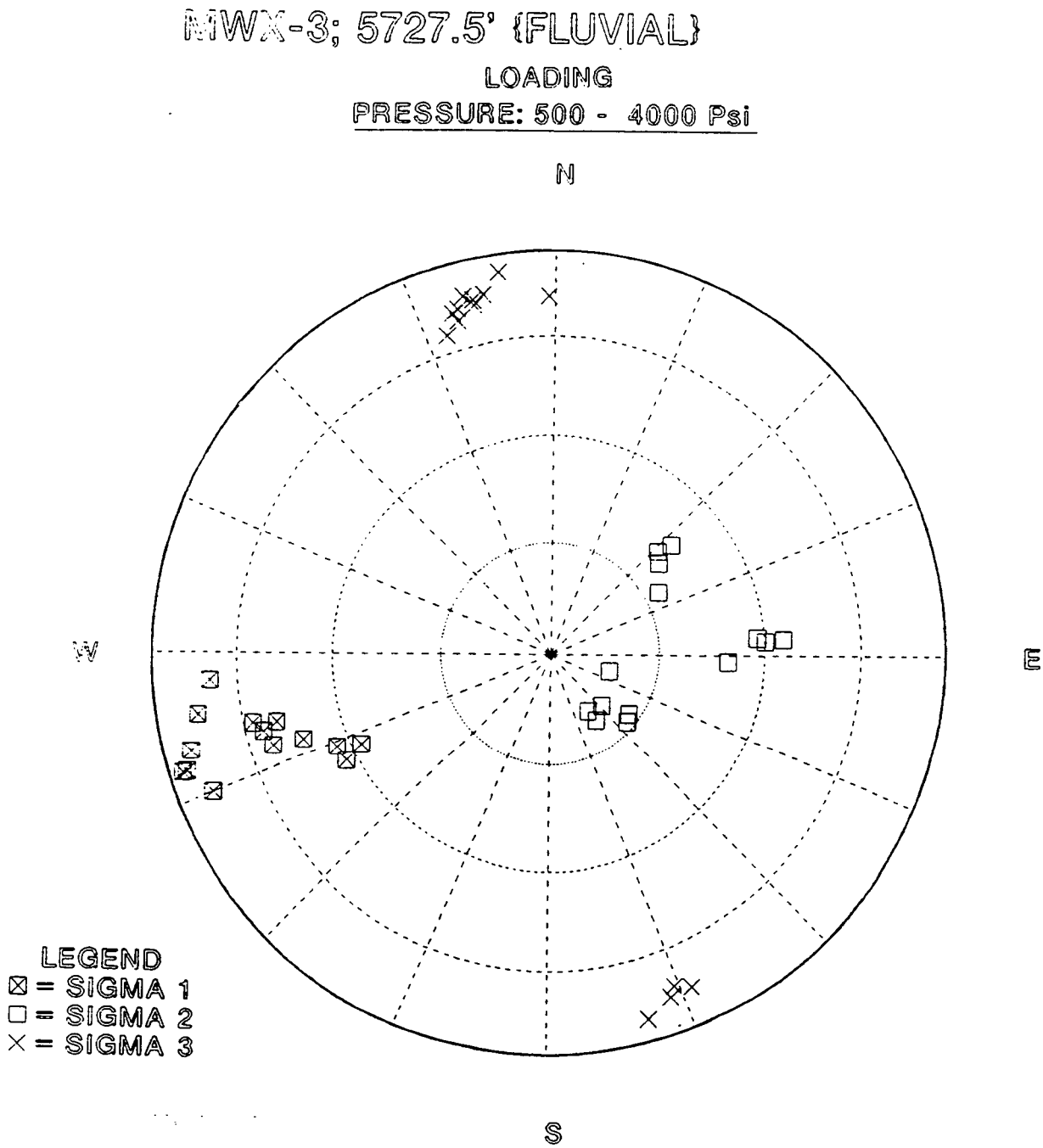

Figure 42. Polar plots of DSCA/DWVA results.

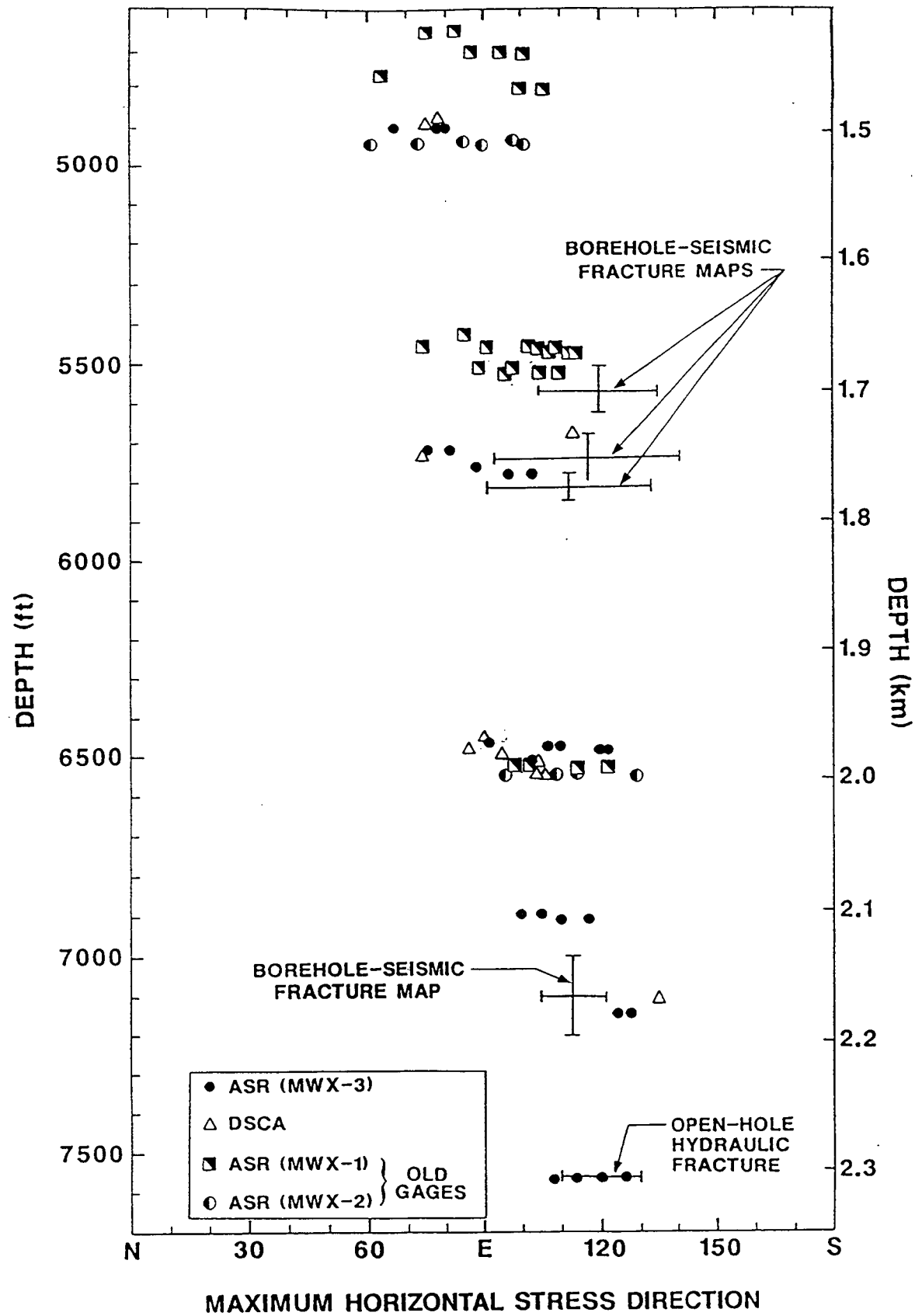

Figure 43. Comparison of DSCA and other orientation techniques from MWX.

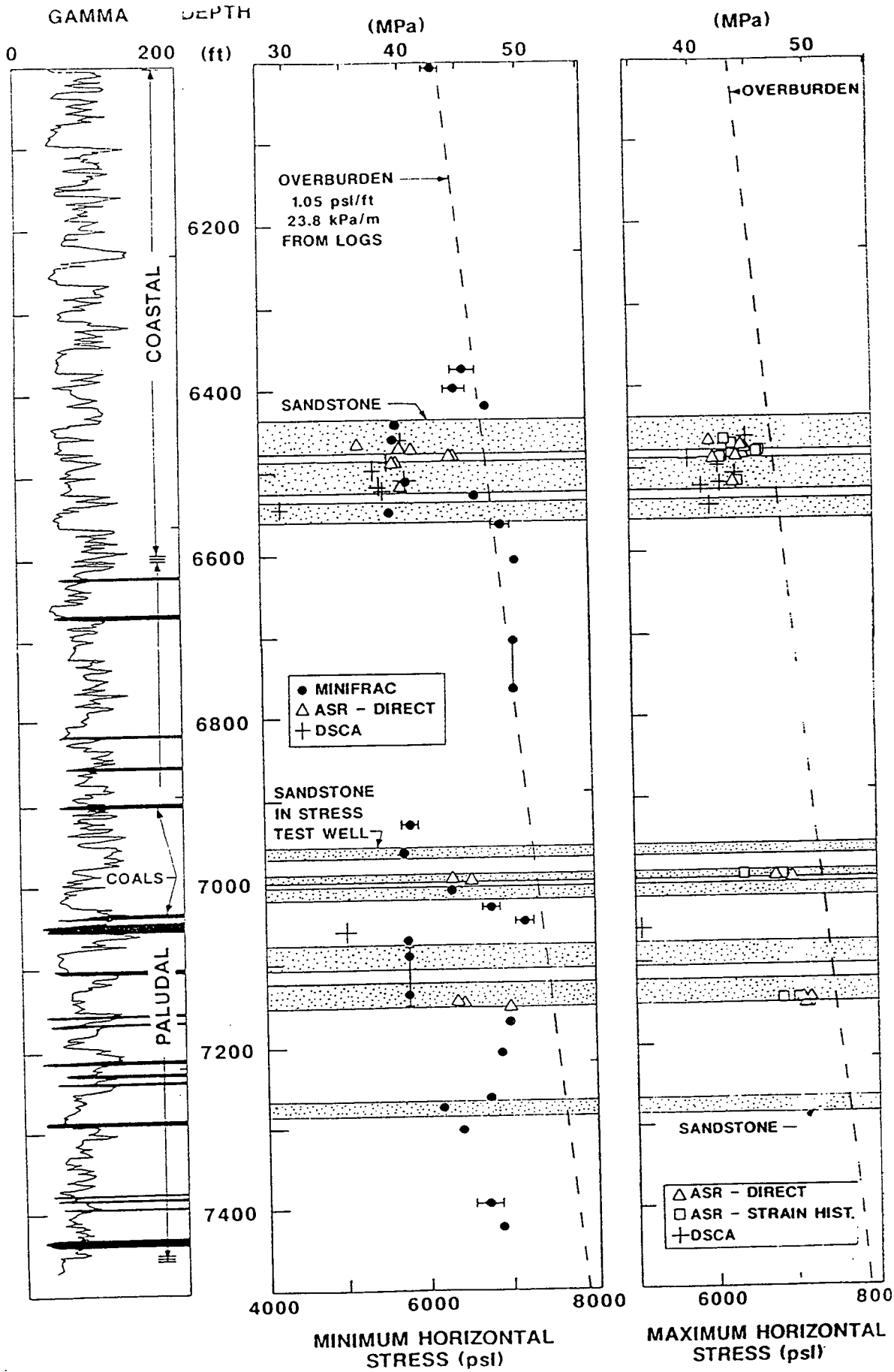

Figure 44. Comparison of DSCA and other magnitude techniques from MWX.

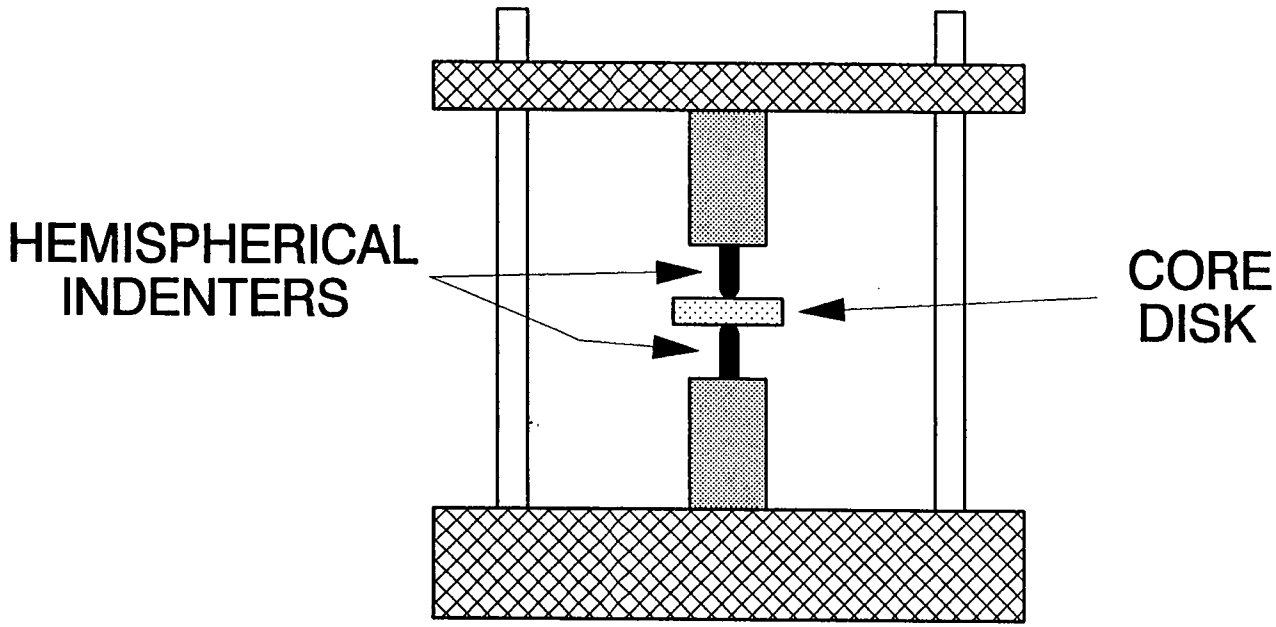

Figure 45. Apparatus for conducting point-load tests.[41]

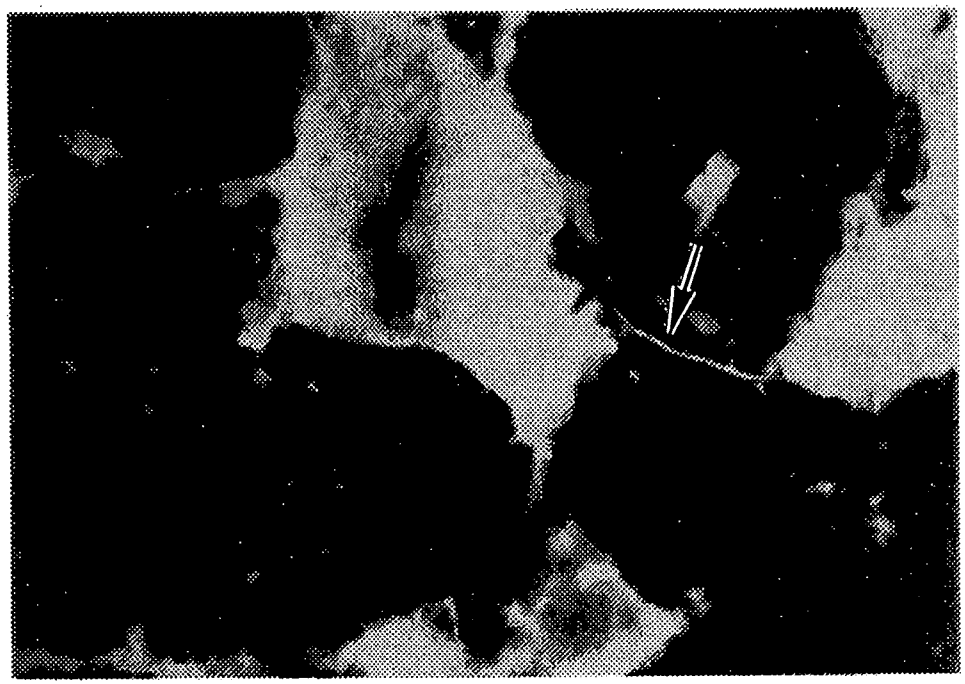

Figure 46. Fluorescent microscopy result showing a relaxation microcrack.

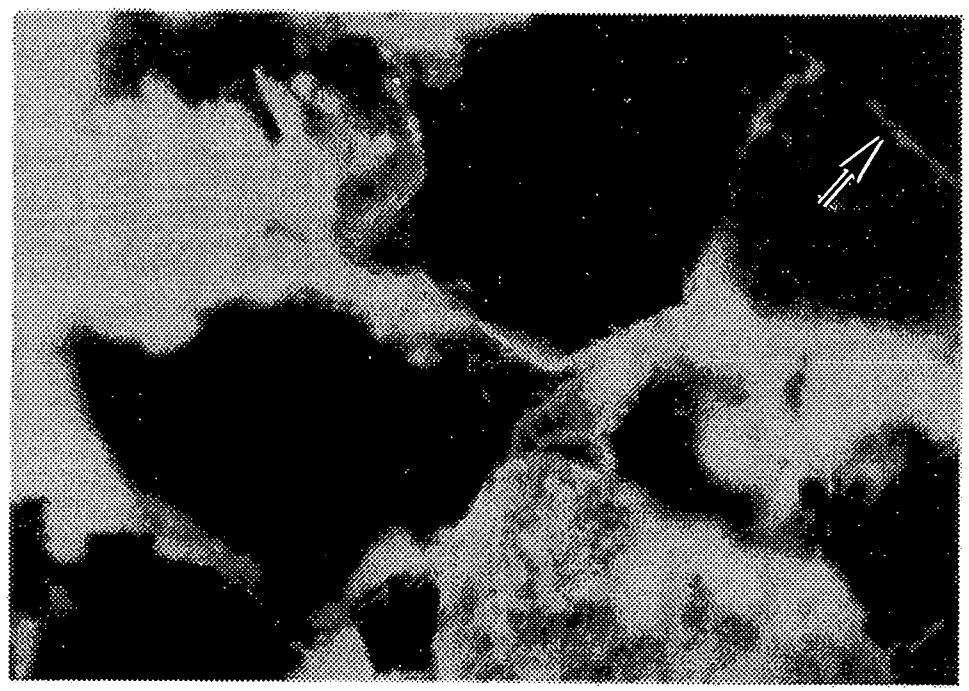

Figure 47. Fluorescent microscopy result showing a tectonic microcrack.

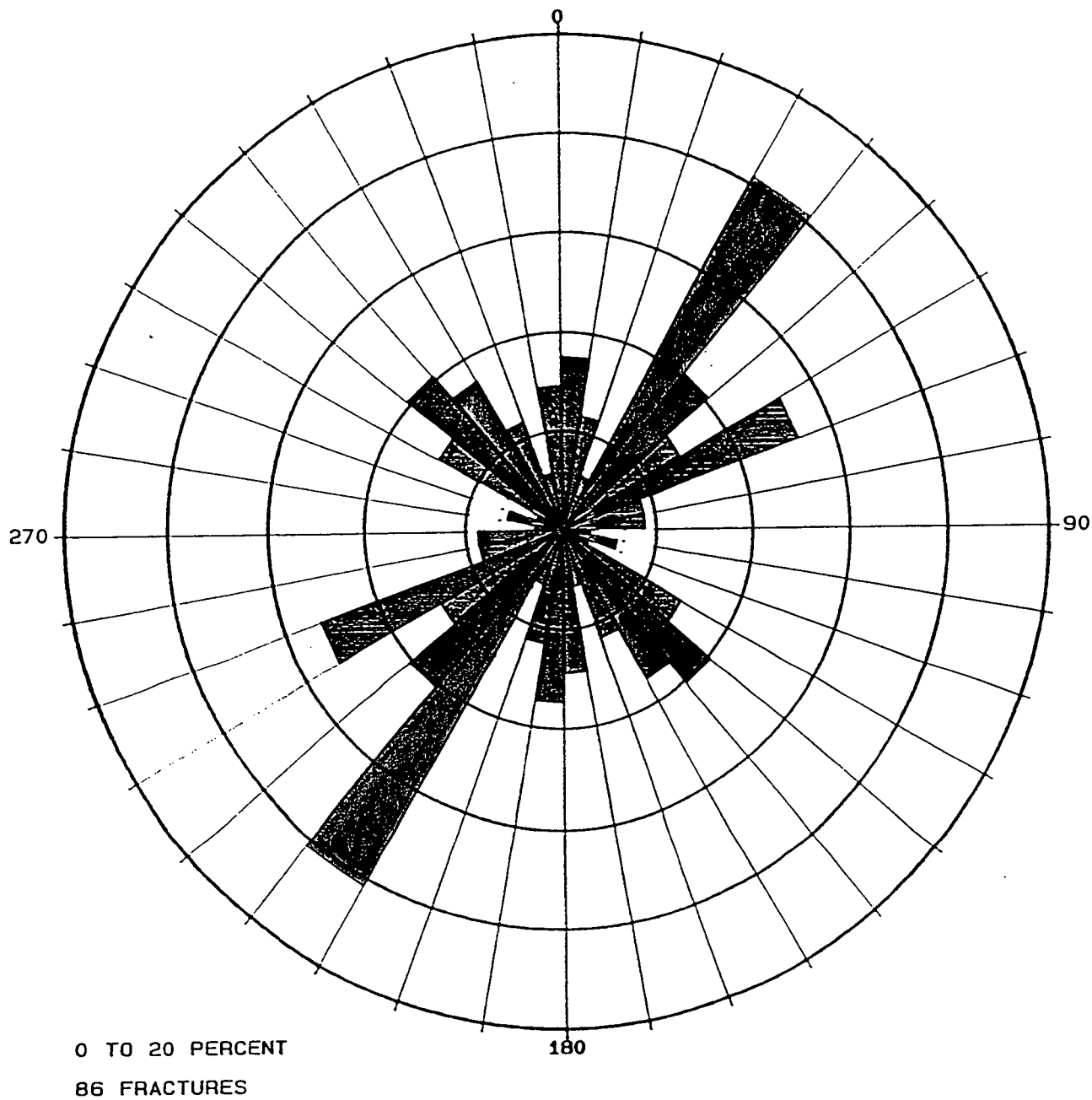

Figure 48. Orientations of MWX microcracks, 6459 ft.

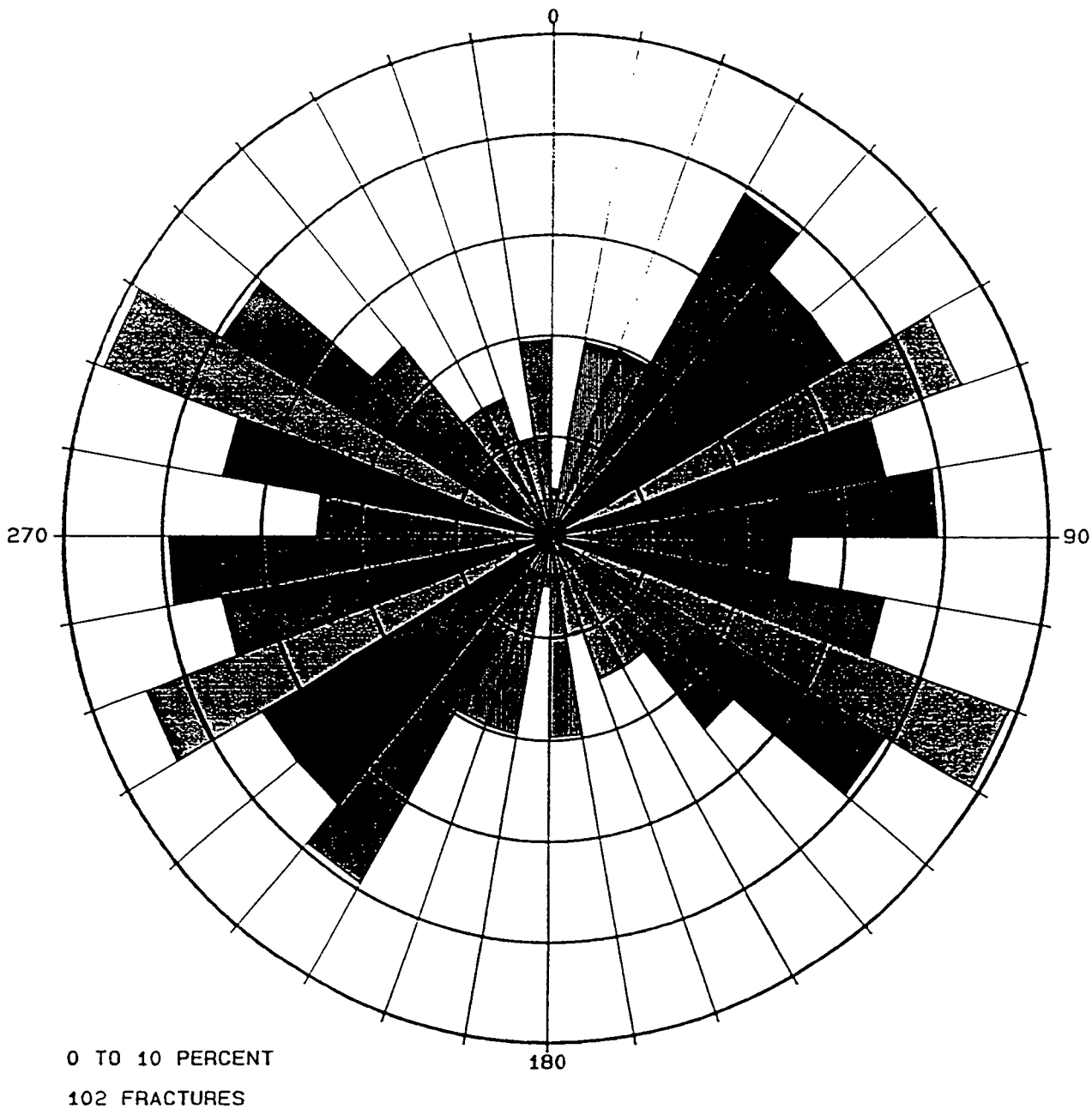

Figure 49 Orientations of MWX microcracks, 5490 ft.

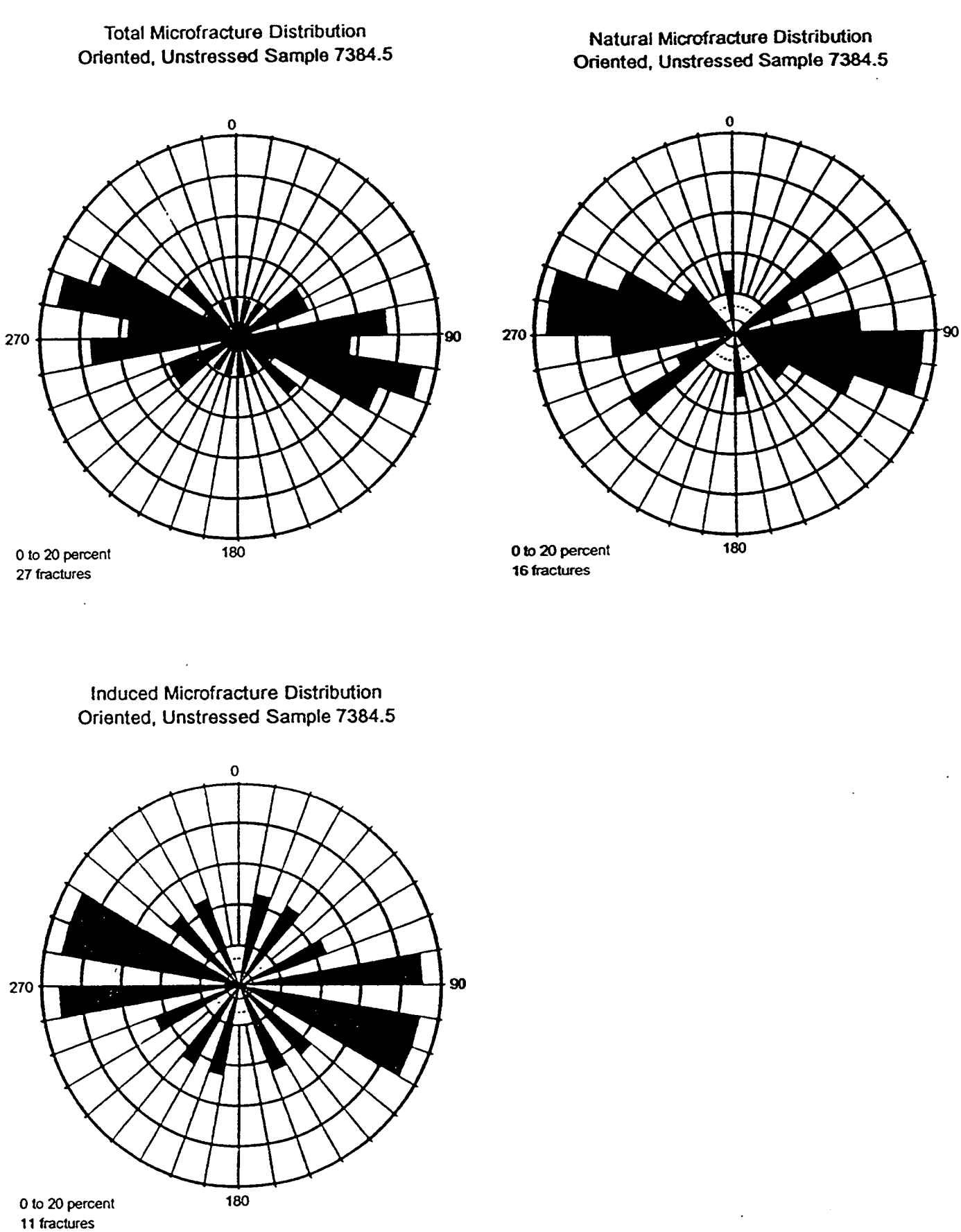

Figure 50. Orientations of SFE-4 microcracks, 7384.5 ft.

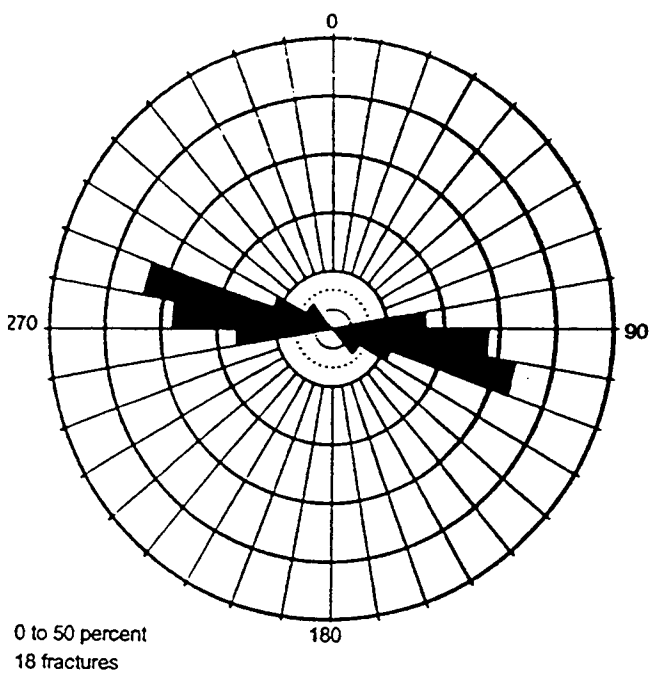

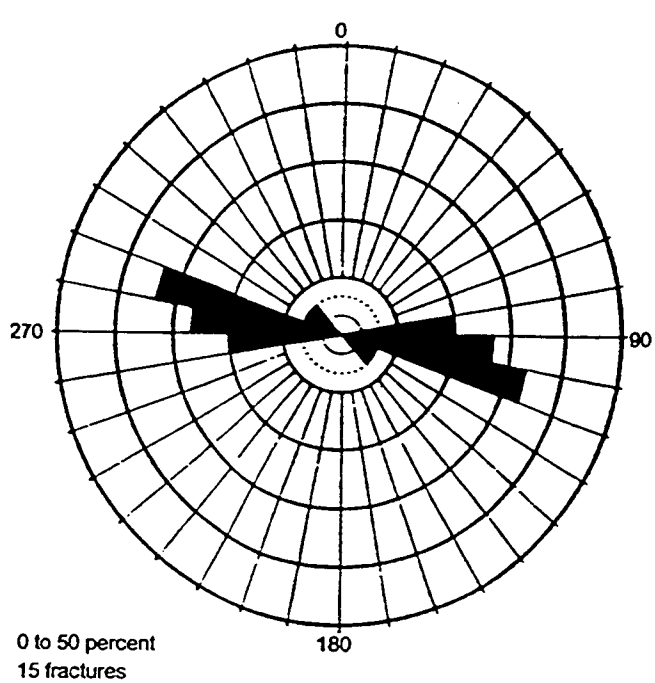

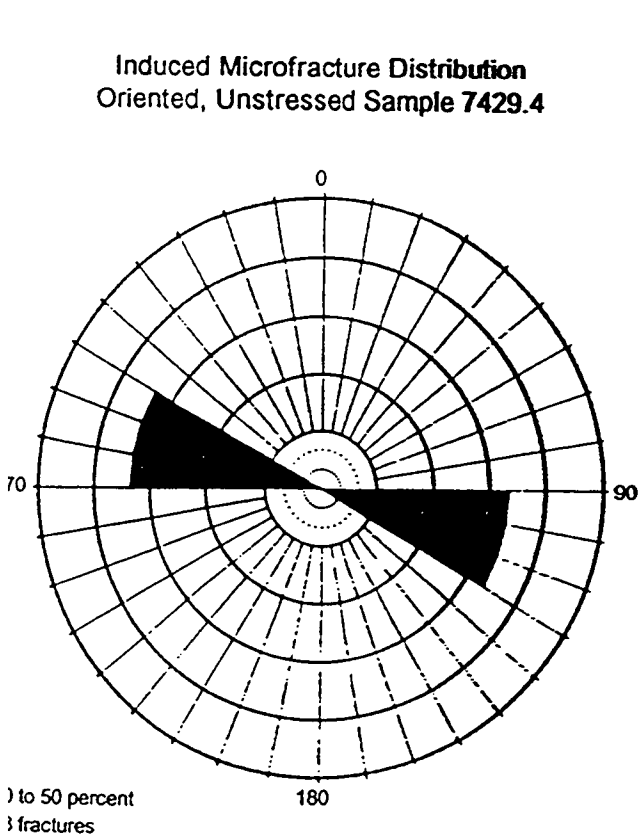

Figure 51. Orientations of SFE-4 microcracks, 7429.4 ft.

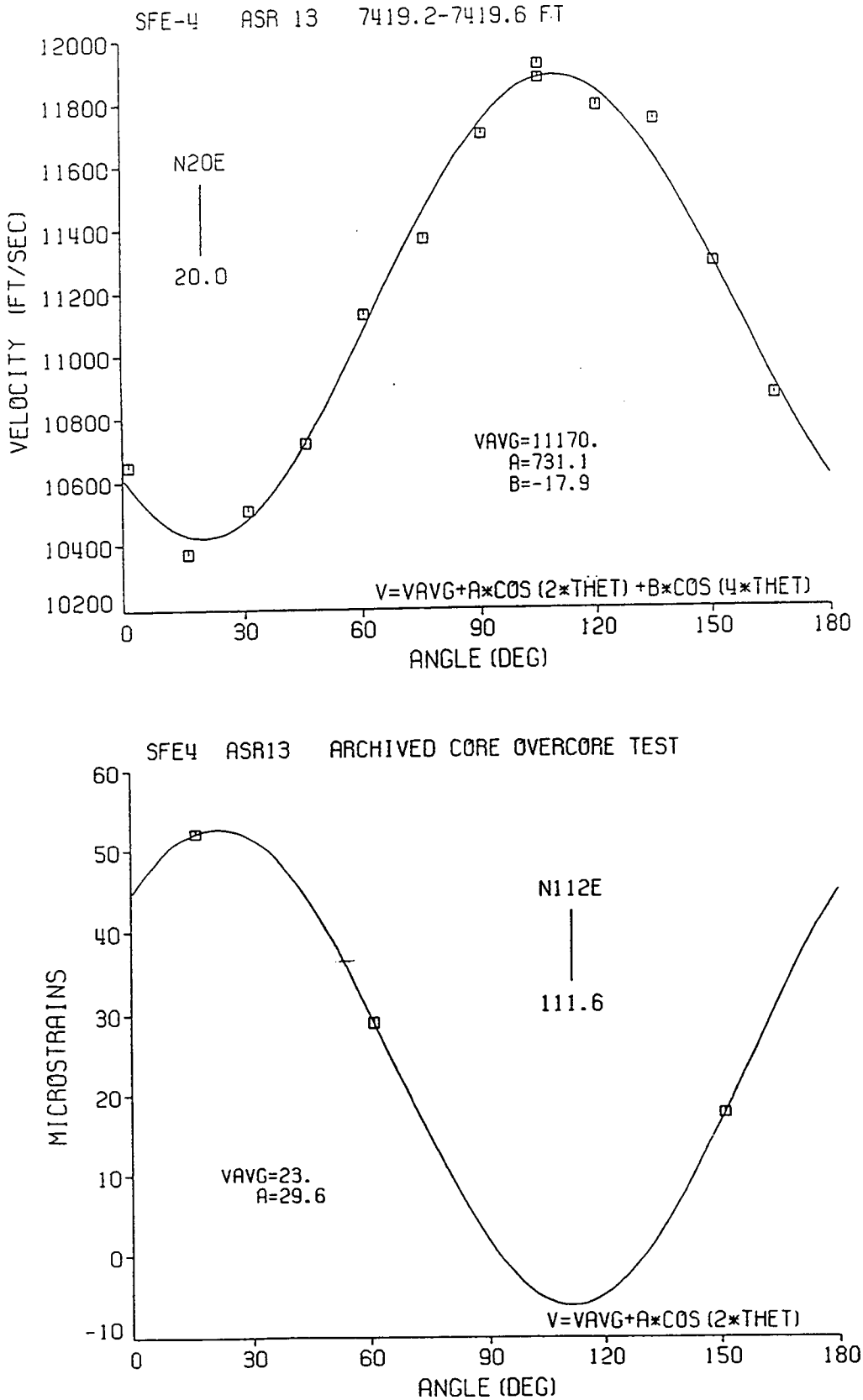

Figure 52. Comparison of overcore and velocity data for SFE-4, ASR-13.

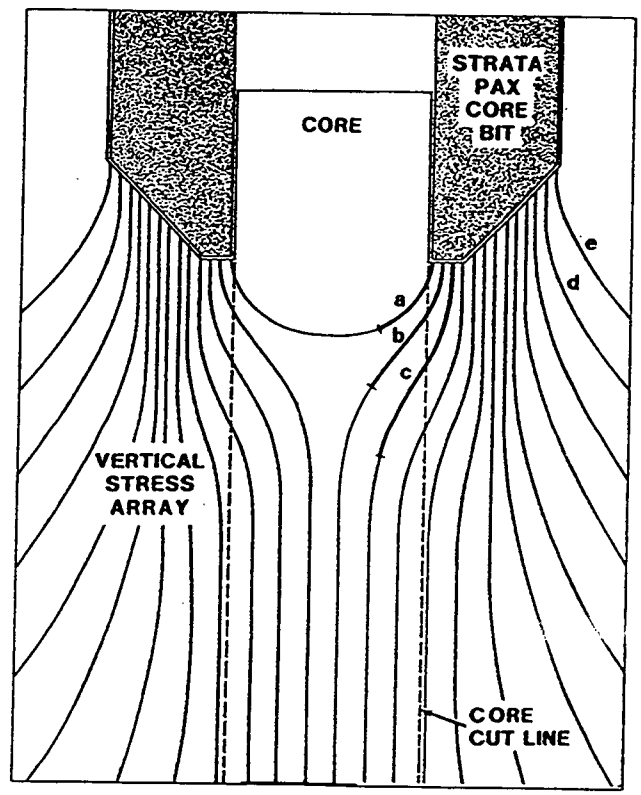

Figure 53. Schematic of bit-induced stress array below core.[45]

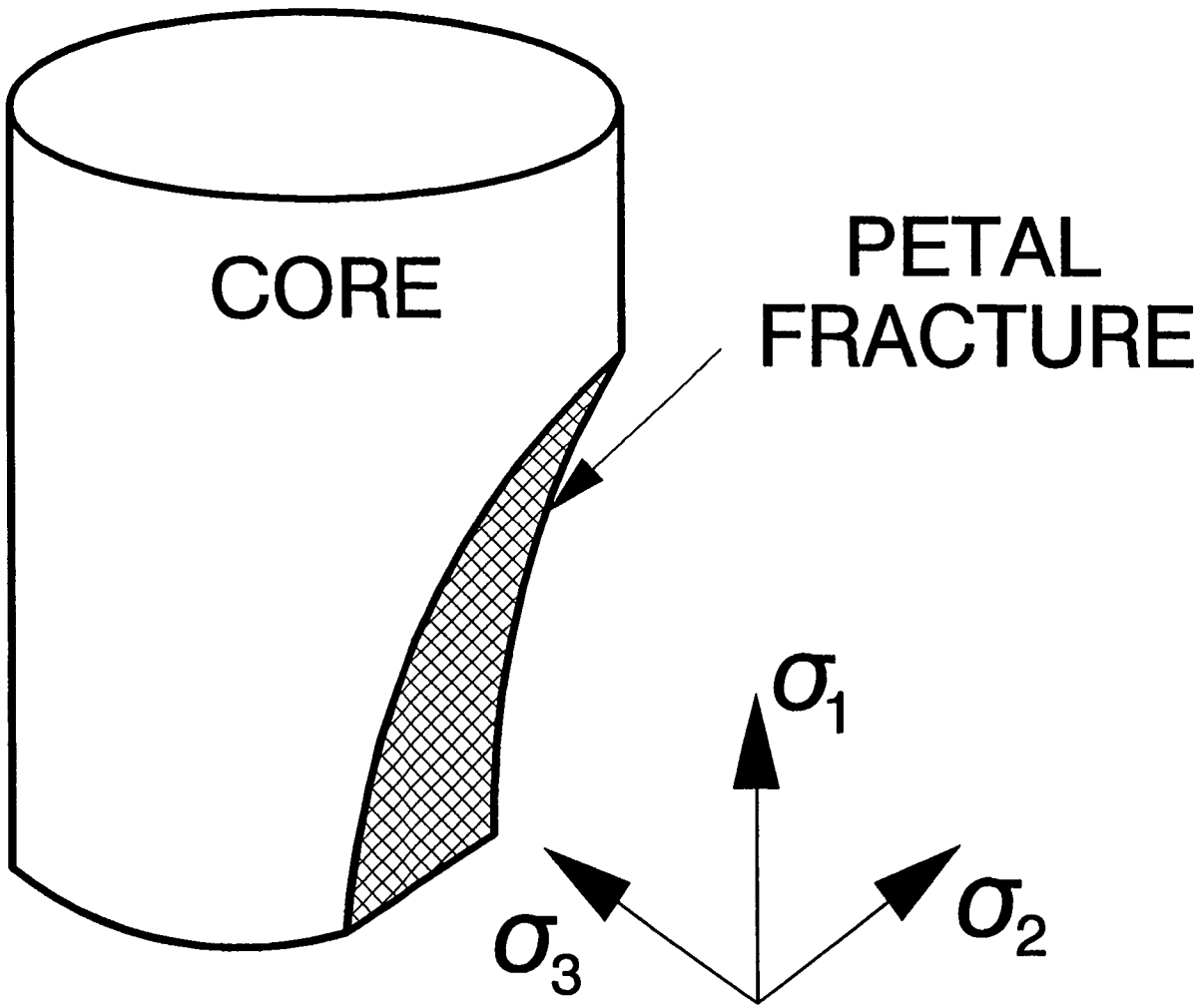

Figure 54. Schematic of petal fracture in core.[45]

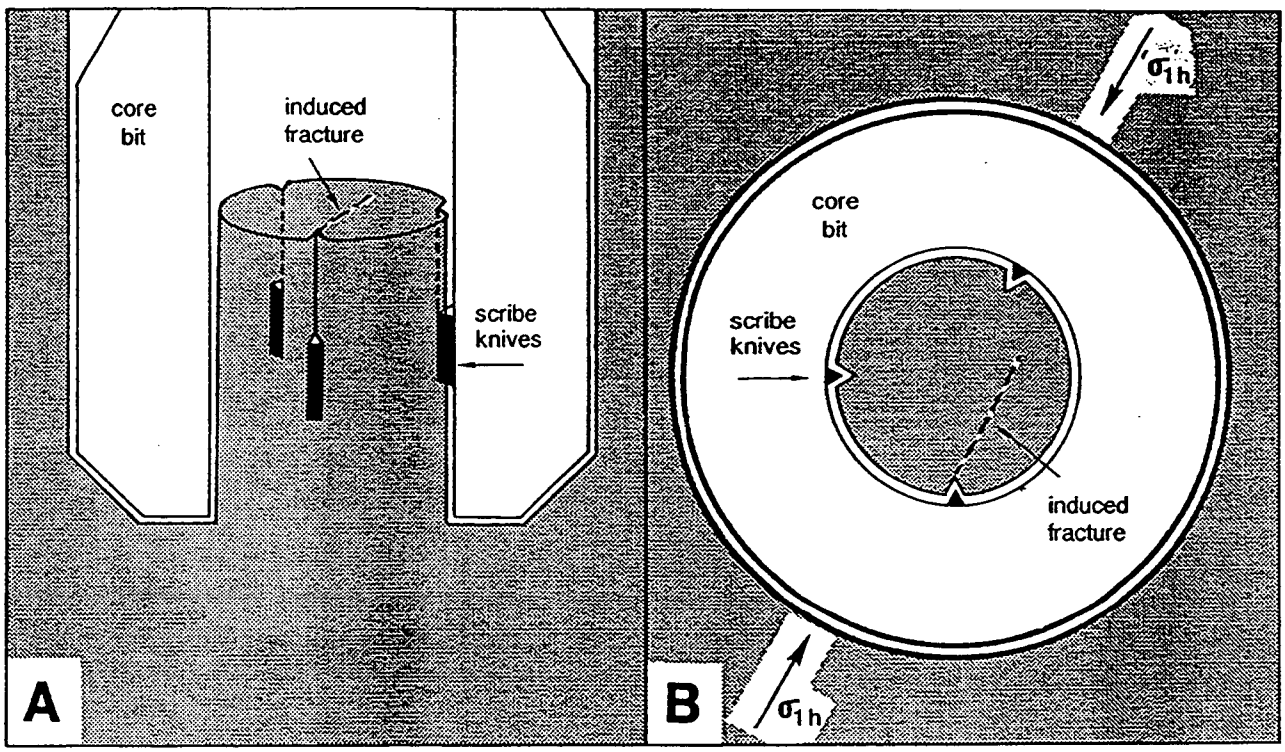

Figure 55. Origin of scribe-line fractures due to wedging of the core by scribing knives. (A) vertical section and (B) horizontal section show relationship between maximum horizontal stress and strike.[45]

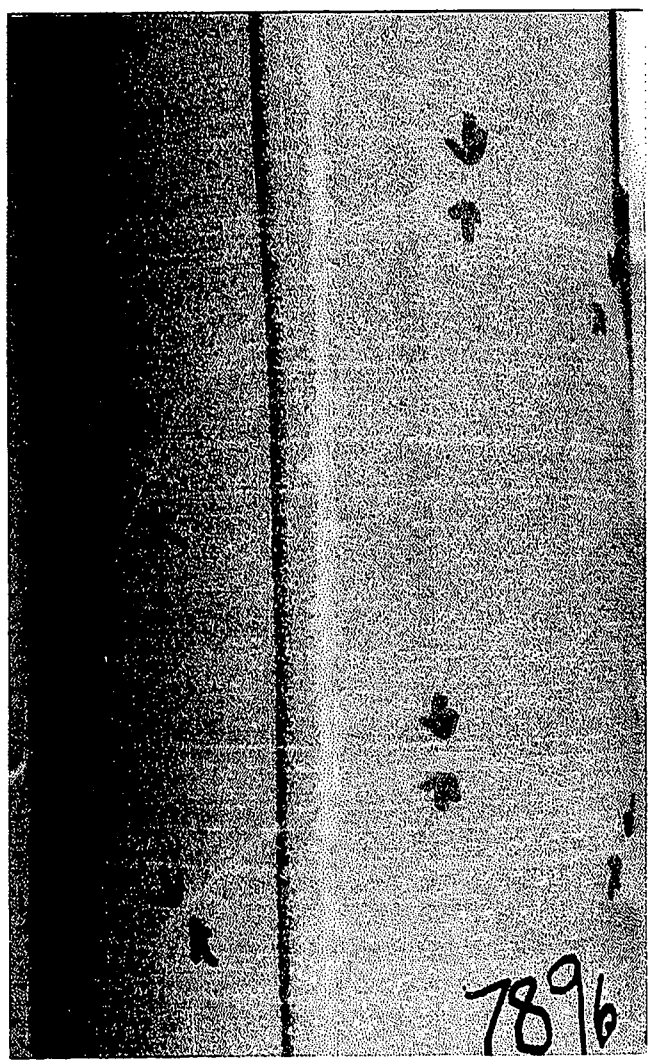

Figure 56. Photograph of two petal fractures in 4-in. diameter MWX core.[45]

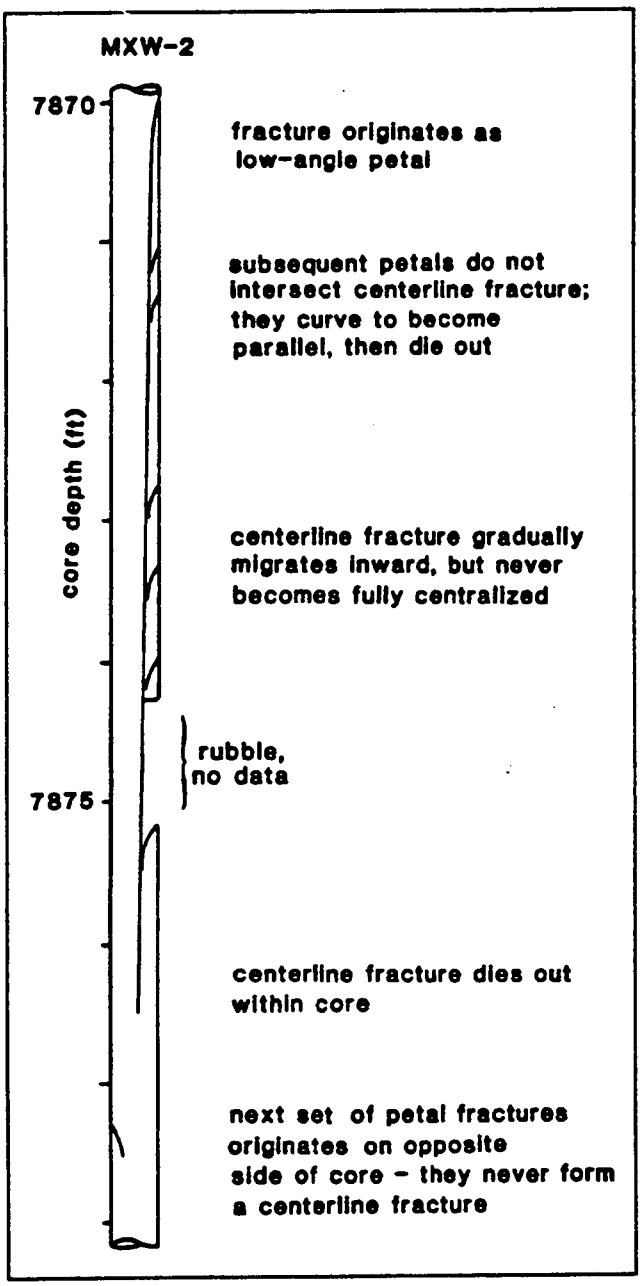

Figure 57. Schematic of petal-centerline fracture and associated petal fractures in core.[45]

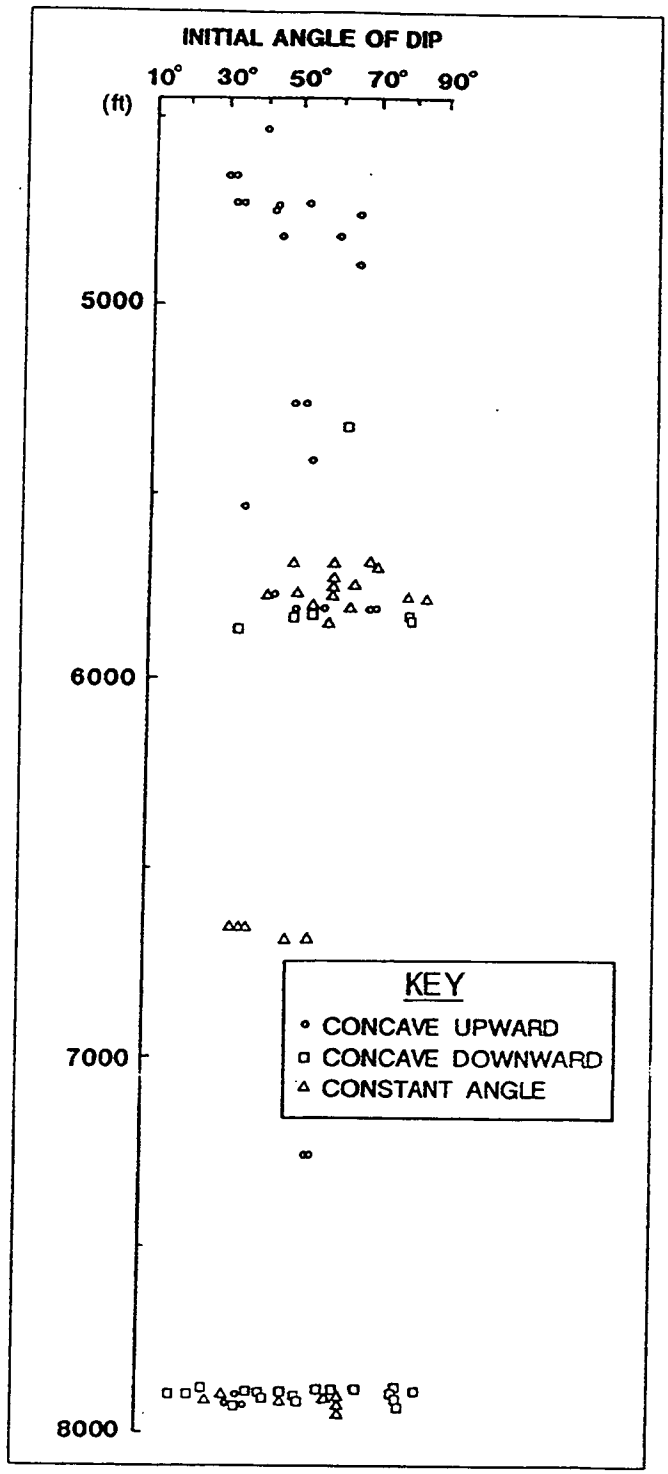

Figure 58. Distribution of petal fractures and petal-fracture dips with depth at MWX.[45]

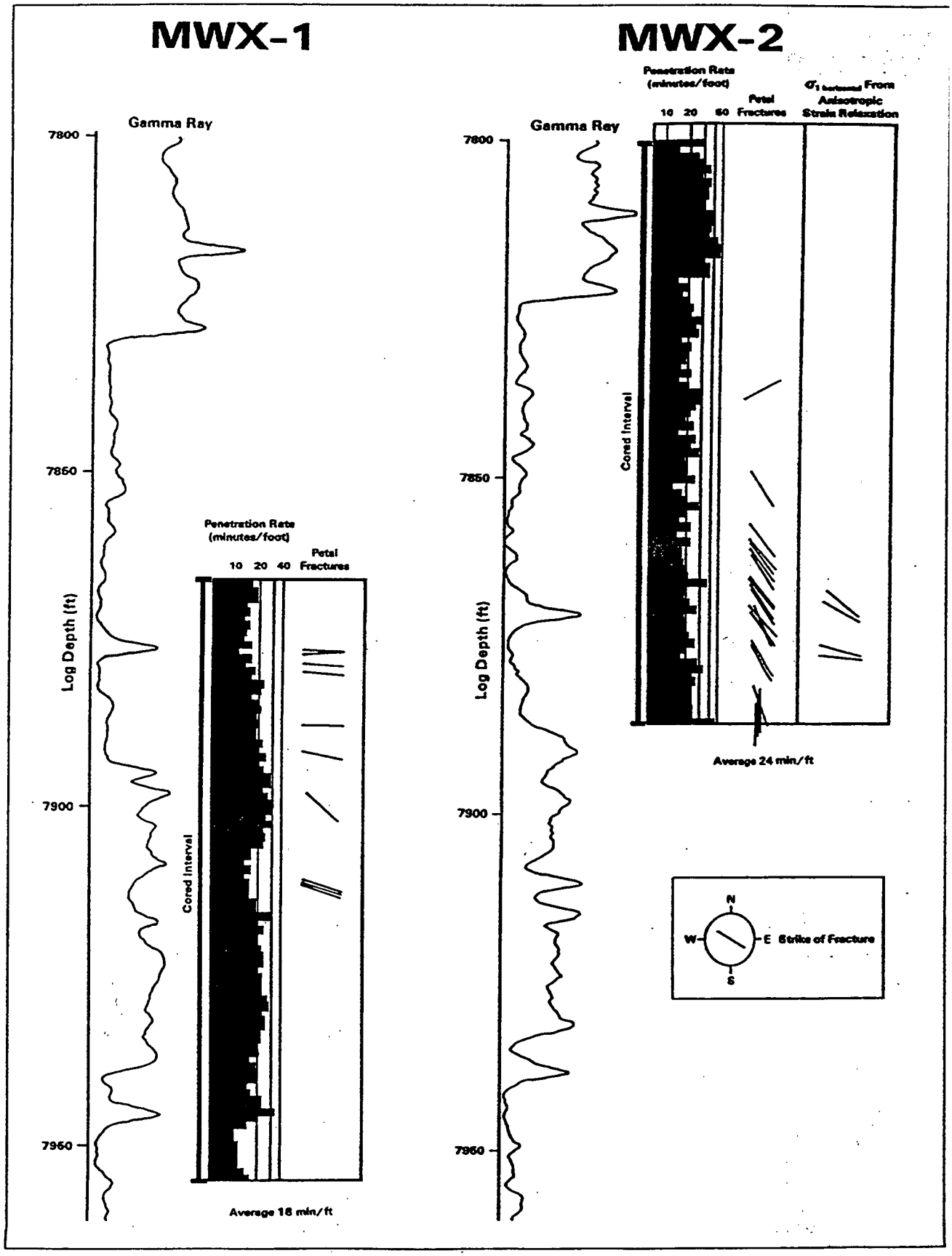

Figure 59. Drilling rates and strikes of petal fractures in oriented core from MWX.[45]

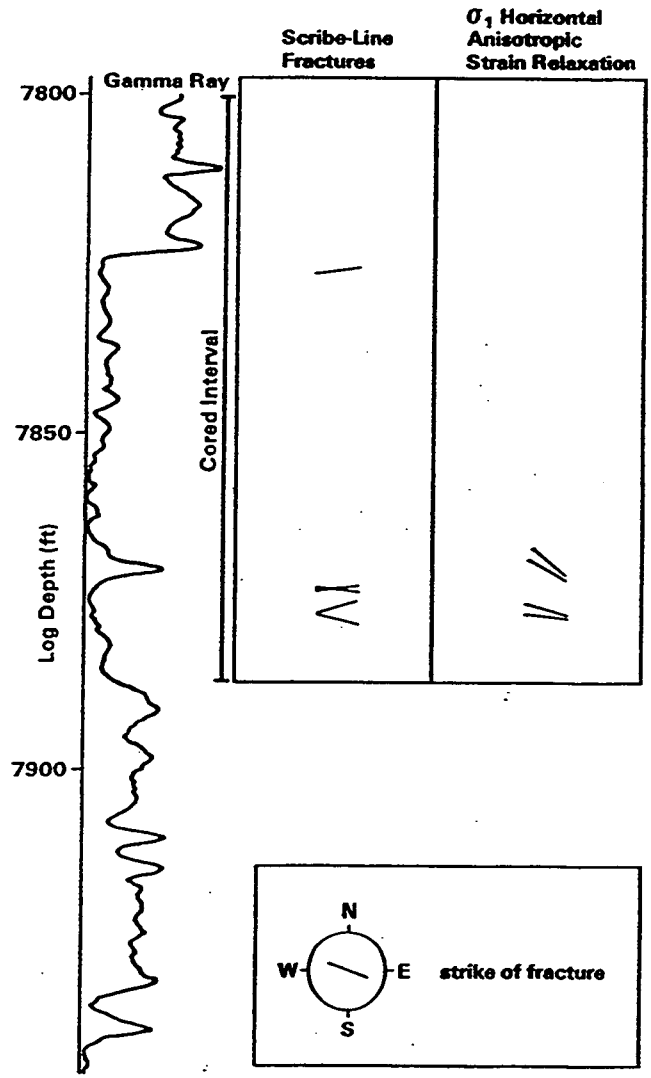

Figure 60. Orientations of five scribe-line fractures in MWX core.[45]

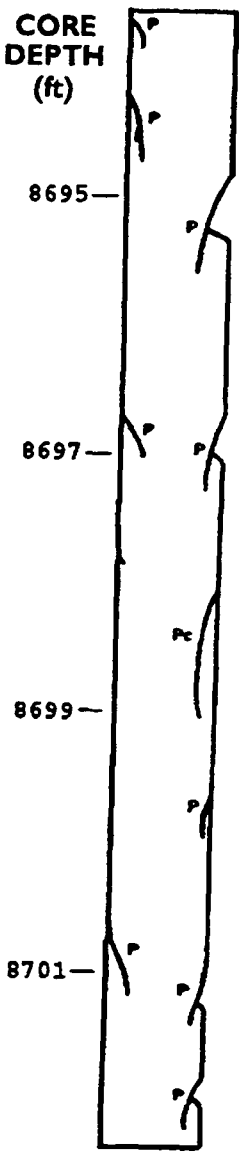

Figure 61. Sketch of aligned petal (P) and petal-centerline (Pc) fractures at SFE-2.51

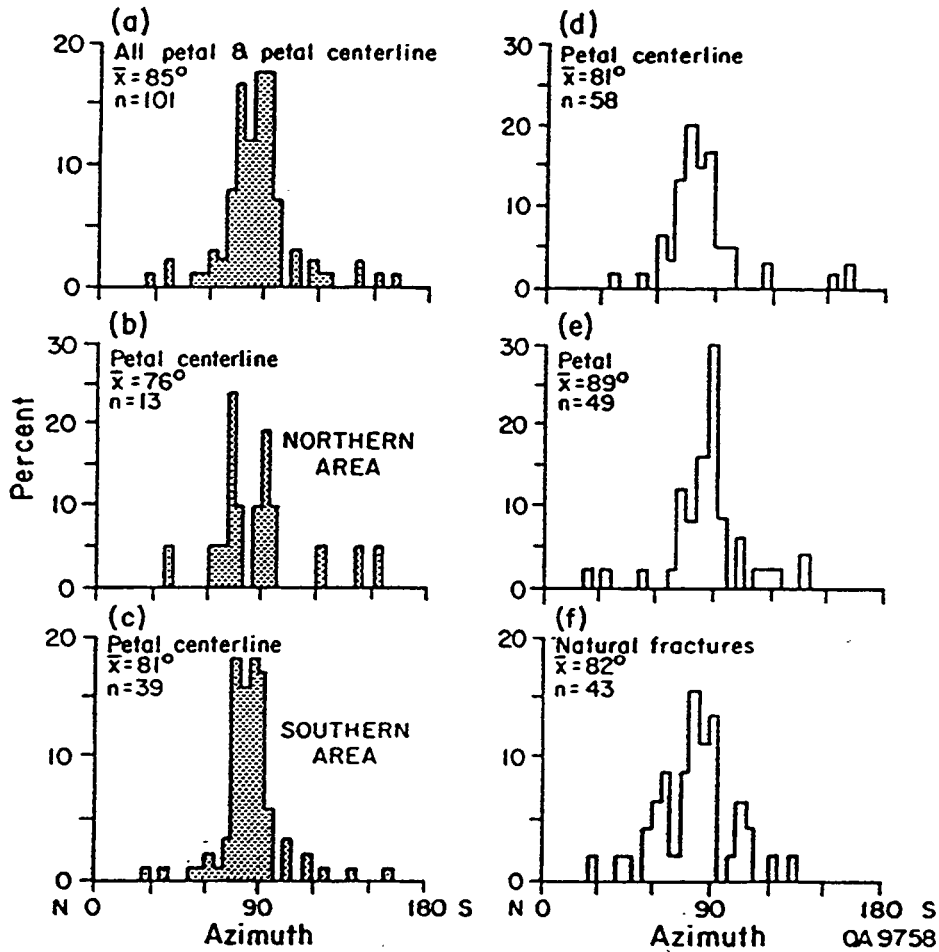

Figure 62. Attitudes of coring induced fractures, SFE-2.[51]